Viscosity of fragile glass-forming melts obtained by high rate calorimetry

Doctoral Thesis
(Dissertation)

to be awarded the degree
Doctor of Engineering (Dr.-Ing.)

submitted by
M.Sc.
Raschid Al-Mukadam
from Neunkirchen (Saar), Germany

approved by the
Faculty of Natural and Materials Science,
Clausthal University of Technology

Date of oral examination
14.03.2023

Dean

Prof. Dr.-Ing. Joachim Deubener

Chairperson of the Board of Examiners

Prof. Dr. Diethelm Johannsmann

Supervising Tutor

Prof. Dr.-Ing. Joachim Deubener

Reviewer

Prof. Dr. Dominique de Ligny

Prof. Dr. rer. nat. Christian Roos

Abstract

Knowledge about the temperature-dependent viscosity behaviour $\eta(T)$ of a glass melt holds strong interest for both, technology and science due to hot-forming and cooling processes as well as to gain deeper knowledge about the melt structure, e.g. the fragility of a melt or the role of the network formers and modifiers. Unfortunately, it is not easy to measure the entire viscosity above the glass transition temperature T_g with comparatively slow running viscometric methods for some glass systems due to crystallisation occurring during the measurements. This crystallisation strongly influences the viscosity of the resulting heterogeneous systems. As a result, a gap in viscosity data is obtained between T_g and the temperature of the stable liquid. Further, it has been demonstrated in the literature that one can superimpose the -lg q_c vs $1/T_f$ curve derived from calorimetry experiments on the lg η vs $1/T$ relationship by using a so-called parallel shift factor lg K. Thus, K enables retrieving η without the need to conduct viscosity measurements. This holds crucial importance since the proneness to crystallise of the glasses studied here prevents determination of liquid viscosity by rheological methods within a wide temperature range above T_g. This cumulative doctoral thesis was designed to test a combined experimental approach based on calorimetry and viscometry to narrow the gap in viscosity data for several fragile glass systems that appears due to fast crystallisation. A new commercial high-rate calorimeter was combined with conventional calorimetry to cover cooling and heating rates up to 40,000 K s^{-1} (2,400,000 K min^{-1}) and thereby receive viscosities from T_g down to $\eta = 10^{4.9}$ Pa s by applying parallel shift factors K_{onset}, K_{peak} and K_{end}. In detail, the fragile melts tested in this study are silicate glasses (lithium disilicate, diopside and standard glass DGG I), a fluorophosphate glass (N-PK52A), tellurite glasses (pure TeO_2 and two sodium tellurite glasses) and Zr–based bulk metallic glasses (Vitreloy 105 and AMZ4). It was found that this combined experimental approach is suitable to narrow the $\eta(T)$ gap for the mentioned melts. New data were obtained from the glass transition region down to $\eta = 10^{6.3}$ Pa s for the fluorophosphate glass, $10^{5.5}$ Pa s for silicate glasses, $10^{5.3}$ Pa s for tellurite glasses and $10^{4.9}$ Pa s for metallic glasses. A subsequent highly-constrained parameterisation of the available viscosity data makes it possible to describe the entire viscosity range. A smaller gap remains in the viscosity data of all glasses after this experimental procedure. Additionally, for pure TeO_2, whose weak glass-forming ability and strong tendency to crystallise prevent reliable measurements in the undercooled state, the parameterisation provides the first experimentally-determined viscosity curve. In case of the metallic glasses, the already-available measured viscosity data from literature suggest the existence of an unusual viscosity behaviour, the fragile-to-strong (F–S) transition. The new data and fits provided in this thesis narrowed down the appearance of this F-S transition to a region at higher temperature.

Danksagung

Als Erstes bedanke ich mich bei meinem Doktorvater Prof. Dr.-Ing. Joachim Deubener für die Bereitstellung dieser Arbeit. Die Jahre unter seiner Betreuung waren lehrreich und die vielen Diskussionen sowie Ideen haben die Arbeit sehr beflügelt.

Bei Prof. Dr. Dominique de Ligny und Prof. Dr. rer. nat. Christian Roos bedanke ich mich für die Übernahme der Korreferate.

Meinen Koautoren und Kollegen Dr. Danilo Di Genova, Dr. Hansjörg Bornhöft, Dr. Alessio Zandonà, Dr. Inga Katharina Götz und Dr. Moritz Stolpe möchte ich herzlich für die gute Zusammenarbeit und die viele Unterstützung danken. Ohne eure Hilfe wäre diese Arbeit nicht so zustande gekommen. Allen Kollegen am Institut für Nichtmetallische Werkstoffe möchte ich danken. Hervorheben möchte ich hierbei insbesondere Dr. Susanne Krüger, Dr. Gundula Helsch, Dr. Philipe Kiefer und Dr. Natalja Romero Sarcos für die zahlreichen Hilfestellungen während der gemeinsamen Zeit im Institut. Weiterhin danke ich Sabrina Schildhauer, Daniel Hart, Dr. Laura Briese, Thorben Welter, Simon Rudolph, Annika Blum, Jessica Löschmann, Thomas Peter, Ralf Putzig, Angelika Ohlendorf, Christian Rust, Michael Zellmann, Polina Notina, Martin Maiwald und Reiner Holly für die Unterstützung bei organisatorischen, sowie technischen Angelegenheiten als auch für die gute Zusammenarbeit. Unbeding zu erwähnen sind zudem Felix Elsner, Dr. Sven Schöbel, Dr. Johannes Unseld und Otto Bauer, die zusammen mit den bereits genannten Doktoranden für den gelegentlichen Ausgleich am Tischkicker sorgten.

Der Deutschen Forschungsgemeinschaft danke ich für die finanzielle Unterstützung im Rahmen des DFG-Projektes DE 598/28-1.

Zum Schluss möchte ich mich bei meiner Familie und meinen Freunden für ihre Unterstützung während meines Aufenthaltes in Clausthal bedanken.

Contents

1 Introduction

The glass-forming ability [1] of a melt is a central aspect that defines not only its large-scale manufacturing potential but also the simplicity by which its viscosity can be measured experimentally. Unfortunately, it is notably difficult to determine the viscosity for melts that tend to crystallise or easily demix above their glass transition temperature T_g [2], given that crystallisation and demixing strongly influence the overall viscosity of the resulting heterogeneous systems [3–8]. One example from manufacturing is the viscosity of all conventional glasses, which holds technological interest as an essential feature for the applicable production and hot-forming processes. Indeed, most metallic glass compositions are characterised by a relatively low glass-forming ability and require high quenching rates [9].

In general, the formation of a glass takes place if the cooling of a melt is sufficiently fast to prevent its crystallisation. Literature [10] has recently proposed an enhanced and more detailed definition of glass: "Glass is a nonequilibrium, noncrystalline condensed state of matter that exhibits a glass transition. The structure of glasses is similar to that of their parent supercooled liquids (SCL), and they spontaneously relax toward the SCL state. Their ultimate fate, in the limit of infinite time, is to crystallize." If such a glass (non-equilibrium) is subsequently heated (**Fig. 1.1**), it first passes through its glass transition region where its structure relaxes to the structure of the SCL state. This SCL is metastable, which means that a thermodynamic barrier must be overcome to start a crystallisation. The glass structure always first relaxes to the structure of the SCL before it can crystallise at any positive temperature after a certain time, which strongly depends on the chemical composition of the system and temperature [10].

The example presented in **Figure 1.1** shows a region between the calorimetric glass transition and the onset of crystallisation T_{cryst}, which represents the SCL state measured with a slow heating rate q_h of 10 K min^{-1} by conventional differential scanning calorimetry (DSC) after cooling the sample with the same rate q_c from its SCL. The fictive temperature T_f (also equilibrium and effective temperature) was first described as the temperature at which the SCL structure is frozen in [14, 15] and later used in terms of its contribution to the structural relaxation process of different glass properties (e.g. enthalpy, specific volume and refractive index) [16–20]. For a DSC experiment with $|q_h| = |q_c|$, the T_f value corresponds to the intercept between the tangent to the glass signal before the glass transition region (at lower temperature) and the tangent to the signal inflection point during the glass transition (at higher temperature) when the endothermal peak starts (calculated as T_{onset} in **Fig. 1.1**). The peak of calorimetric glass transition (T_{peak}) corresponds to the minimum of the signal during the glass transition, while the endset (T_{end}) can be constructed from the intercept between the tangent to the signal of the relaxed liquid after the glass transition region and the tangent to the second signal inflection point during the

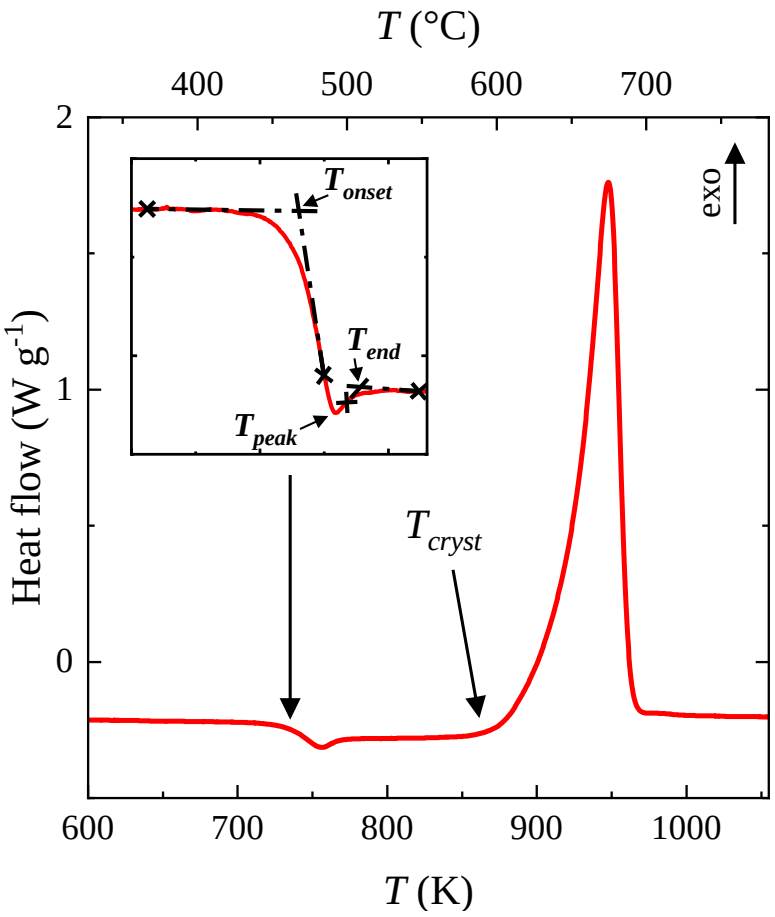

Figure 1.1: Measured heat flow as a function of temperature for a stoichiometric lithium disilicate glass [11–13] at a heating rate of 0.17 K s^{-1} (10 K min^{-1}) after cooling with the same rate from the SCL.

glass transition at a higher temperature than T_{peak}. T_f can also be called the standard glass transition temperature T_g if the glass was measured with q_h = 10 K min^{-1} after cooling the sample with $|q_c| = |q_h|$ from its SCL state [21]. This behaviour of a glass of lithium disilicate composition was illustrated for a wide range of matching cooling and heating rates $q_{c,h}$ ($q_{c,h} \mathrel{\hat{=}} |q_c| = |q_h|$) in a time-temperature-transformation (TTT) diagram (**Fig. 1.2**). In cotrast to the rate-dependent glass transition ($T_f(q_{c,h})$), the crystallisation process of a liquid occurs due to a combination of crystal nucleation and crystal growth. The kinetics of the liquid-to-crystal transformation can be described by the Johnson-Mehl-Avrami-Kolmogorov theory (JMAK) [22–26]. For **Fig. 1.2**, the time and temperature to crystallise a fraction of $\alpha = 10^{-6}$ was calculated following the parameters of lithium disilicate from the literature [27, 28]. Further, the average structural relaxation time was obtained by first calculating the viscosity curve using the MYEGA model [29, 30] (**Eq. 1.1**) and applying **Eq. 1.2** [31, 32] with a shift factor of lg K = 11.2 [5] on the viscosity to transform the data into a corresponding cooling/heating rate and finally into the time necessary to relax the glass to its SCL for heating from room temperature (**Eq. 1.3**). Further on, the corresponding temperature that was reduced by the room temperature can

be divided by the cooling rate to obtain the time necessary to relax a glass to its SCL at every temperature. In addition, the calorimetric glass transition T_f measured with different $q_{c,h}$ is presented and matched with the average structural relaxation curve.

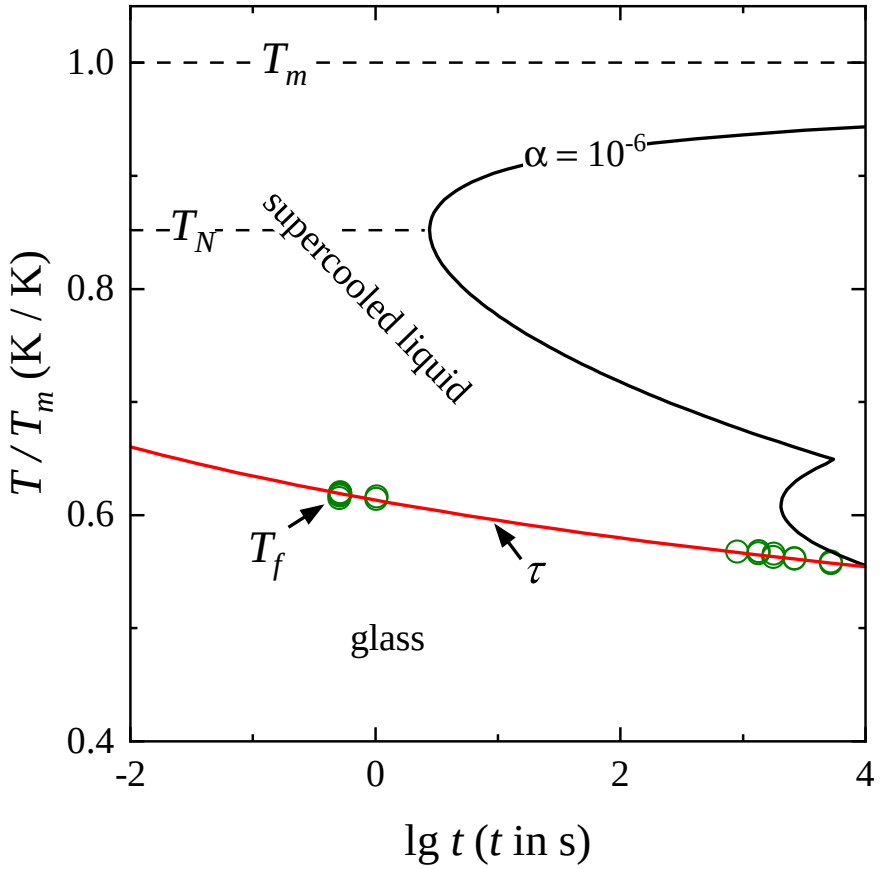

Figure 1.2: TTT diagram of lithium disilicate melt for a crystallised fraction of α = 10^{-6} (black line) together with average structural relaxation time τ (red line) and the calorimetric glass transition T_f measured for different $q_{c,h}$ (green circles). The melting temperature T_m and the "nose" temperature T_N (the time to crystallize α = 10^{-6} is the shortest at T_N) are added.

$$\lg \eta = \lg \eta_\infty + (12 - \lg \eta_\infty)\frac{T_g}{T} exp\left[\left(\frac{m}{12-\lg \eta_\infty} - 1\right)\left(\frac{T_g}{T} - 1\right)\right] \quad (1.1)$$

$$\lg q_{c,h} = \lg K - \lg \eta(T) \quad (1.2)$$

$$\tau = \frac{T - 293}{q_{c,h}} \quad (1.3)$$

Figure 1.2 shows that the α = 10^{-6} and τ curves change their courses with different slopes, whereby the slope of the relaxation curve is lower in comparison to the slope

of the transformation curve for $T < T_N$. These different slopes result in an increasing gap between glass transition and crystallisation with an increasing heating/cooling rate. Generally, the slope of the lines can be explained considering the activation energy *E* for each process [33]. With the increase of heating rates, both T_f and T_{cryst} move to higher temperatures, but T_f requires more activation energy to shift, and T_f will be left behind by T_{cryst} [34]. For crystallisation, which has a complex temperature dependence, *E* cannot be described by a single Arrhenius equation, which is the basis of the often-used Kissinger equation [35]. Instead, the already mentioned JMAK theory is appropriate for this purpose. In the case of T_f, *E* can be obtained by, for instance, using the Vogel-Fulcher-Tammann equation (VFT) [36–38]:

$$\lg \eta(T) = A + \frac{B}{T - T_0} \tag{1.4}$$

where *A*, *B* and T_0 are constants. The corresponding Arrhenius plot ($\lg \eta$ vs. T^{-1}) shows a non-linear trend and the slope represents *E* (*R* is the gas constant), which decreases with increasing *T* [33]:

$$\frac{d \lg \eta}{d\, T^{-1}} = \frac{BT^2}{(T - T_0)^2} = \frac{E}{R} \tag{1.5}$$

However, the knowledge of increasing space between T_f and T_{cryst} with increasing $q_{c,h}$ is not the only important behaviour of glass to be highlighted here. Additionally, it is necessary to mention the influence of the thermal history on the glass structure. The kinetics of the whole glass transition can be obtained by the Tool-Narayanaswami-Moynihan model (TNM) [15, 39, 40], whereby for a narrow temperature range a single constant *E* is frequently used [33]. However, for a large *T*-range, **Eq. 1.4** and **1.5** demonstrate that a non-linear trend for $\eta(T)$ is correct and that *E* is not a constant. Thus, the approach of Moynihan et al. [16, 41] linking *E* from calorimetric experiments with the rate-dependent glass transition $T_f(q_{c,h})$:

$$\frac{d \lg q_{c,h}}{d\, T_f^{-1}} = -\frac{E}{R} \tag{1.6}$$

is actually non-linear and has to be extended to serve a broader range of $q_{c,h}$ and to obey the non-Arrhenius dependence of η. Then, one has [32]:

$$\frac{d \lg \eta}{d\, T^{-1}} = \frac{d \lg q_{c,h}^{-1}}{d\, T_f^{-1}} = \frac{E_\eta(T)}{R} = \frac{E_q(T)}{R} \tag{1.7}$$

Eq. 1.7 also describes a linear relation between the cooling rate and viscosity at the fictive temperature $T = T_f$ [32]:

$$\frac{d \lg q_c}{d \lg \eta} = -1 \tag{1.8}$$

and, thus, confirms the observation previously described by Scherer [31]:

$$\lg \eta(T) = \lg K - \lg q_{c,h} \tag{1.9}$$

Eq. 1.9 emphasises that the lg η vs T^{-1} relationship can be superimposed on the -lg q_c vs T_f^{-1} curve by using the parallel shift factor lg *K*.

If unmatching cooling and heating rates ($|q_c| \neq |q_h|$) are used, differences between fictive and real temperatures occur. These differences are artefacts and stem from the thermal history. The first upscan reveals the relaxation of the initial glass towards the SCL state, whereas the second upscan shows the thermally equilibrated glass. In this example, a release of enthalpy ΔH (hysteresis) can be observed between the first and second upscan. The recently-released publication of Scarani et al. [42] extensively compared the difference between matching and unmatching cooling and heating rates when using **Eq. 1.9** with a combination of conventional and high-rate calorimetry for DGG standard glass. **Figure 1.3** clearly shows how strongly the fictive temperature is influenced if $|q_c|$ is unequal to $|q_h|$. The data reveal that T_f is shifted to a higher temperature if $|q_c|$ is lower than $|q_h|$ and vice versa to a lower temperature if $|q_c|$ is higher than $|q_h|$. Additionally, it is shown that the data with matching $q_{c,h}$ display the shape of the viscosity curve, which is constantly shifted by a factor of lg *K* = 11.2.

Another important point to consider is the target temperature or waiting time between the successive cooling cycles to allow structural relaxation of the sample. As summarised by Deubener [2] for silicate glasses, a time-dependent viscosity can be observed after the temperature changes in the glass transition range, more precisely the equilibration time of the viscosity takes longer than needed to set a new temperature. Deubener illustrates that for silicate glasses the structural relaxation time is two orders of magnitude longer than the Maxwell stress relaxation time. This observation is in line with the experimental study of Masuhr et al. [44] for bulk metallic glasses (BMGs).

This study was designed to introduce and demonstrate the results of an updated method based on the TNM approach to reproduce the kinetic fragility of liquids correctly by means of calorimetry even for fragile liquids. The viscosity of such fragile liquids is inaccessible in the $\eta(T)$ gap between T_g and the temperature of the stable liquid due to crystallisation occurring during the measurements with comparatively slow running viscometric methods.

However, the low scanning rates ($\leq$ 30 K min^{-1}) of conventional calorimeters limit the accessible range of viscosity around 10^{12} Pa s. With the aim of determining lower viscosity through this approach, the experiments must be conducted with higher scanning rates. For this purpose, a second DSC with an active cooling device and a Flash-DSC (FDSC) – which made the use of novel accessible high scanning rates possible – were implemented to cover cooling and heating rates from $\sim$0.02 K s^{-1} (1 K min^{-1}) up to

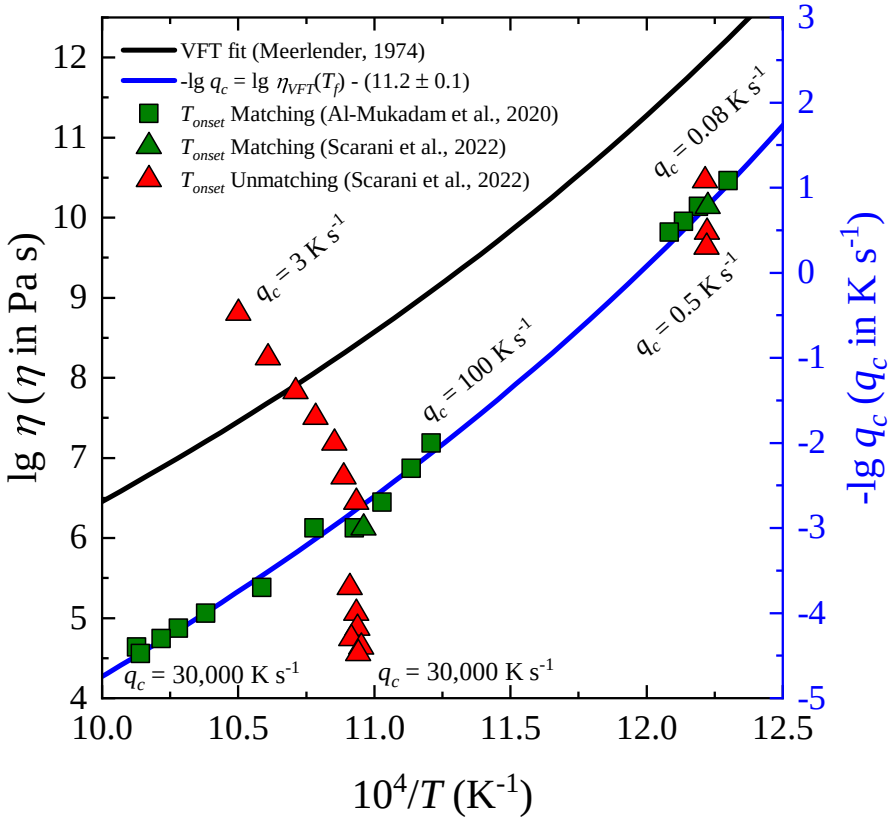

Figure 1.3: Arrhenius plot of viscosity calculated with **Eq. 1.4** (black line) and reciprocal cooling rate calculated with **Eq. 1.9** using lg K = 11.2 [5] (blue line). Fictive temperature (T_{onset}) of standard glass DGG I [43] measured with matching (green symbols) and unmatching (red symbols) cooling and heating rates between 0.08 K s^{-1} and 30,000 K s^{-1} were added. The unmatching cycles were always measured with q_h = 1,000 K s^{-1} when using $q_c \geq$ 100 K s^{-1} and q_h = 0.17 K s^{-1} when $q_c \leq$ 0.5 K s^{-1}. Figure modified after [42].

40,000 K s^{-1} (2,400,000 K min^{-1}).

Afterwards, this shift factor concept is extended to be applicable to three well-defined points (T_{onset}, T_{peak} and T_{end}) of the calorimetric glass transition region [5] to cover a larger range of viscosity from a single experiment:

$$\lg \eta(T_{onset}, T_{peak}, T_{end}) = \lg K_{onset,peak,end} - \lg q_{c,h} \tag{1.10}$$

By using a FDSC and the three fixed points T_{onset}, T_{peak} and T_{end}, it is possible to generate viscosity data in the $\eta(T)$ gap, ranging from the glass transition region ($\eta = 10^{12}$ Pa s) through the softening point ($\eta = 10^{6.6}$ Pa s) to $\eta = 10^{4.9}$ Pa s.

The motivation for this research is whether this updated approach is successful given the high scanning rates made accessible by the FDSC, and how well these newly-derived viscosity data fit with data from slow running devices or the literature. As mentioned before, it was shown [32] with experimental data for a small temperature range that the

lg η vs T^{-1} relationship can be superimposed on the -lg q_c vs T_f^{-1} curve which can be tested now with the FDSC experimentally for a large temperature range. Another point of interest is whether the approach can be used for glasses with different fragilities. Recent literature [45] described an increasing deviation of calorimetric fragility from kinetic fragility when measuring glasses with higher fragility by conventional DSC. This observation was explained by the inherent assumption of the used equations that the correlation of -lg q_c vs T_f^{-1} is based on an Arrhenius behaviour near T_g whereas a non-Arrhenius behaviour is correct across the whole temperature range. Consequently, the methodology was tested on several different glass systems in this study.

First, chapter 3 discusses the attempt to generate new viscosity data for a commercial fluorophosphate N-PK52A glass [46] and two model glasses of close stoichiometry, namely diopside (Di [11]) and lithium disilicate (LS2 [12, 13]). This was possible by applying the same approach to the standard glass DGG I [43]. The same methodology was utilised in chapter 4 to investigate pure TeO_2 glass by a necessary detour of measurements of two sodium tellurite glasses with a better glass-forming ability. Finally, in chapter 5 the focus is placed on investigations into new viscosity data of two Zr–based BMGs, namely Vitreloy 105 and AMZ4.

2 Overview of publications

2.1 Paper 1: Silicate and fluorophosphate glasses

- Authors and their contribution to the publication
  - R. Al-Mukadam: Conceptualization, Methodology, Data curation, Writing - review & editing, Investigation, Visualization, own contribution $\approx$ 70%
  - D. Di Genova: Conceptualization, Methodology, Writing - original draft, Data curation, Investigation, Visualization
  - H. Bornhöft: Investigation
  - J. Deubener: Writing - review & editing, Resources, Funding acquisition
- Year: 2020
- Title: **High rate calorimetry derived viscosity of oxide melts prone to crystallization**
- Scientific Journal: Journal of Non-Crystalline Solids
- Volume: 536
- Page: 119992
- DOI: https://doi.org/10.1016/j.jnoncrysol.2020.119992
- Content and relevance for the thesis:

This study was designed to introduce a first approach to determine the viscosity of melts prone to crystallisation. The glass systems examined in this case are a commercial fluorophosphate N-PK52A glass [46] and two model glasses of close stoichiometry, i.e., diopside (Di [11]) and lithium disilicate (LS2 [12, 13]).

Viscosity was determined by using three different DSC devices to study the T_f/q_c relationship of melts over five orders of magnitude of cooling rate, ranging from $\sim$0.08 K s^{-1} (5 K min^{-1}) up to 5,000 K s^{-1} (300,000 K min^{-1}), and then a chemically-independent *K* factor on the data by use of a basic equation from [31, 32] was applied:

$$\lg \eta(T_{onset}, T_{peak}) = \lg K_{onset}, K_{peak} - \lg q_{c,h} \tag{2.1}$$

Viscosity measurements in the range between $\sim 10^9$ and $\sim 10^{12}$ Pa s were performed using micropenetration viscometry and from 10^0 to 10^3 Pa s using concentric cylinder viscometry.

In order to arrive at the correct *K* factor for translating calorimetric data into viscosity, the standard glass DGG I [43] was used to calibrate the viscosimetric devices and the relationship between viscosity and calorimetry, which results in a global lg K_{onset} = 11.19 $\pm$ 0.06 and lg K_{peak} = 9.68 $\pm$ 0.08. As a result, these global shift factors are used to obtain new viscosity data for the Di, LS2 and N-PK52A glasses that agree with their measured viscosity data from viscometry. Following this, the MYEGA equation [29, 30] was used to parameterise the measured and DSC-derived viscosities to contribute a highly-constrained parameterisation of the viscosity of the melts examined in this study.

Accordingly, a $\eta(T)$ gap ranging from the glass transition region (η = 10^{12} Pa s) towards the softening point (η = $10^{6.6}$ Pa s) – which has been inaccessible so far due to crystallisation occurring during the measurements – has become accessible and allows expanding the existing data in literature for the glasses in this study.

2.2 Paper 2: Sodium tellurite and pure TeO_2 glasses

- Authors and their contribution to the publication
  - R. Al-Mukadam: Conceptualization, Validation, Data curation, Investigation, Visualization, Writing - original draft, own contribution $\approx 80\%$
  - A. Zandona: Conceptualization, Validation, Data curation, Investigation, Visualization, Writing - original draft
  - J. Deubener: Writing - review & editing, Supervision, Project administration, Funding acquisition
- Year: 2021
- Title: **Kinetic fragility of pure TeO_2 glass**
- Scientific Journal: Journal of Non-Crystalline Solids
- Volume: 554
- Page: 120595
- DOI: https://doi.org/10.1016/j.jnoncrysol.2020.120595
- Content and relevance for the thesis:

The publication describes a procedure that allows the production of a single-component oxide glass of pure TeO_2 by ultrafast quenching in a high-rate calorimeter. This melt system is known to crystallise directly in the $\eta(T)$ region below the melting temperature T_m, whereas a glass of this composition can only be produced by fast quenching very small sample volume or by the addition of chemical dopants/pollutants. Furthermore, it presents an approach to obtain new viscosity data by combining calorimetric with viscosimetric measurements of pure TeO_2 and sodium tellurite glasses.

The pure TeO_2 glass (100Te) was synthesised by heating up the raw material of high purity in a flash differential scanning calorimeter (FDSC) above the melting point and subsequently quenching it with high rate. Additionally, two sodium tellurite glasses (80Te20Na and 86Te14Na) with an improved glass-forming ability are produced by conventional melting in a muffle furnace. Viscosity measurements in the range between $\sim 10^{12.2}$ and $\sim 10^{9.6}$ Pa s were performed using micropenetration viscometry and were in very good agreement with the data available from the literature. The characteristic calorimetric temperatures T_{onset} and T_{peak} were achieved by using conventional DSC and FDSC devices with cooling/heating rates ranging from $\sim$0.02 K s^{-1} (1 K min^{-1}) up to

30,000 K s^{-1} (1,800,000 K min^{-1}). Using the measured viscosity data from the sodium tellurite glasses, it was possible to find the common best-fitting lg K_{onset} = 10.77 $\pm$ 0.06, which was used to translate all calorimetric T_{onset} values into viscosity by use of the equation from [31, 32]. Following this, a common lg K_{peak} = 9.73 $\pm$ 0.10 was collected from the FDSC data by aligning the T_{peak} values to the T_{onset} course. The application of this K_{onset} and K_{peak} to the calorimetric data of pure TeO_2 resulted in viscosity data ranging from η = $10^{9.4}$ to $10^{5.7}$ Pa s. Finally, the measured and calorimetric derived viscosities of 100Te and 80Te20Na were added together with values from the literature determined at high temperature. This dataset is used to parameterise the viscosity applying the MYEGA equation [29, 30] to supply a constrained parameterisation (extrapolated infinite temperature viscosity, fragility index, glass transition temperature) of the viscosity of these melts.

The results of the study provide the first experimentally-derived viscosity curve for pure TeO_2, whose strong tendency to crystallise and poor glass-forming ability prevent reliable data in the undercooled state. The T_g value stemming from the MYEGA fit is clearly lower than the scattered determinations reported in the literature and the determined fragility index *m* is so far the highest one reported for a single-component oxide glass.

2.3 Paper 3: Metallic glasses

- Authors and their contribution to the publication
  - R. Al-Mukadam: Conceptualization, Investigation, Validation, Writing - review & editing, own contribution ≈ 70%
  - I.K. Götz: Resources, Writing - review & editing, Funding acquisition
  - M. Stolpe: Resources, Writing - review & editing
  - J. Deubener: Deubener: Resources, Writing - original draft, Supervision, Project administration
- Year: 2021
- Title: **Viscosity of metallic glass-forming liquids based on Zr by fast-scanning calorimetry**
- Scientific Journal: Acta Materialia
- Volume: 221
- Page: 117370
- DOI: https://doi.org/10.1016/j.actamat.2021.117370
- Content and relevance for the thesis:

The publication explores the hitherto unexploited viscosity region between the glass transition temperature (T_g) and the melting temperature for Zr–based BMGs, namely Vitreloy 105 ($Zr_{52.5}Cu_{17.9}Ni_{14.6}Al_{10}Ti_5$) and AMZ4 ($Zr_{59.3}Cu_{28.8}Al_{10.4}Nb_{1.5}$). An experimental determination of the viscosity is hindered by crystallisation, which leads to a huge data gap between high- and low-temperature viscosity measurements of ∼11 (Vitreloy 105) and ∼13 (AMZ4) orders of magnitude in viscosity. Furthermore, the existing measured viscosity data from literature suggest the existence of an unusual viscosity behaviour, the fragile-to-strong (F–S) transition, which has been attributed to liquid-liquid transitions and was examined more closely in this case.

Conventional DSC and FDSC devices with cooling/heating rates ranging from ∼0.083 K s^{-1} (5 K min^{-1}) up to 40,000 K s^{-1} (2,400,000 K min^{-1}) were applied to achieve the characteristic calorimetric temperatures T_{onset}, T_{peak} and T_{end}. Afterwards, all fictive temperatures were transformed into viscosity data by applying the parallel shift factors lg K_{onset} = 11.2 ± 0.1, lg K_{peak} = 9.8 ± 0.2 and lg K_{end} = 9.2 ± 0.2, which were found for the reference soda-lime-silica glass DGG I [5] and represent compositionally-independent factors.

This new calculated viscosity data confirms the strong regime of both liquids down until lg η = 4.9–5.5 ($\sim 0.78 T_g/T$) in good agreement with measured low-temperature viscosity from the literature [47, 48]. Additionally, the strong regime could be described well by the MYEGA equation [29, 30]. With further consideration of the measured high temperature viscosity data from literature – which shows a fragile behaviour – the temperature region of a F-S transition can be narrowed down. By applying a generalised version of the MYEGA equation introduced by Zhang et al. [49, 50] – which uses a strong term dominant at low temperatures and a fragile term dominant at high temperatures – the whole viscosity range could be described in quantitative terms. In addition, under use of the first derivative of the viscosity behaviour, the maximum of the F–S crossover was found at approximately $0.69 T_g/T$ (Vitreloy 105) and $0.66 T_g/T$ (AMZ4).

3 High rate calorimetry derived viscosity of oxide melts prone to crystallisation

R. Al-Mukadam, D. Di Genova, H. Bornhöft, J. Deubener

Institute of Non-Metallic Materials, Clausthal University of Technology, Zehntner Str. 2a, 38678 Clausthal-Zellerfeld, Germany

Abstract

A gap in viscosity data spreads between glass transition and liquidus temperature for glass compositions, which are prone to crystallisation. Alternatively, differential scanning calorimetry (DSC) is used to calculate viscosity as both the cooling rate in a DSC experiment and the shear viscosity at the fictive temperature are related by a constant shift factor. However, the low cooling rate ($\leq$ 30 K min^{-1}) of conventional calorimeters limits the accessible range of viscosities around 10^{12} Pa s. This study reports on measurements using a Flash DSC (FDSC) with cooling rates up to 3 × 10^5 K min^{-1}. Under such extreme conditions, the fictive temperature is shifted considerably to higher temperatures and viscosity is accessible down to the softening point (viscosity = $10^{6.6}$ Pa s) without the occurrence of crystallisation during measurements. We provide a composition-independent shift factor to retrieve the viscosity of silicate and fluorophosphate melts over six orders of magnitude.

Keywords: fast scanning calorimetry; Flash DSC; viscosity; lithium disilicate glass; diopside glass; fluorophosphate glass

3.1 Introduction

Glass formation takes place upon the cooling of a melt fast enough to avoid its crystallisation. This process roots to the dependence of the timescale of structural relaxation τ of the melt with temperature T; the higher is T, the shorter is τ. This timescale controls the syn-cooling viscous delay of nucleation and crystallisation, and such retardation underpins the glass formation. Therefore, when studying the glass formation ability of a given system, of particular interest is the i) dependence on the temperature of the melt viscosity η and ii) cooling rate q_c dependence of fictive temperature T_f, which represents the temperature at which the liquid structure appears frozen on the timescale of observation. It is known that η correlates inversely with T, whereas T_f correlates positively with q_c, which means that a rapidly cooled melt has a higher T_f than a slowly cooled melt. Importantly, as demonstrated by Scherer [31] and Yue et al. [32], the lg η vs 1/T relationship can be superimposed on the -lg q_c vs 1/T_f curve by using the so-called parallel

shift factor lg *K*. This aspect assumes extraordinary importance as the use of lg *K* allows to retrieve η without the need to perform viscosity measurements, when the relationship between -lg q_c and 1/T_f is known. This is key since viscosity measurements often cannot be performed due to the rapid crystallisation and/or volatilisation of the sample. Therefore, knowledge of the relationship between q_c and T_f lies at the core of our understanding of glass formation process and thereby research on glass in materials and Earth sciences.

Broadly, DSC is the prevailing thermal analysis technique used to retrieve the relationship between q_c and T_f. Conventional high-temperature DSC equipment can impose to the sample a scanning rate ranging from ∼0.0016 to 0.5 K s^{-1}, which corresponds to 0.1 and 30 K min^{-1} , respectively. Recently, chip-based fast scanning calorimeters, the so-called "Flash-DSC" (FDSC) have been developed to explore the kinetics of glass transition over a wide range of temperature (178–1273 K) and elevated rates, up to scan rate of 5 × 10^4 K s^{-1} in heating and 4 × 10^4 K s^{-1} in cooling [21, 51, 52]. This now opens the opportunity to examine an exceptionally wide range of $T_f(q_c)$ and thus $\eta(T)$ of systems with low glass-forming ability, which are prone to crystallisation and/or exsolution of volatile phases if studied at standard rates with conventional DSC.

Here, we present the first attempt to retrieve the viscosity of melts prone to crystallisation by using a chemically-independent *K* factor and three different DSC devices. To this aim, we use a Flash-DSC, a second DSC with an active cooling device, and a third conventional DSC to study the T_f/q_c relationship over five orders of magnitude of cooling rate, from ∼0.08 K s^{-1} (5 K min^{-1}) up to 5000 K s^{-1} (3 × 10^5 K min^{-1}). This allows us to determine the melt viscosity of the commercial fluorophosphate N-PK52A glass [46] and two model glasses of close stoichiometry, i.e. diopside (Di [11]) and lithium disilicate (LS2 [12, 13]) in a $\eta(T)$ interval that has been inaccessible so far, i.e. from the glass transition range (η = 10^{12} Pa s) down to the softening point (η = $10^{6.6}$ Pa s), without crystallisation occurring during measurements.

3.2 Experimental and analytical methods

3.2.1 Glasses

We selected two glasses [diopside (Di) and lithium disilicate (LS2)] from previous studies [11–13] together with a commercial fluorophosphate N-PK52A glass [46]. The crystallisation and viscosity of Di, LS2 glasses have been extensively studied over decades [53–61] and combined with N-PK52A glass encompass a broad range of chemistry and fragility [62], thus representing the best candidates to explore both the $\eta(T)$ and $T_f(q_c)$ dependences over a wide interval of T and q_c. Viscometry was calibrated using the standard soda-lime silicate DGG I glass [43]. The chemistry of all four glasses is reported in **Table 3.1**, whilst the errors in chemical analysis are reported in ref. [46] for N-PK52A,

Fanara et al. [11] for Di, Krüger and Deubener [13] for LS2, and Meerlender [43] for DGG I. Constant composition of the fluorophosphate N-PK52A glass as analyzed by X-ray fluorescence (S4 Pioneer, Bruker AXS) before and after concentric cylinder viscometry indicated negligible evaporation of light elements.

Table 3.1: Chemical composition (mol%) of the investigated glasses. See references for the errors in chemical analysis.

Glass Ref.	DGG I [43]	Di [11]	LS2 [12, 13]	N-PK52A [46] in wt%
SiO_2	70.9	49.9	67.3	
TiO_2	0.1			
Al_2O_3	0.7			10-20
F^-				20-30
F_2O_3	0.1			
MgO	6.2	24.8		1-10
CaO	7.1	25.3		1-10
BaO				10-20
SrO				10-20
Na_2O	14.3			
K_2O	0.2			
Li_2O			32.5	
P_2O_5				10-20
Nb_2O_5				<1
SO_3	0.3			

3.2.2 Differential scanning calorimetry (DSC)

The fictive temperature T_f of the glasses was determined by measuring the change in the heat flow with temperature during a DSC upscan at a given heating rate (q_h). The upscan followed a downscan at a cooling rate $|q_c|$ equal to $|q_h|$. With this approach of matching cooling and heating rates $q_{c,h}$, the so-called onset of the calorimetric glass transition T_{onset} corresponds to T_f [17, 32, 63] determined by the enthalpy-matching method [16, 64, 65]. The T_{onset} represents the intercept between the tangent to the heat flow curve of the glass (i.e. before the glass transition region) and the tangent to the inflection point during the glass transition as illustrated in **Fig. 3.1**. We also determined the temperature corresponding to the heat flow peak undershoot (hereinafter referred to as T_{peak}) during the glass transition (**Fig. 3.1**).

The conventional DSC 404 F3 Pegasus (Netzsch, Selb, Germany) was used to measure T_{onset} and T_{peak} at $q_{c,h}$ equal to 5, 10, 15 and 20 K min^{-1} (0.08, 0.17, 0,25 and 0.33 K s^{-1}, respectively) under N_2 5.0 atmosphere (80 ml min^{-1} flow rate) using a PtRh20 crucible. Here, we used from ∼10 to ∼45 mg of DGG I glass to explore the effect of sample mass on

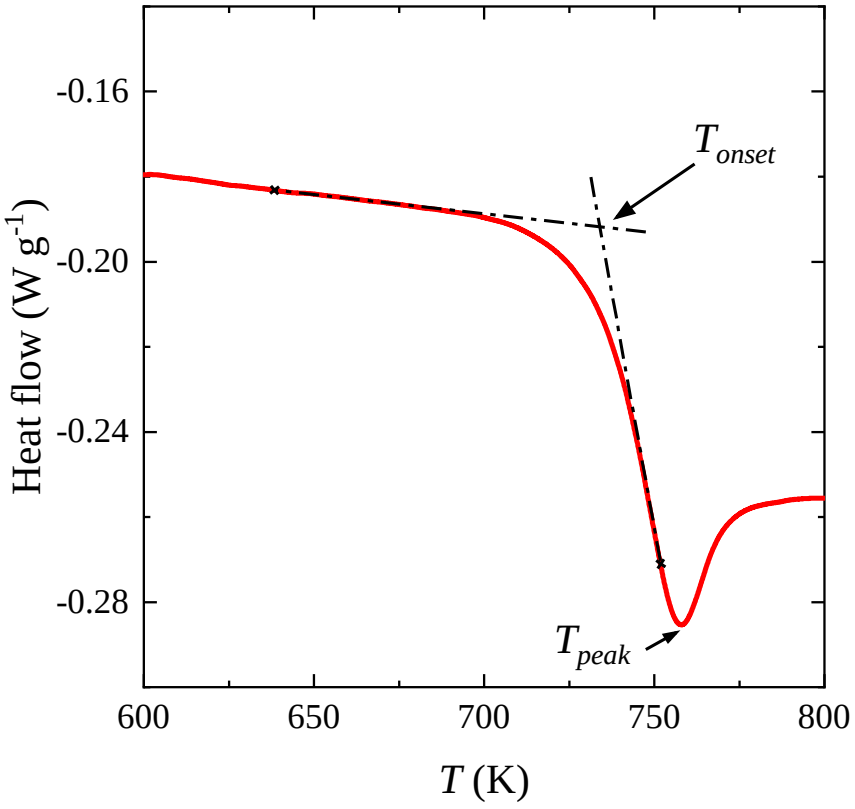

Figure 3.1: Measured heat flow as a function of temperature for LS2 glass at a heating rate of 0.17 K s^{-1} (10 K min^{-1}) after cooling at 0.17 K s^{-1} through the glass transition region. The characteristic temperatures T_{onset} and T_{peak} are shown.

the thermal retardation of T_{onset} and T_{peak}, especially at the fastest $q_{c,h}$ of 20 K min^{-1}. We used 20 ± 5 mg of glass for all the other samples. Prior to sample analysis, temperature and sensitivity calibration was performed using melting temperature and enthalpy of fusion of reference materials (pure metals of In, Sn, Bi, Zn, Al, Ag and Au) up to 1337 K. Baseline measurements were made at the different $q_{c,h}$, where two empty PtRh20 crucibles were loaded into the DSC. Each sample was heated at 0.08 K s^{-1} (5 K min^{-1}) from room temperature to 323 K and kept at this temperature for 40 min in order to achieve DSC signal equilibrium. Subsequently, in order to erase the thermal history of the sample, the temperature was raised with a heating rate of 0.33 K s^{-1} (20 K min^{-1}) to ∼60 K above the T_{peak} and, afterwards, decreased to 323 K at 0.17 K s^{-1} (10 K min^{-1}). From here, we applied the 4 cycles of $q_{c,h}$ following the sequence of 0.17, 0.33, 0.25, and finally 0.08 K s^{-1}, namely 10, 20, 15 and 5 K min^{-1}.

The TGA/DSC 3+ (Mettler-Toledo, Greifensee, Switzerland) equipped with a water cooling device was employed to extend the relationship between T_{onset} and T_{peak} with $q_{c,h}$ up to 0.5, 1 and 2 K s^{-1} (30, 60 and 120 K min^{-1}, respectively). Here, we used ∼5 up to ∼30 mg of glass for all samples and the measurements were performed under N_2 5.0 atmosphere (60 ml min^{-1} flow rate) using a PtRh20 crucible. We employed the same

temperature protocol used with the previous DSC for starting the measurement.

Finally, the Flash DSC 2+ (Mettler-Toledo, Greifensee, Switzerland) equipped with the UFH 1 sensor allowed us to achieve a $q_{c,h}$ interval ranging from 1 × 10^0 to 3 × 10^4 K s^{-1}. Before measuring the characteristic glass transition temperatures of the sample, we performed the two-step thermal treatment of an empty sensor according to the temperature programs provided by the manufacturer. Initially, the temperature of the chip and sensor support was set at 300.2 K. Once thermal equilibrium was reached, we carried out the so-called "conditioning" program, which consists of a series of heating and cooling steps at the maximum operating temperature. Such a temperature program is required to remove the thermal history of the chip. Afterwards, the thermocouple correction program was also performed. In order to obtain an optimal signal to noise ratio, we used a sample mass that ranged from ∼10 to ∼300 ng, which was estimated by using the intensity of the glass transition step obtained by FDSC and conventional DSC [52, 66]. As an example, we show in **Fig. 3.2** the N-PK52A sample (density ρ equal to 3.7 g cm^{-3} [46]) for which we obtained a mass of ∼90 ng. After the FDSC measurement was performed, aluminum (melting temperature T_m = 933.6 K) or indium (T_m = 429.8 K) was placed on the reference side of the chip sensor and measured with the same temperature program used for the sample. We used aluminum for Di, DGG I and LS2 that were measured at relatively high temperatures, whereas for the N-PK52A sample indium was used as the maximum temperature achieved during the measurement was 923.2 K. The difference between the measured T_m and the reference value at a given q_h was used for the correction of T_{onset} and T_{peak}. The maximum deviation between the reference melting temperature occurred for the aluminum standard and ranged from 1 K up to 5 K at the highest heating rate (3 × 10^4 K s^{-1}) in agreement with previous studies [52]. During the measurements a constant gas flow of Ar 5.0 with 40 ml min^{-1} was used.

3.2.3 Viscometry

High viscosity measurements between ∼10^9 and ∼10^{12} Pa s were performed using micropenetration viscometry on doubly polished glassy disks (3 mm thick). We used a vertical dilatometer (Bähr VIS 404, Hüllhorst, Germany) equipped with a micropenetration setup consisting of a rod of SiO_2 pushing a sapphire sphere of radius r = 0.75 mm. The force applied on the sample via the pushing rod was adjusted to 3.92 N by loading 400 g of load when measuring viscosity between 10^{10} and 10^{12} Pa s. We reduced the force to 1.96 N by loading 200 g of load to measure viscosity below 10^{10} Pa s. The temperature was controlled with a S-type thermocouple (Pt-PtRh) placed at ∼ 2 mm from the sample surface. As discussed recently by Behrens et al. [67] which used the same apparatus, the thermal gradient along the sample axis was less than ± 1 K mm^{-1}. Thereby, the maximum temperature error on is ± 5 K when considering the accuracy of the

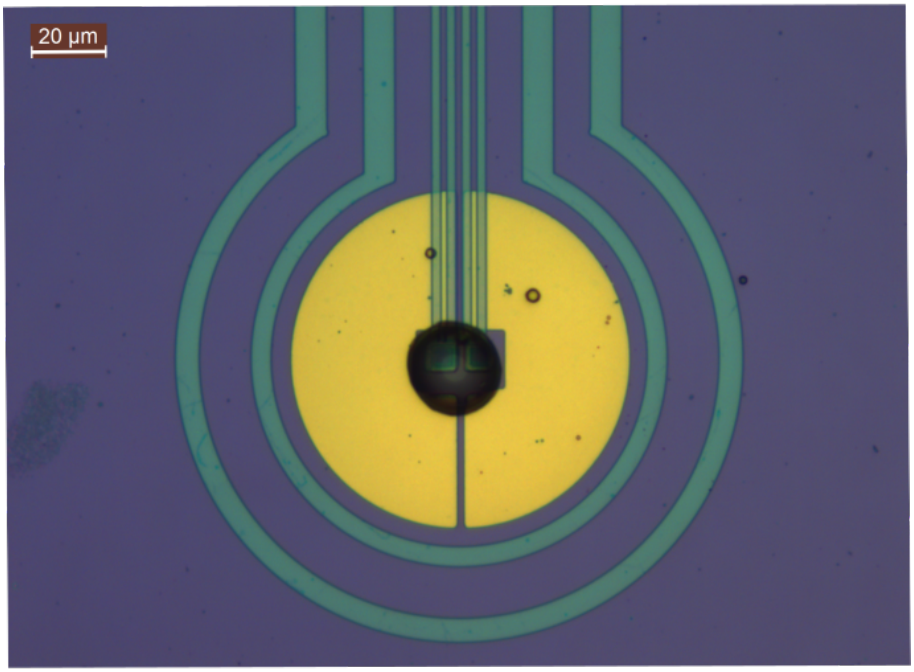

Figure 3.2: N-PK52A glass (~ 20 μm diameter) on the UFH 1 sensor of the Flash DSC 2+.

S-type thermocouple and its distance from the sample. We followed the procedure adopted by Di Genova et al. [68] to achieve the thermal equilibration of the sample at the target temperature (i.e. measuring temperature). A heating rate of 0.17 K s^{-1} (10 K min^{-1}) was imposed to the sample up to a temperature of 100 K lower than the measuring temperature and then a rate of 0.08 K s^{-1} (5 K min^{-1}) was used for the last 100 K. After reaching the final dwell temperature, the samples were allowed to relax for approximately 600 s before the load was applied. The indentation depth of the sapphire sphere into the sample was measured as a function of time using a linear variable displacement transducer and viscosity was determined according to Douglas et al. [69]. The viscosity measurements of the standard glass DGG I were also used to calibrate the vertical dilatometer. The certified viscosity data [43] were reproduced with a standard deviation of $\pm$ 0.1 in lg units.

Low viscosity measurements ranging from 10^0 to 10^3 Pa s were performed using concentric cylinder viscometry (Haake RV 20, Karlsruhe, Germany) for DGG I, LS2 and N-PK52A melts. The torque reading of the device was calibrated at strain rates from 0.1 to 96 s^{-1} using the standard DGG I [43, 70] and the error in viscosity was found to be $\pm$ 0.02 lg units, which is in line with that reported by Deubener et al. [70] who used the same experimental setup. For all experiments, we used data where a linear stress strain-rate relation was measured suggesting pure Newtonian flow behavior of crystal-free melts.

For the Di glass, only high-viscosity measurements were performed due to the limited amount of sample available. However, we selected viscosity data from the literature [53, 55, 56, 60, 61] necessary to obtain the full picture of the $\eta(T)$ relationship.

3.2.4 Calibration of the relationship between viscosity and characteristic temperatures

The standard glass DGG I was used to calibrate our devices (micropenetration and concentric cylinder viscometers) and the relationship between viscosity and the characteristic temperatures T_{onset} and T_{peak}. This was possible because for this glass certified data over the entire viscosity range from ~10 to ~10^{12} Pa s are provided. **Fig. 3.3** shows the certified viscosity points together with those measured (**Fig. 3.3A**) and the characteristic temperatures of the glass transition in Arrhenian diagrams (**Fig. 3.3B**). The inspection of **Fig. 3.3A** shows an excellent agreement between measured and standard viscosity. On the other hand, the inspection of **Fig. 3.3B** reveals that for each DSC method an upper limit in $q_{c,h}$ is evident at which the characteristic temperatures increasingly deviate (red symbols) from the anticipated Arrhenian behavior. A sample mass-dependent thermal lag, which will be discussed in detail in Section 3.4 is assumed to cause this deviation. The affected data were discarded from further evaluation.

In order to establish the shift factors (lg K_{onset} and lg K_{peak}) connecting viscosity lg η at T_{onset} and T_{peak} and calorimetry data we used **Eq. (3.1)** [31, 32]:

$$\lg K_{onset}, K_{peak} = \lg \eta(T_{onset}, T_{peak}) + \lg q_{c,h} \tag{3.1}$$

where $q_{c,h}$ represents the cooling/heating rate (K s^{-1}) at which T_{onset} and T_{peak} were measured by DSC. In order to obtain the viscosity at the different characteristic glass transition temperature, the VFT temperature dependence of the certification letter of DGG I was used (lg $\eta = A_{VFT} + \frac{B}{T(K)-T_0}$, where A_{VFT} = -2.5835 lg Pa s, B = 4331.6 K and T_0 = 520.79 K). The results are listed in **Tab. 3.2**, and by combining the average obtained from each DSC a global lg K_{onset} = 11.19 $\pm$ 0.06 and lg K_{peak} = 9.68 $\pm$ 0.08 could be established. The value for lg K_{onset} is similar to that provided by the literature [31, 32], whilst for lg K_{peak} our result matches that reported in [52], which performed an exclusive calibration of the FDSC device.

3.3 Results

3.3.1 Glass transition temperature

From the measurements performed at relatively slow $q_{c,h}$ (i.e. using conventional and water-cooled DSC) we obtained that the characteristic glass transition temperatures varied between 729.9 K [T_{onset} at 0.08 K s^{-1} (5 K min^{-1}), sample LS2] and 1057.3 K [T_{peak} at 2 K s^{-1} (120 K min^{-1}), sample Di]. With the fast $q_{c,h}$ measurements using the FDSC the characteristic glass transition temperatures ranged from 780.9 K (T_{onset} at 50 K s^{-1},

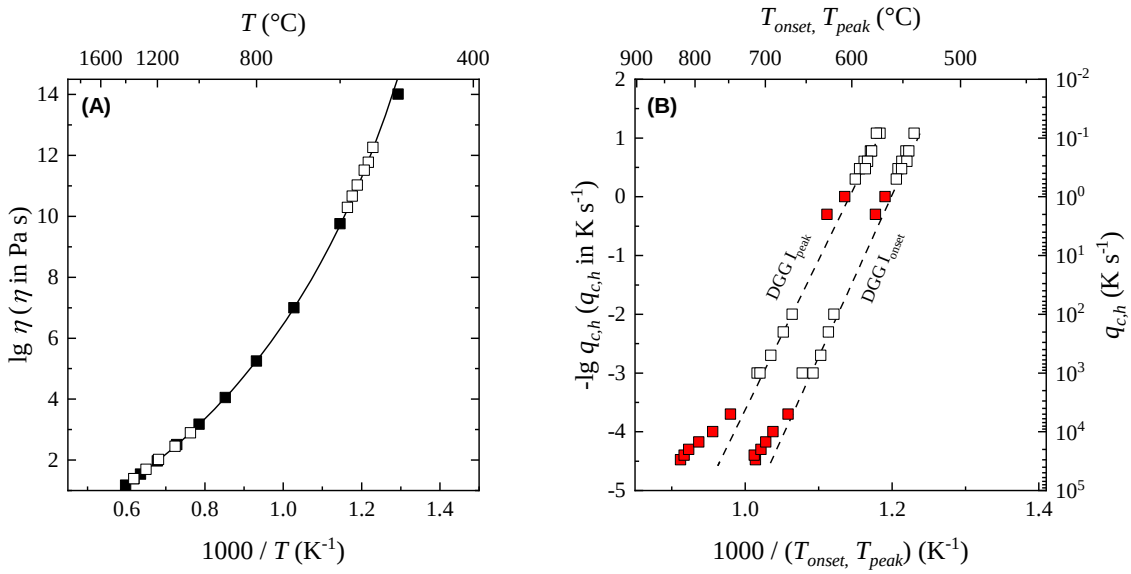

Figure 3.3: Arrhenian diagram of viscosity (A) and characteristic glass transition temperatures (B) of the standard soda-lime silicate glass DGG I. Panel A shows the certified data (black symbols), the VFT dependence (line) provided by the certificate, and the viscosity measured in this study (empty symbols). Note that red symbols in panel B indicate a deviation from the expected linear trend (dashed lines) due to thermal lag at high cooling/heating rates for the water-cooled and Flash DSC devices. Error bars are smaller than symbols (see text for details). (For interpretation of the references to colour in this figure legend, the reader is referred to the web version of this article.)

sample N-PK52A) to 1151.5 K (T_{peak} at 5000 K s^{-1}, sample Di). All results of DSC measurements were plotted in **Fig. 3.4** against the inverse of the temperature and compiled in **Table 3.3**.

3.3.2 Viscosity

The results from micropenetration (high viscosity interval) and concentric cylinder viscometry (low viscosity interval) are summarized in **Table 3.4** and illustrated in **Fig. 3.5**. In general, the measured viscosity by micropenetration ranged from $10^{9.55}$ Pa s (1044.0 K) for the diopside glass to $10^{12.30}$ Pa s (746.2 K) for the N-PK52A glass. For diopside glass, we also reported in **Fig. 3.5** data (gray triangles) provided by previous studies [53, 55, 56, 60, 61] and found an excellent agreement within the experimental error. Therefore, we can assume that the low viscosity data can be incorporated into our study. **Fig. 3.5** clearly underlines the wide gap in the determination of viscosity data from rheometric methods. For concentric cylinder viscometry, data below the lowest temperature for LS2 and N-PK52A samples were discarded since a constant torque reading was not achieved, suggesting a progressive crystallisation of the sample.

Table 3.2: Characteristic glass transition temperatures of the standard glass DGG I and calculated shift factor according to **Eq. (3.1)**. The star (*) indicates a deviation from the Arrhenian behavior due to thermal lag (**Fig. 3.3B**). Corresponding shift factors were not calculated. The characteristic glass transition temperatures were determined within ± 1 K for conventional and water-cooled DSC, and a maximum of ± 5 K for the FDSC (see text for details).

DSC-Type	$q_{c,h}$ (K s^{-1})	$q_{c,h}$ (K min^{-1})	T_{onset} (K)	T_{peak} (K)	lg K_{onset} (**Eq. 3.1**)	lg K_{peak} (**Eq. 3.1**)
Conventional	0.08	5	813.0	844.9	11.16	9.70
	0.17	10	820.3	854.2	11.10	9.63
	0.25	15	824.0	860.6	11.10	9.56
	0.33	20	827.6	865.1	11.06	9.52
Water-cooled	0.08	5		848.3		9.52
	0.17	10	817.6	853.0	11.23	9.68
	0.25	15	819.5	857.1	11.32	9.69
	0.33	20	824.4	859.3	11.21	9.74
	0.50	30	829.1	869.4	11.17	9.54
	1	60	839.8*	880.4*		
	2	120	849.2*	899.8*		
Flash	100	6000	892.1	939.8	11.08	9.76
	200	12,000	898.0	950.5	11.20	9.80
	500	30,000	906.7	966.3	11.34	9.84
	1000	60,000	927.8	983.9	11.06	9.77
	1000	60,000	915.2	980.2	11.40	9.85
	5000	300,000	944.6*	1020.3*		
	10,000	600,000	963.3*	1046.1*		
	15,000	900,000	972.7*	1067.2*		
	20,000	1,200,000	978.7*	1083.1*		
	25,000	1,500,000	987.5*	1090.4*		
	30,000	1,800,000	986.1*	1096.4*		

3.4 Discussion

The **Fig. 3.4** illustrates the relationship between -lg $q_{c,h}$ and the inverse of two characteristic glass transition temperatures (T_{onset} and T_{peak}) over five orders of magnitude of $q_{c,h}$, which we obtained by combining the results from three DSC devices. For all samples, the Arrehenian behavior can be observed from -lg $q_{c,h}$ ∼1 s K^{-1}, which corresponds to the lowest rate ($q_{c,h}$ = 5 K min^{-1}) used with conventional high-temperature DSC, to -lg $q_{c,h}$ ∼ -3.7 s K^{-1} ($q_{c,h}$ = 5000 K s^{-1}) explored by FDSC. We observed a deviation from the Arrehenian behaviour for -lg $q_{c,h} <$ -3.7 s K^{-1} for all samples, which corresponds to a $q_{c,h} >$ 5000 K s^{-1}. Furthermore, the same behavior was observed regardless of the sample mass for LS2 and N-PK52A at $q_{c,h}$ equal to 1 and 2 K s^{-1} that represent the high rates for the water-cooled DSC. We argue that the deviation from the linear trend stems from the combined effects of the thermal lag of the DSC sensors, the sample properties (i.e. mass, volume and thermal conductivity) and the used $q_{c,h}$. All these effects ultimately result in a shift to higher temperature of the T_{onset} and a delay in the release of the excess enthalpy (T_{peak}) of the glass upon dynamic heating.

The thermal lag of the FDSC sensor was recently observed and discussed by Schawe

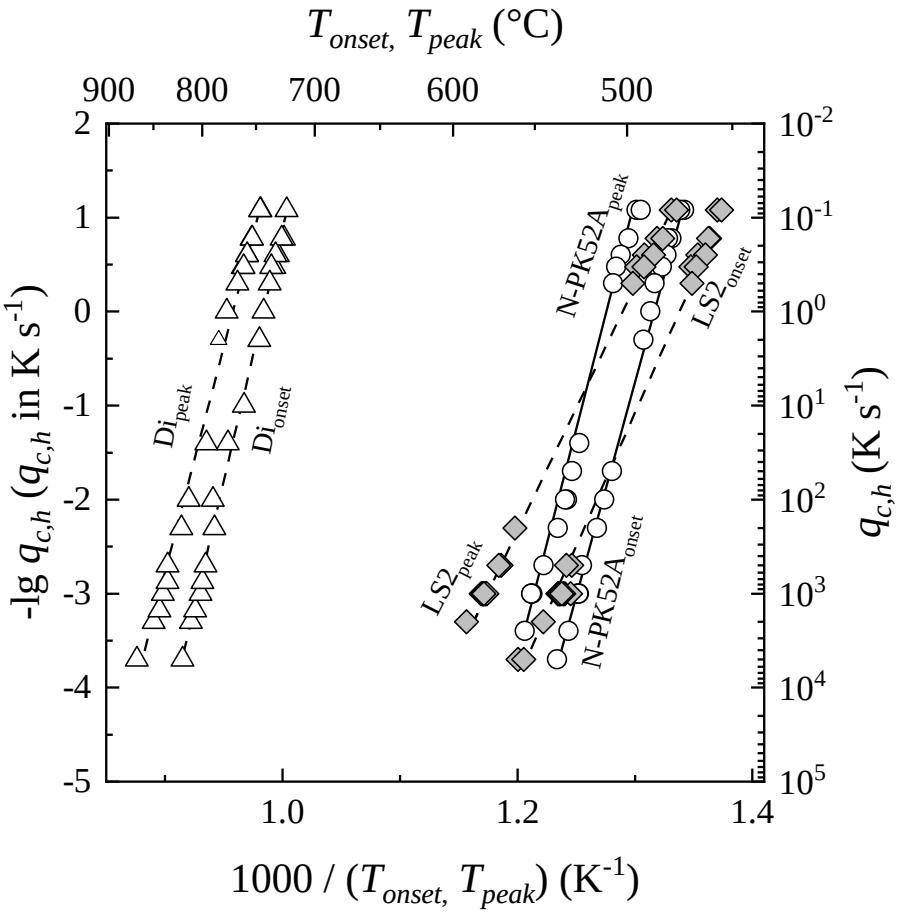

Figure 3.4: T_{onset} and T_{peak} with heating rate following equal cooling rate through the glass transition region of Di, LS2 and N-PK52A. Error bars are smaller than symbols (see text for details).

and Hess [52] who used DGG I glass. They concluded that thermal lag of the UFH 1 sensor, which is in the order of 0.4 ms, is relevant from $q_{c,h}$ higher than 5000 K s^{-1} when using $\sim$ 50 ng of glass. Here, we further explore the thermal lag effect on T_{onset} and T_{peak} by combining different DSC devices and simultaneously varying the sample mass. We aim to provide optimal conditions for retrieving the effective relationship between $q_{c,h}$, T_{onset} and T_{peak}. This is crucial because a limited range of $q_{c,h}$ is often studied, which would therefore lead to an apparent dependence of T_{onset} and T_{peak} on $q_{c,h}$. This aspect has a profound implication for the correct estimation of the melt viscosity via DSC, especially when the relationship between $q_{c,h}$, T_{onset} and T_{peak} is extrapolated outside the measured interval. Concerning the thermal lag observed in the relatively low $q_{c,h}$ region typical of conventional DSCs ($q_{c,h}$ ranging from 5 K min^{-1} to 2 K s^{-1}), we found that with $\sim$ 25 mg of sample the thermal lag is avoided from 5 K min^{-1} to 15 K min^{-1}. However, less sample ($\sim$ 15 mg) was needed to obtain reliable results up to 60 K min^{-1} and, eventually, we used $\sim$10 mg for the Di sample to measure T_{onset} and T_{peak} at 2 K s^{-1}, which is characterized by a relatively high DSC signal-to-noise ratio that allowed the use of a small amount of sample. Obviously, the sample density plays also a key role in defining the optimal amount

Table 3.3: Characteristic temperatures of the glass transition T_{onset}, T_{peak} of Di, LS2 and N-PK52A glasses as determined by conventional DSC, water-cooled DSC, and FDSC. The characteristic glass transition temperatures were determined within $\pm$ 1 K for conventional and water-cooled DSC, and a maximum of $\pm$ 5 K for the FDSC (see text for details).

	Di		LS2		N-PK52A	
$q_{c,h}$ (K s^{-1})	T_{onset} (K)	T_{peak} (K)	T_{onset} (K)	T_{peak} (K)	T_{onset} (K)	T_{peak} (K)
0.08	996.3	1019.0	729.9	751.4	745.2	768.5
0.08		1019.3	728.0	748.8	747.0	766.2
0.17	998.7	1026.9	733.4	758.4	751.2	775.6
0.17	1000.6	1026.3	733.9	755.5	752.9	772.4
0.25	1004.0	1031.1	738.9	764.5	754.9	780.9
0.25	1005.9	1031.0	735.4	759.9	753.6	776.3
0.33	1006.9	1034.9	742.1	768.4	758.0	785.6
0.33	1009.4	1034.1	739.7	764.8	755.8	778.8
0.50	1011.0	1039.8	741.6	770.3	759.5	780.3
1	1016.3	1049.9				
2	1019.8	1057.3				
10	1033.7					
25	1048.8	1069.2				798.3
50					780.9	802.2
100	1062.8	1086.5			785.0	805.0
100						806.0
200	1061.3	1094.0		834.8	788.7	810.1
500	1069.9	1108.2	802.4	843.2	796.7	818.0
500			805.3	844.6		
750	1072.8	1108.5				
1000	1074.9	1113.0	809.8	854.0	799.4	824.6
1000			810.1	852.5	798.6	825.1
1000			807.2	852.9	798.7	825.2
1000			806.2	852.4		
1000			803.1	851.7		
1000			808.7	854.7		
1000			809.1	855.3		
1000			806.9	854.2		
1000			809.0	854.2		
1000			808.0	853.7		
1500	1080.0	1116.8				
2000	1084.1	1123.0				
2500					804.1	829.0
5000	1092.8	1141.5			810.4	842.6

of material and indeed for the densest glass used in our study (N-PK52A, ρ = 3.7 g cm^{-3} [46]) we used $\sim$ 5 mg that resulted in a thermal lag only for T_{peak}.

Once the relationship between the characteristic temperatures $T_{onset}(q_{c,h})$ and $T_{peak}(q_{c,h})$ of **Tab. 3.2** and viscosity was retrieved for the standard soda-lime silicate glass

Table 3.4: Viscosity of disilicate (LS2), diopside (Di) and fluorophosphate (N-PK52A) glasses. The error associated with micropenetration viscometry is ± 0.1 lg units, whilst for concentric cylinder viscometry is ± 0.02 lg units.

Di		LS2		N-PK52A	
T (K)	lg η (Pa s)	T (K)	lg η (Pa s)	T (K)	lg η (Pa s)
999.2	11.92	731.0	12.08	746.2	12.30
999.4	11.96	740.9	11.46	751.3	11.85
1004.6	11.53	750.7	10.93	930.2	1.99
1006.3	11.49	750.5	10.91	930.2	1.88
1009.2	11.35	760.4	10.37	960.2	1.07
1009.4	11.28	770.5	9.92	960.2	1.07
1014.7	11.01	780.3	9.53	960.2	1.07
1016.4	10.93	790.2	9.11	993.2	0.46
1019.4	10.75	1289.2	1.57	993.2	0.47
1029.0	10.27	1289.2	1.57	1025.2	0.04
1029.4	10.25	1319.2	1.43	1025.2	0.03
1036.3	9.92	1319.2	1.43		
1044.0	9.55	1348.2	1.30		
		1348.2	1.30		
		1403.2	1.10		
		1403.2	1.10		
		1448.2	0.93		
		1448.2	0.93		
		1495.2	0.78		
		1495.2	0.78		
		1528.2	0.67		
		1528.2	0.66		

DGG I using **Eq. (3.1)**, we applied the parallel shift factors lg K_{onset} = 11.19 ± 0.06 and lg K_{peak} = 9.68 ± 0.08 for the DSC data of the Di, LS2 and N-PK52A glasses (**Fig. 3.6**). Notably, the derived viscosity for Di, LS2 and N-PK52A in the low-temperature regime investigated by the two low $q_{c,h}$ DSCs agree with the measured viscosity by micropenetration (blue stars) in the high viscosity interval (between 10^9 and 10^{12} Pa s). Therefore, we conclude that within the chemical interval investigated in this study, the calculated K_{onset} and K_{peak} are independent of chemical composition. Moreover, we observed that the FDSC-derived viscosity virtually fills the $\eta(T)$ gap in which crystallisation occurs for most of the synthetic and natural systems with low ability to form glass [12, 13, 71–74].

Finally, we parameterized the measured and DSC-derived viscosities using the MYEGA equation (**Eq. 3.2**) [29, 30] to provide a highly-constrained parameterization of the viscosity of our melts over the temperature interval studied here:

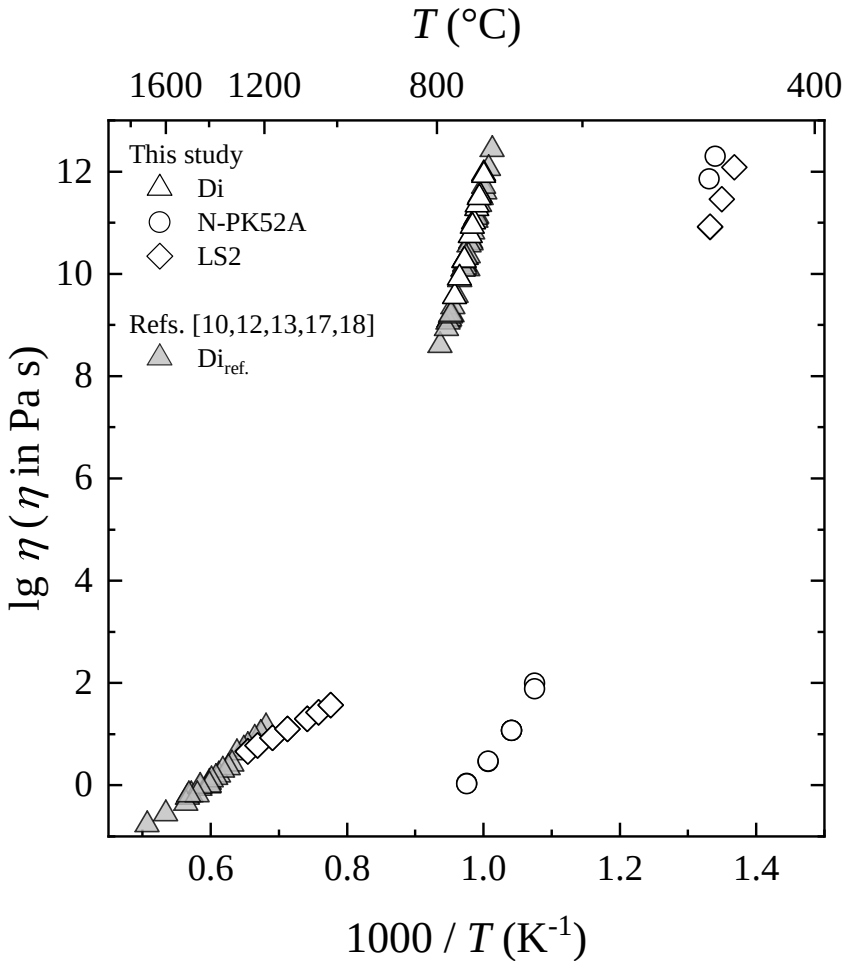

Figure 3.5: Viscosity of Di, LS2, and N-PK52A melts. The figure emphasizes the broad gap in viscosity data due to the ease with which the supercooled melts crystallise. Error bars are smaller than symbols (see text for details).

$$\lg \eta = \lg \eta_\infty + (12 - \lg \eta_\infty)\frac{T_g}{T} exp\left[\left(\frac{m}{12-\lg \eta_\infty} - 1\right)\left(\frac{T_g}{T} - 1\right)\right] \quad (3.2)$$

The obtained MYEGA parameters η_∞, *m* and T_g are reported in **Table 3.5**. The lg η_∞ ranges between -5.96 for N-PK52A and -0.73 for LS2, whilst for Di is equal to -2.02 Pa s. These results are in agreement with previous findings for oxides glass-forming melts [30]. The derived fragility *m* for Di is 62.7 and agrees with data provided in the literature (*m* = 58.6 [75]). The LS2 exhibits the lowest fragility of 47.4 (*m* = 45.4 [76]), whereas the N-PK52A was found to have the highest fragility of 72.3. Finally, we also calculated the *m* parameter using only the measured viscosity for LS2 and N-PK52A samples whose viscosity was weakly constrained in the low temperature range (**Fig. 3.5**). We obtained *m* = 43.4 $\pm$ 0.5 for LS2 and *m* = 82.0 $\pm$ 2.2 for N-PK52A, which are respectively $\sim$10% lower and higher than values given in **Table 3.5**. Therefore, the use of FDSC-derived viscosities provides a better constraint to the estimation of the *m* parameter that is not only

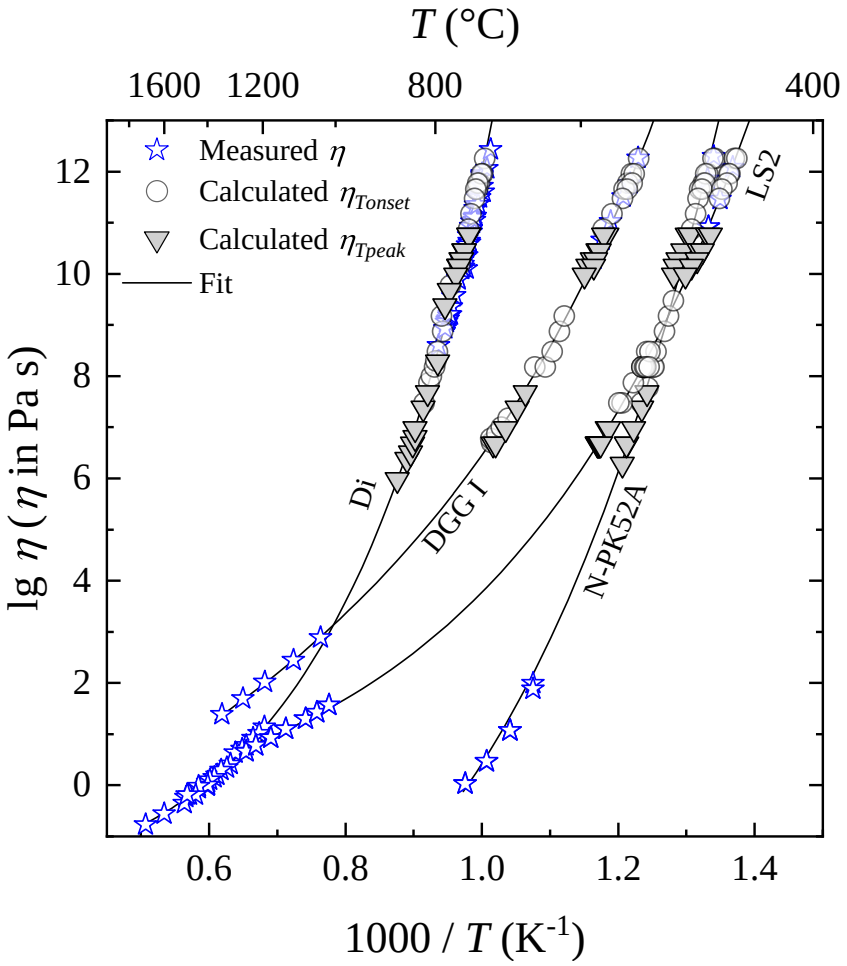

Figure 3.6: Measured viscosity data of samples used in this study (blue stars, data from **Fig. 3.5**) together with DSC-derived viscosity using **Eq. (3.1)** , T_{onset} (empty circles), T_{peak} (gray triangles) and the parallel shift factors (lg K_{onset} and lg K_{peak}) provided in this study. Lines represent fitting according to Waterton-Mauro (WM called also MYEGA) equation [29, 30] and parameters listed in **Table 3.5** for Di, LS2 and N-PK52A melts. Error bars of both measure and calculated viscosities are smaller than symbols (see text for details).

important for modelling the viscosity as a function of temperature, but is also used to link the melt structure to viscosity through the measurement of the configuration heat capacity [45, 77, 78].

Table 3.5: Fit parameters and standard errors of estimation for the MYEGA [30] equation (**Eq. 3.2**) using the DSC derived viscosity data of Di, LS2 and N-PK52A melts.

Sample	lg η_∞ (Pa s)	m	T_g (K)
Di	-2.02 ± 0.10	62.7 ± 0.8	1000.4 ± 0.5
LS2	-0.73 ± 0.07	47.4 ± 0.4	732.6 ± 0.4
N-PK52A	-5.96 ± 0.54	72.3 ± 1.6	752.2 ± 0.6

We conclude that the provided K_{onset} and K_{peak} can be used for relatively strong glass formers systems such as the standard soda-lime silicate glass DGG I (m = 37.8 [79]) and,

importantly, more fragile systems such as LS2, Di and notably also for the fluorophosphate N-PK52A. We emphasize that all these fragile glasses are prone to crystallise rapidly above the glass transition temperature when using conventional DSC and viscometry. The implications of such universality in retrieving the melt viscosity of glass-forming systems over six orders of magnitude and a broad landscape of chemical composition by using a single parallel shift factor are profound and diverse. First and foremost, it is now possible to formulate better parameterizations of the viscosity of technical and natural melts by accessing the $\eta(T)$ where melt crystallisation occurs rapidly. Simultaneously, the use of FDSC will stimulate future work on the effect of crystallisation and volatiles species on the viscosity of melts. This is fundamental for the formation and reforming of glass-ceramics [80], for the viscous sintering of glass matrix composites for sealant [81] and packaging applications [82, 83], as well as the study of magma dynamics [84–88].

3.5 Conclusions

In this study, we combined fast scanning calorimetry with two conventional DSC equipment and viscometers to retrieve the viscosity of the glass-forming melts over six orders magnitude, from $\sim 10^6$ up to $\sim 10^{12}$ Pa s. We demonstrate that the parallel shift factors (lg K_{onset} and lg K_{peak}) are independent of the chemical composition of relatively strong and fragile glass-forming silicate and fluorophosphate systems. The obtained lg K_{onset} and lg K_{peak} can be used over an interval of heating rate ranging from 5 K min^{-1} up to 5000 K s^{-1}. We also provide constraints on the effect of sample mass on the thermal lag of the characteristic glass transitions (T_{onset} and T_{peak}). With the use of fast scanning calorimetry and parallel shift factors here provided, it is now possible to access the critical viscosity region where crystallisation and/or volatilisation occur within the time-scale of conventional DSC and viscometry equipment. This has profound implication for materials and Earth sciences.

4 Kinetic fragility of pure TeO_2 glass

R. Al-Mukadam, A. Zandona, J. Deubener

Clausthal University of Technology, Institute of Non-Metallic Materials, 38678 Clausthal-Zellerfeld, Germany

Abstract

Pure TeO_2 glass was prepared in a flash differential scanning calorimeter by applying fast quenching rates to a TeO_2 melt. Matching cooling and heating rates of up to 30,000 K s^{-1} were then used to determine the respective fictive temperatures, corresponding to viscosity values as low as $10^{5.3}$ Pa s. The interdependence between calorimetric data and viscosity was verified and fine-tuned for this compositional system utilizing sodium tellurite glasses. The fragility index of pure TeO_2 (m = 64) is by far the highest reported for a single-component oxide melt.

Keywords: Glass; TeO_2; Sodium tellurite; FDSC; Fragility; Viscosity

4.1 Introduction

The glass forming ability [1] of a melt is a key feature that defines not only its large-scale manufacturing potential, but also the ease by which its physical properties can be experimentally measured. As a prime example, viscosity determinations are particularly challenging for melts that tend to readily demix or crystallise above their glass transition temperature (T_g), since these processes are known to strongly affect the overall rheology of the resulting heterogeneous systems [3–8]. Calorimetry has indeed been suggested as a less demanding alternative to indirectly retrieve the viscosity of a melt near its T_g, based on the fundamental relation [31, 32]:

$$\lg \eta(T_{onset}, T_{peak}, T_{end}) = -\lg q_{c,h} + \lg K_{onset,peak,end} \tag{4.1}$$

where η stands for the viscosity of the melt. T_{onset}, T_{peak} and T_{end} represent well-defined points in the calorimetric glass transition region [5, 89], whereas $q_{c,h}$ defines the matching cooling and heating rates used during the measurements; finally, lg K_{onset}, lg K_{peak} and lg K_{end} are compositionally independent factors, respectively calibrated to the average values (with margins of error) of 11.2 ± 0.1, 9.8 ± 0.2 and 9.2 ± 0.2 [5]. As shown recently, this approach allows an accurate characterization of the near-T_g rheology of readily crystallizing silicate melts [5].

It is clear that a broad-range viscosity determination using **Eq. (4.1)** can be crucially limited by the maximum heating and cooling rates achievable using the available analytical

instrumentation. Yet, the ground-breaking development of fast scanning calorimetry has recently enabled to apply matching heating and cooling rates up to 30,000 K s^{-1}, yielding viscosity values η as low as 10^6 Pa s [52, 89]. In this work, the applicability of **Eq. (4.1)** is extended to tellurite melts, providing a valid experimental scheme to precisely determine the viscosity of poor and conditional glass formers. Eventually, this work presents the first full viscosity curve for a pure TeO_2 melt, which can otherwise only be turned into a glass by ultrafast quenching of very small samples or by the addition of chemical dopants/pollutants [90–95].

4.2 Experimental

4.2.1 Glass preparation and characterization

High-purity TeO_2 powder (Alfa Aesar, 99.99%) was melted in situ on the measuring sensor of a flash differential scanning calorimeter (see Section 2.4). It was heated up to 47 K above its melting point (T_m = 1005.8 K) and subsequently quenched at high rate. Complete melting occurred within a few milliseconds; material contamination can be considered negligeable, since the chip surface displayed no sign of cracking or chemical reactions (**Fig. 4.1**). The pure TeO_2 glass is hereinafter referred to as 100Te.

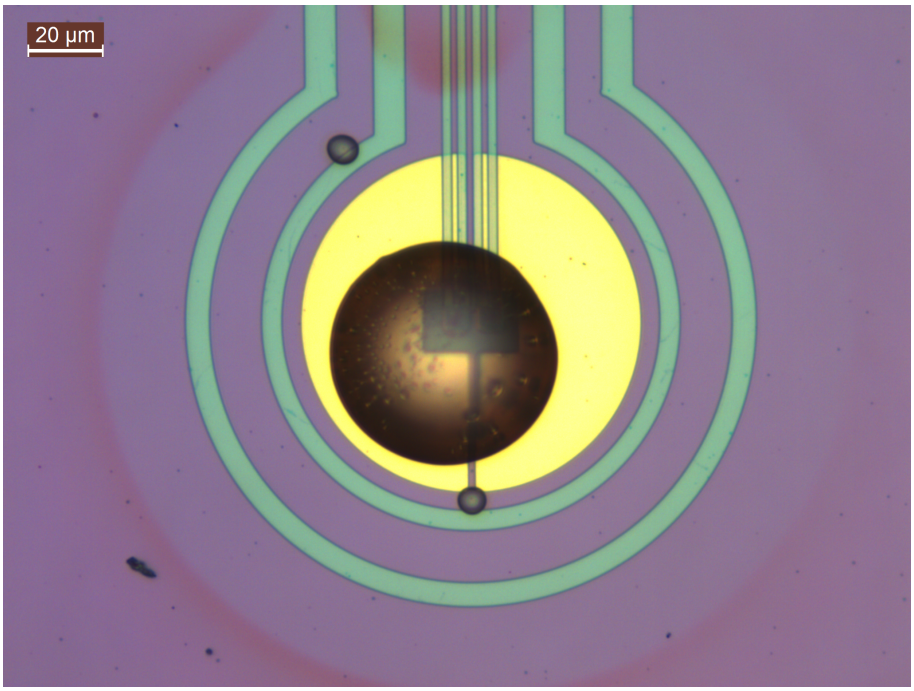

Figure 4.1: Pure TeO_2 glass (100Te), quenched with a cooling rate of 1,000 K s^{-1} on the measuring area (golden circle) of a UFH 1 sensor of the Flash DSC 2+.

The above-mentioned TeO_2 raw material and Na_2CO_3 (Sigma-Aldrich, ACS reagent primary standard, anhydrous, 99.95 – 100.05% dry basis) were mixed for the production

of two distinct glass samples (ca. 5 g each). The two mixtures were melted in a muffle furnace at 973 K in Pt-crucibles, poured on a steel plate and then cooled down in a second furnace from 423 K to room temperature with 5 K h^{-1}. Chemical analyses of the two samples performed by X-ray fluorescence (S4 Pioneer;Bruker AXS, Karlsruhe, Germany) yielded in mol%: 80(1) TeO_2 · 20(1) Na_2O (hereinafter sample 80Te20Na) and 86(1) TeO_2 · 14(1) Na_2O (hereinafter sample 86Te14Na). Numbers in parentheses give uncertainty of the last digit. These compositions were selected because they are situated in a compositional range exhibiting relatively high glass stability [96].

4.2.2 Raman spectroscopy

A confocal Raman microscope (Senterra, Bruker Optik GmbH, Ettlingen, Germany), equipped with a 20x and a 50x objective and a 532 nm diode laser was used to control the glassy state of the specimens; the laser power was set at 10 mW. The spectra were recorded at room temperature in the range 50–1550 cm^{-1}, with a resolution of 4 cm^{-1}. In the case of 100Te, the very small size of the sample employed for the FDSC measurements (**Fig. 4.1**) and the strong fluorescence stemming from the measuring chip noticeably reduced the quality of the obtained spectrum. The appearance of a "ripple" artefact stemming from the edge filter of the spectroscope did not compromise the evaluation of the spectra.

4.2.3 Differential scanning calorimetry (DSC)

A conventional DSC (DSC 404 F3 Pegasus; Netzsch, Selb, Germany) was used for the measurements. The temperature and sensitivity calibration of the instrument was performed prior to the experiments using melting temperatures and enthalpy of fusion of reference materials (pure metallic In, Sn, Bi, Zn, Al, Ag and Au) up to 1337 K. Several fictive temperatures T_f of the glasses 80Te20Na and 86Te14Na were then determined according to the procedure already defined elsewhere [5, 89]: the samples (ca. 16 mg) were cooled to room temperature with rates q_c of 1, 5, 10, 15, or 20 K min^{-1} from ca. 20 K above the glass transition peak (to ensure "equilibration" in the undercooled liquid state) and then measured with a matching heating rate q_h. Before this, a baseline correction measurement was performed with two empty lidded PtRh20 crucibles (height ≈ 2.6 mm, diameter ≈ 6.5 mm) under nitrogen atmosphere (100 ml min^{-1}), using the above-described temperature program. This procedure could not be used for the 100Te melt, due to its strong tendency to crystallise at these comparatively low cooling/heating rates [93].

The so-called onset of the calorimetric glass transition (T_{onset}) was determined from the heat flow curves during the heating segments; it corresponded to the intercept between the tangent to the glass signal (i.e. before the glass transition region) and the tangent to the signal inflection point during the glass transition. This point is equal to T_f [17, 63, 94]

determined by the enthalpy matching method [16, 64, 65]. As for T_{peak} and T_{end} [5, 89], they were not evaluated due to the likely appearance of artefacts caused by a crystallisation of the samples.

4.2.4 Flash Differential Scanning Calorimetry (FDSC)

The above-described glasses (80Te20Na, 86Te14Na and 100Te) were characterized by high-rate calorimetry FDSC (Flash DSC 2+; Mettler Toledo, Greifensee, Switzerland) using UFH 1 chips. The characteristic glass transition temperatures T_{onset} and T_{peak} were determined by the same method described in Section 2.3, with $q_{c,h}$ up to 30,000 K s^{-1}. The applicability of this procedure to silicate and fluorophosphates glasses has been demonstrated in previous studies by Al-Mukadam et al. [89] and Schawe and Hess [52].

The sample support temperature was set to 293.2 K; a constant flow of Argon (Ar 5.0, 40 ml min^{-1}) served as purge gas for all experiments. Two pre-measurement steps, i.e. conditioning and thermocouple correction, were performed without sample according to the producers' guidelines, reducing the temperature inaccuracy to $\leq$ 2 K. For the actual measurements, a single grain of material was placed in the centre of the chip (golden circular area in **Fig. 4.1**). It was heated up once over the liquidus temperature T_{Liq} to achieve good thermal contact between glass and sensor surface. The mass of the samples was estimated in the range 0.2 – 0.4 μg, comparing the intensity of the glass transition step obtained by FDSC and conventional DSC [52, 66]. After measuring the glass with the procedure used for the conventional DSC (adjusted to the high rates of FDSC), indium was placed on the reference side of the chip and the same program was run another time. The difference between the measured T_m for indium and its reference value (T_m = 429.8 K) was used for the correction of T_{onset} and T_{peak} obtained using a given q_h. A plot of these values against $q_{c,h}$ in logarithmic scale enabled to select trust-worthy data points for the viscosity determination, based on their overall adherence to a linear trend.

4.2.5 Viscometry

Viscosity measurements ranging from $\sim 10^{12.2}$ to $\sim 10^{9.6}$ Pa s were performed using a micro-penetration setup on a vertical dilatometer (Bähr VIS 404, Hüllhorst, Germany). Samples were prepared as doubly polished glass blocks (thickness $\approx$ 3 mm) that were placed under a SiO_2 glass rod, pushing a sapphire sphere (r = 0.75 mm) into the glass block with a force of 3.92 N (400 g load). An S-type thermocouple (Pt-PtRh) placed at $\sim$2 mm distance from the sample monitored the temperature. As shown by Behrens et al. [67], the temperature error corresponds to $\pm$ 5 K if one considers the distance to the sample and the accuracy of the thermocouple. The indentation depth of the sapphire sphere into the glass block was measured as a function of time and temperature using a linear variable

displacement transducer; viscosity was determined according to Douglas et al. [69].

4.3 Results and discussion

4.3.1 Raman spectroscopy

The Raman spectra obtained from the samples are displayed in **Fig. 4.2**. They were compared and found to satisfactorily match the literature references for amorphous TeO_2 [93] and for sodium tellurite glasses [97, 98]: characteristic features of the amorphous materials included the broad bands at ∼450, ∼665 and ∼720 cm^{-1}. No sign of partial crystallisation or phase separation could be detected.

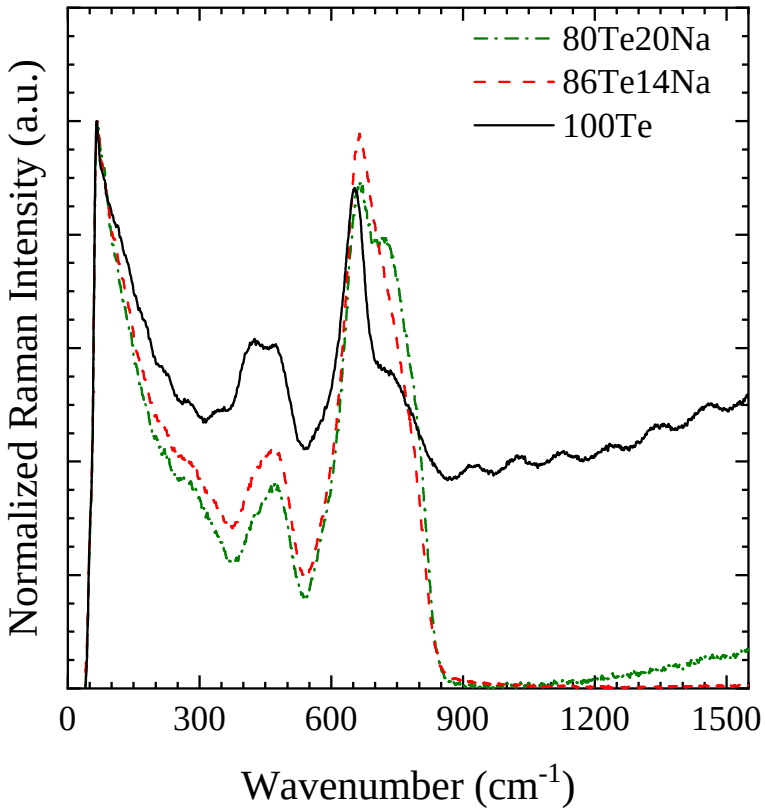

Figure 4.2: Raman spectra obtained from the as-cast 80Te20Na and 86Te14Na samples and from the 100Te glass, quenched on the measuring chip of the FDSC as in **Fig. 4.1** (mind the "ripple" artefact stemming from the edge filter of the Raman spectroscope).

4.3.2 Viscometry

The viscosity data obtained by micropenetration measurements of samples 80Te20Na and 86Te14Na are listed in **Tab. 4.1** and plotted in **Fig. 4.3**. They generally exhibit a very good agreement with the available literature sources [99, 100]. A linear interpolation

of the data enabled the determination of lg K_{onset} and lg K_{peak}, as described in the next section. The viscometric fragility index [101] was determined as 72(1) for 80Te20Na and 70(1) for 86Te14Na.

Table 4.1: Results of micropenetration viscometry performed on samples 80Te20Na and 86Te14Na. The error is estimated as ± 0.1 lg units.

80Te20Na		86Te14Na	
T (K)	lg η (Pa s)	T (K)	lg η (Pa s)
521.0	12.2	533.7	12.2
525.8	11.5	538.7	11.6
530.6	10.8	543.5	10.9
535.5	10.2	548.4	10.3
540.4	9.6	553.3	9.7

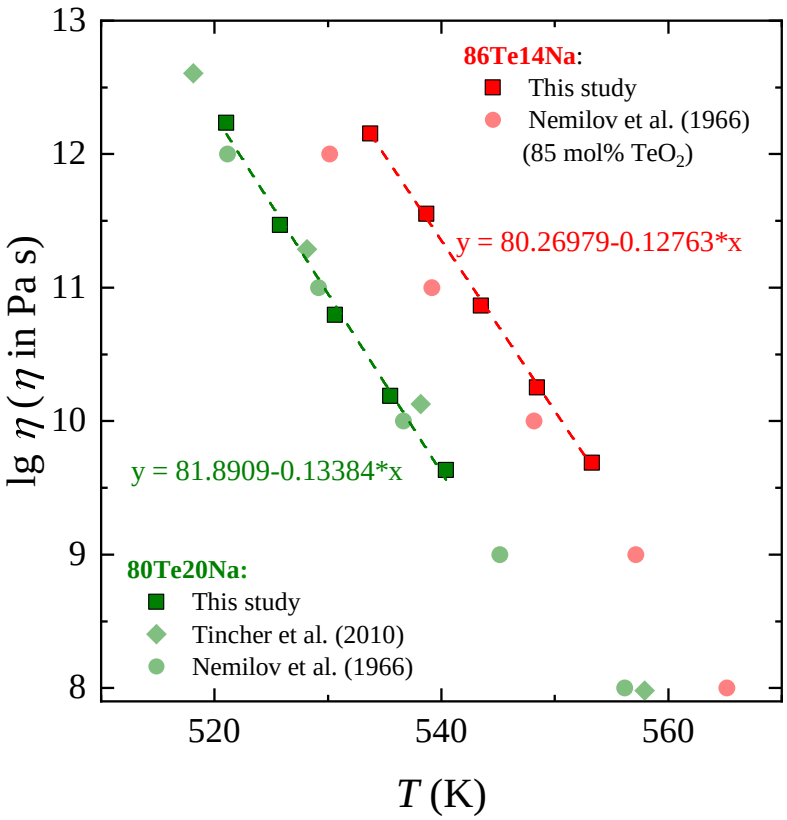

Figure 4.3: Viscosity data measured by micropenetration on samples 80Te20Na and 86Te14Na, in comparison with selected literature references [99, 100]. Linear fits through micropenetration points are provided with the corresponding equation.

4.3.3 Calorimetry

The values of T_{onset} and T_{peak} were obtained by conventional DSC and FDSC with cooling/heating rates $q_{c,h}$ ranging from 0.02 K s^{-1} (or 1 K min^{-1}) to 30,000 K s^{-1} (or 1,800,000 K min^{-1}). After trimming of the FDSC data (see Section 2.4), satisfactory linear trends of T_{onset} and T_{peak} could be obtained for the three examined samples against the employed $q_{c,h}$ in logarithmic scale (**Fig. 4.4A**). All accepted T_{onset} and T_{peak} are listed in **Tab. 4.2**.

Table 4.2: Characteristic glass transition temperatures T_{onset} and T_{peak} of glasses 80Te20Na, 86Te14Na and 100Te as determined by conventional DSC and FDSC, with the associated viscosities calculated using **Eq. (4.1)**. T_{onset} and T_{peak} were determined with a maximum uncertainty of ± 2 K for conventional DSC and ± 5 K for FDSC.

$q_{c,h}$ (K s^{-1})	T_{onset} (K)			lg η (Pa s)	T_{peak} (K)			lg η (Pa s)
	80Te20Na	86Te14Na	100Te	at T_{onset}	80Te20Na	86Te14Na	100Te	at T_{peak}
0.02	517.4	530.4		12.6				11.5
0.08	523.2	535.3		11.9				10.8
0.17	525.6	538.4		11.6				10.5
0.25	527.1	540.2		11.4				10.3
0.33	528.5	541.6		11.3				10.2
10				9.8		563.5	596.0	8.7
25			585.1	9.4				8.3
50			589.8	9.1		567.9	603.5	8.1
100		560.1	592.2	8.8	558.7	571.6	607.8	7.7
250	551.2	565.8	596.7	8.4	565.6		611.2	7.3
500	554.2	568.0	601.0	8.1	569.4		615.4	7.0
750	556.9	570.0	603.6	7.9	572.9		619.2	6.9
1,000	558.1	571.7	605.2	7.8	574.4	588.0	620.3	6.7
2,500	564.5	575.2	612.4	7.4	580.6	592.3	627.7	6.3
5,000	569.5	578.9	616.5	7.1	585.0	596.4	632.5	6.0
7,500	573.5	580.8	619.1	6.9		597.8	636.8	5.9
10,000	574.9	582.0	620.3	6.8		600.7	639.9	5.7
15,000	578.1		624.8	6.6		603.6		5.6
20,000	580.1			6.5		605.5		5.4
30,000	583.2		630.9	6.3		608.1		5.3

Using the linear interpolations shown in **Fig. 4.3** for samples 80Te20Na and 86Te14Na, it was possible to determine the common best-fitting lg K_{onset} = 10.77 ± 0.06, which was used to translate all calorimetric T_{onset} values into viscosity according to **Eq. (4.2)**. Subsequently, a common lg K_{peak} = 9.73 ± 0.10 was obtained from the FDSC data by adjusting the T_{peak} values to the T_{onset} trend. It is important to point out that this K_{peak} agreed closely with the values previously computed for other melts [5, 89], while the obtained lg K_{onset} differs noticeably from the average value of 11.2 ± 0.1 reported in the past. This might be related to the highly fragile nature of these glasses, as suggested before [102]. The resulting viscosity points have been summarized in **Fig. 4.4B**, together with those determined by direct viscometry.

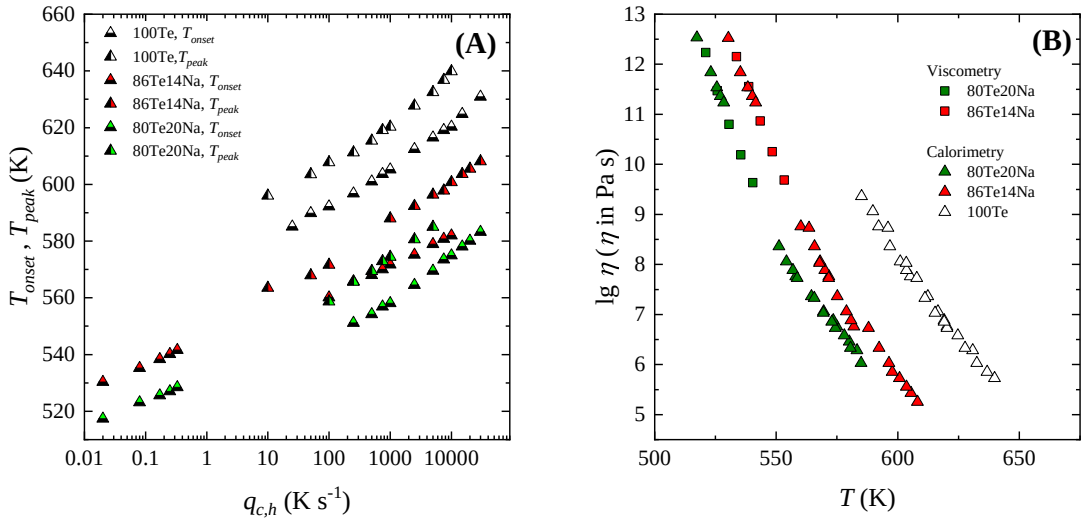

Figure 4.4: A) Plot of T_{onset} and T_{peak} values obtained from DSC and FDSC, against the respective cooling/heating rates $q_{c,h}$; B) viscosity data obtained by direct micropenetration viscometry and calorimetry for samples 80Te20Na, 86Te14Na and 100Te.

The experimental data of samples 100Te and 80Te20Na was combined with the values determined at high temperature (rotating crucible viscometry) by Tokunaga et al. [103] for the same compositions; full viscosity curves were subsequently fitted using the MYEGA equation (**Eq. (4.2)**) [29, 30]:

$$\lg \eta = \lg \eta_\infty + (12 - \lg \eta_\infty)\frac{T_g}{T} exp\left[\left(\frac{m}{12-\lg\ \eta_\infty} - 1\right)\left(\frac{T_g}{T} - 1\right)\right] \quad (4.2)$$

The obtained MYEGA parameters lg η_∞, m and T_g are reported in **Tab. 4.3**, while the respective curves are plotted in **Fig. 4.5** with the data used for the computation.

Table 4.3: Fit parameters and estimated standard errors obtained by applying the MYEGA [29, 30] equation (**Eq. 4.2**) to the viscosity data of the glasses 80Te20Na and 100Te, reported in **Fig. 4.5**.

Sample	lg η_∞ (Pa s)	m	T_g (K)
80Te20Na	-3.08 $\pm$ 0.12	71.5 $\pm$ 1.1	521.8 $\pm$ 0.4
100Te	-2.97 $\pm$ 0.10	64.4 $\pm$ 1.2	559.5 $\pm$ 0.8

The results of the fit provide the first experimentally determined viscosity curve for pure TeO_2, whose poor glass forming ability and strong tendency to crystallise generally prevent reliable measurements in the undercooled state. The resulting fragility index m of 64(1) is by far the highest reported for a single-component oxide glass, since all others (SiO_2, GeO_2, P_2O_5, As_2O_3) have yielded strong Arrhenius behaviors and m values between 17 and 20, with the intermediate exception of B_2O_3 (m = $\sim$45). This must be related to the extraordinarily modest resistance against viscous flow that is offered by the structural

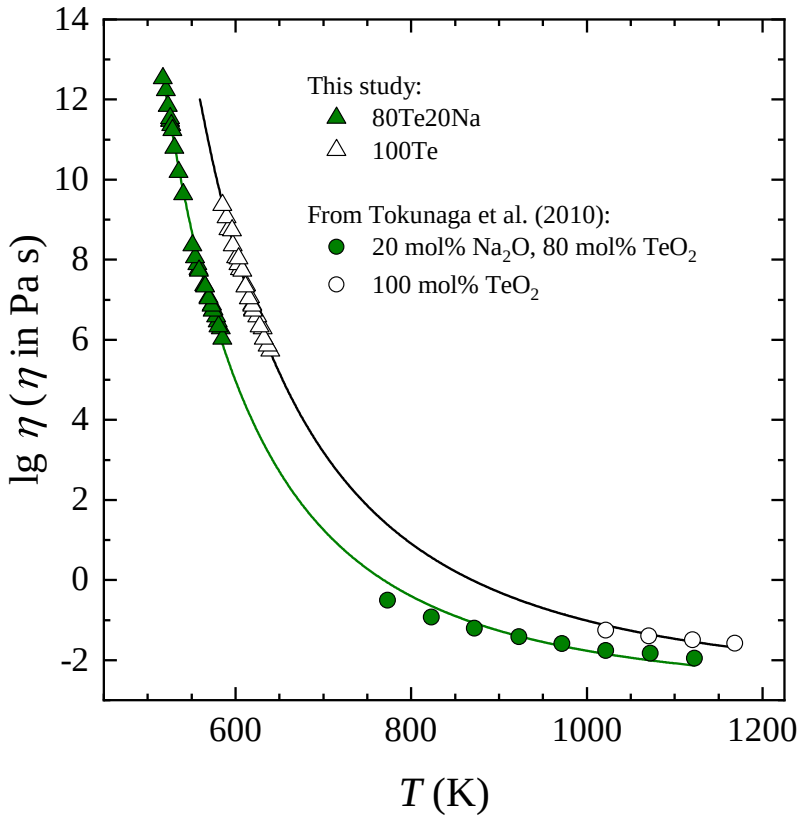

Figure 4.5: MYEGA fits based on calculated and measured viscosity data from this study and literature [103].

units composing the TeO_2 melt. Indeed, recent studies suggest a substantial short-range disorder around the Te atom, whose comparably weak interaction with oxygen (mind also the presence of a lone electron pair) expresses in the lack of a clear cutoff between bonding and non-bonding partners, with an average coordination number close to 4 [94, 95, 104–106]. A plot of the viscosity versus the reduced temperature T_g/T (Angell-plot) emphasizes the exceptional role of the fragile TeO_2 melt among the single glass-forming oxides (**Fig. 4.6**).

The MYEGA fit also yielded a T_g value of 559.5 $\pm$ 0.8 K, noticeably lower than the scattered determinations reported in the literature [92, 93, 112–115], which are however likely to be affected by sample contamination and/or unsufficient relaxation of the superquenched melt (**Fig. 4.7**). On the other hand, the values obtained within this work for η = 10^{12} Pa s in the TeO_2–Na_2O system closely agree with those available in the literature [100]. In fact, investigations in borate and silicate systems have frequently highlighted non-linear trends for T_g as the first mol% of modifier are added to the glass former endmember [116–118].

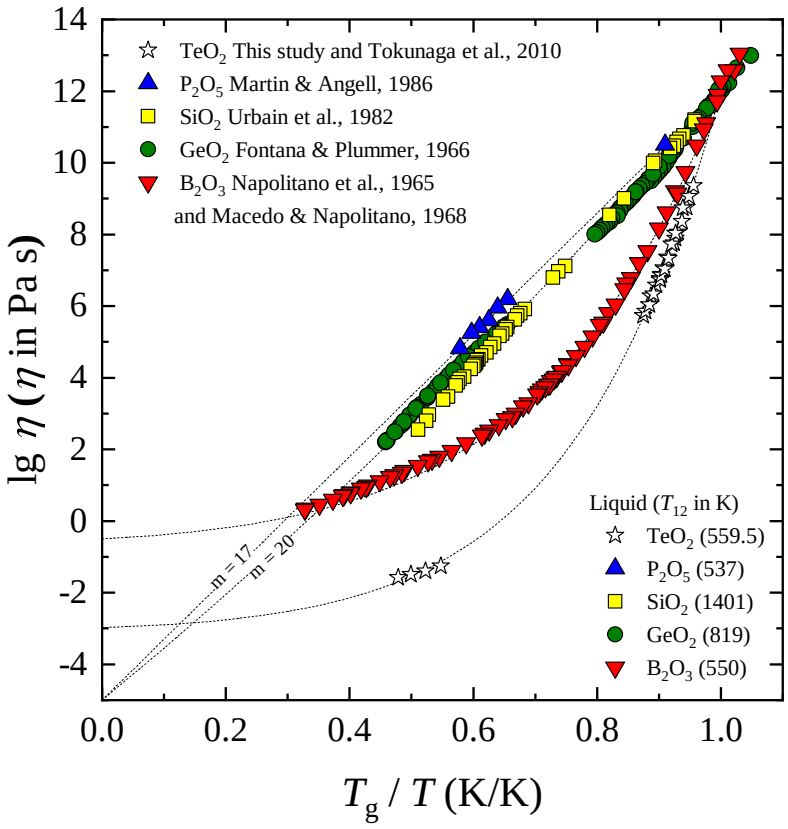

Figure 4.6: T_g/T-scaled representation of the temperature dependence of the viscosity (Angell-plot) of single oxide glass-forming melts ($T_g = T_{12} = T(\eta = 10^{12}$ Pa s)). Data: Martin & Angell (1986, P_2O_5) [107], Urbain et al. (1982, SiO_2) [108], Fontana & Plummer (1966, GeO_2) [109], Napolitano et al. (1965, B_2O_3) [110] and Macedo & Napolitano (1968, B_2O_3) [111].

4.4 Conclusions

With the aim of determining the full viscosity curve of pure TeO_2 melt, a combined experimental approach based on calorimetry and viscometry has been successfully tested in tellurite compositions. Fragility index m and glass transition T_g values obtained by this method for a pure TeO_2 melt are provided and discussed.

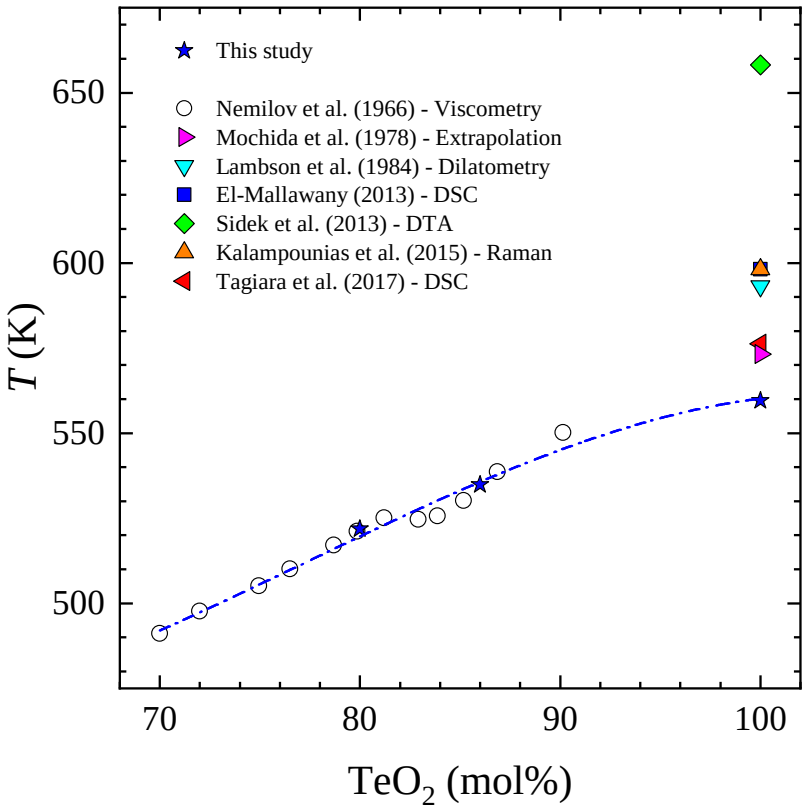

Figure 4.7: Values of T_g obtained within this work, plotted as a function of TeO_2 content in the Na_2O–TeO_2 compositional system, in comparison with various literature sources [92, 93, 100, 112–115]. The line is obtained as a polynomial interpolation of the data from this work and from Nemilov et al. (1966) [100].

5 Viscosity of metallic glass-forming liquids based on Zr by fast-scanning calorimetry

R. Al-Mukadam[a], I.K. Götz[b], M. Stolpe[c], J. Deubener[a]

[a]Clausthal University of Technology, Institute of Non-Metallic Materials, Zehntnerstraße 2a, 38678 Clausthal-Zellerfeld, Germany
[b]Uppsala University, Department of Physics and Astronomy, Materials Physics, Box 516, 751 20 Uppsala, Sweden
[c]Heraeus AMLOY Technologies GmbH, Heraeusstraße 12-14, 63450 Hanau, Germany

Abstract

Fast-scanning calorimetry was applied to retrieve the viscosity of supercooled liquids of the Zr–based bulk metallic glasses (BMGs) Vitreloy 105 and AMZ4 for temperatures from standard glass transition down to $\sim 0.78 T_g/T$. Characteristic temperatures of the glass transition were translated into viscosity values by means of composition-independent shift factors based on the equivalency between structural relaxation and viscous flow. The extended MYEGA model with a fragile term dominant at high-temperatures and a strong term dominant at low-temperatures describes the entire viscous range. The analysis revealed that Vitreloy 105 and AMZ4 are strong liquids for lg $\eta \geq$ 4.9-5.5. In turn, the fragile-to-strong crossover is centred on $0.69 T_g/T$ for Vitreloy 105 and on $0.66 T_g/T$ for AMZ4. The extent of the fragile-to-strong transition was found to be larger for Vitreloy 105 than for AMZ4, while their values agreed well with the inverse relation between transition factor and kinetic fragility of the strong regime established for BMG-forming liquids.

Keywords: BMG; Vitreloy 105; AMZ4; viscosity; fragility; fragile-to-strong crossover; fast-scanning calorimetry

5.1 Introduction

The viscosity of metallic glasses is of technological interest as an important feature for the applicable production and hot- forming processes [9]. Additive manufacturing, which has emerged as a possibility to attain high quenching rates locally and build up bulk pieces layer-by-layer, is no exception. Most metallic glass compositions are characterised by a rather low glass forming ability and require high cooling rates [9]. The experimental determination of the viscosity between the glass transition temperature (T_g) and the melting temperature is often hindered by crystallisation, which leads to a data gap between high- and low-temperature viscosity measurements.

A range of metallic glass formers have been identified to exhibit unusual viscosity behaviour that hints toward a fragile-to-strong (F–S) transition. Amongst them are Zr–based bulk metallic glasses, such as Vitreloy 106, 106a, 105, and 101 [47], Vitreloy 1 [119], and AMZ4 [48]. For these systems, the high and low-temperature fragilities do not match, which has emerged as a common feature for bulk metallic glass (BMG) formers [120]. Hereby, the fragility characterizes how rapidly the viscosity of a BMG liquid increases as it is cooled toward T_g. Frequently used descriptions of the viscosity behaviour, amongst them the Vogel-Fulcher-Tammann-Hesse (VFTH) [36–38] and Mauro-Yue-Ellison-Gupta-Allan (MYEGA) [29, 30] fits, therefore fail to describe these systems. Direct observations of F–S transitions have been hindered by the experimental difficulties in accessing the viscosity as in between T_g and liquidus, where the crystallisation rate reaches its maximum, the timescales are often too short for classical viscometric techniques. An exception is Vitreloy 1 ($Zr_{41.2}Ti_{13.8}Cu_{12.5}Ni_{10.0}Be_{22.5}$), for which Way et al. [119] could observe a viscosity crossover with a hysteresis path upon heating and cooling. Vitreloy 1 is an archetypal strong system and the crossover occurs above the melting point upon heating, which makes it suitable for study with conventional calorimetry [121]. Other Zr–based systems without Beryllium show intermediate fragilities [120], which is more typical for metallic glasses in general [9]. For these Vitreloy systems (106, 106a, 105, and 101), a low temperature strong and high temperature fragile behaviour was observed and the transition therefore postulated in the intermediate inaccessible undercooled liquid [47].

The origin of the F–S crossovers has been attributed to liquid-liquid transitions. Since the first observations in 1979 [122, 123], transitions from one initial to another amorphous state have been found in a wide range of systems [124]. Linking the dynamic crossover to changes in thermodynamic properties and structure has thus been explored to understand this phenomenon [120]. For Zr–based compositions, the structural changes have been explored for Vitreloy 1 [121] and Vitreloy 106a [125]. Wei et al. [121] found a peak in heat capacity coinciding with the drop in viscosity as well as changes in the temperature-dependence of the structure factor for Vitreloy 1. Stolpe et al. [125] examined the structure of $Zr_{58.5}Cu_{15.6}Ni_{12.8}Al_{10.3}Nb_{2.8}$ (Vitreloy 106a) bulk metallic glass forming liquid from above the liquidus down to the glass transition and connected the results hinting at a phase transition in the deeply undercooled liquid state at around $1.2T_g$ to previous viscosity measurements. In addition to this, numerous other studies report evidences for transitions in the liquid or supercooled liquid state of other metallic glass forming alloys, that are considered as origin of experimentally observed differences in their low and high temperature fragilities [126–131]. It is concluded from these experiments that the dynamic crossovers are linked to order-disorder transitions in the liquid state, associated with structural changes in the short- and medium-range order originating from the formation of locally favoured structures, i.e. energetically preferred cluster structures

that are characterized by a higher symmetry and lifetime compared to the average liquid structure [132, 133].

Experimental assessments of this phenomenon are complicated by the fact that the supposed structural transitions often take place in the deeply supercooled liquid state of these alloys, i.e. in vicinity of the maximum crystallisation rates, so that very fast measurements are needed to identify their thermophysical, dynamic or structural signatures. Conventional rheological measurements, e.g. Couette-viscometry or 3-point beam bending relaxation studies, or measurements of the structural relaxation times and diffusivity by scattering methods such as quasi-elastic neutron scattering normally require observation times of several seconds or minutes up to hours, while the times for nucleation and crystal growth are usually much shorter. As a consequence, the supercooled melt crystallises, preventing an assessment of the liquid dynamics over the full temperature range from above the liquidus down to the glass transition temperature. This leaves an empty region in the intermediate viscosity range of the Angell-plot (a T_g-scaled Arrhenius plot of the dynamics), sometimes referred to as "no man's land" [134].

Due to the aforementioned difficulties, the collection of experimental data in the intermediate viscosity range has been limited. Most bulk metallic glass forming compositions do not allow for enough time to perform conventional viscosity measurements throughout the supercooled liquid region due to rapid crystallisation [120]. This experimental limitation can be circumvented by employing fast-scanning calorimetry (FDSC), as demonstrated by Al-Mukadam et al. for oxide melts [89, 135]. With heating and cooling rates up to 40,000 K s^{-1} this method yields access to the deeply undercooled liquid state making it possible to broaden the accessible temperature range.

Here we apply FDSC to extract the viscosity data in the previously unexploited temperature range corresponding to the deeply undercooled liquid state above the glass transition temperature for the Vitreloy 105 ($Zr_{52.5}Cu_{17.9}Ni_{14.6}Al_{10}Ti_5$) and AMZ4 ($Zr_{59.3}Cu_{28.8}Al_{10.4}Nb_{1.5}$) bulk metallic glass forming alloys. Our results show that the low temperature fragility of these alloys is maintained down to relative inverse temperatures of about $0.78T_g/T$, suggesting dynamic crossovers to occur at around 0.6-0.7T_g/T in good agreement to previous studies on Zr–based bulk metallic glass forming liquids.

5.2 Viscosity-temperature relationships

Different equations with three constants have been developed to account for the deviation from an Arrhenian temperature dependence of the viscosity. The viscosity of bulk metallic glass formers is traditionally expressed by the empirical VFTH model [36–38] in the form [101]:

$$\eta = \eta_\infty exp\left(\frac{D^* T_0}{T - T_0}\right) \tag{5.1}$$

with the adjustable parameters η_∞, D^* and T_0. The prefactor, η_∞, in **Eq.(5.1)** is frequently said to be equal to hN_a/V_m where *h* and N_a are the Planck's and Avogadro's constants, respectively, and V_m the molar volume. For the studied BMG, η_∞ is close to 4×10^{-5} Pa s and this value was kept constant by previous researchers if low-temperature viscosity data (close to the glass transition) were evaluated [47, 48, 136]. In order to reflect the stability of the short- and medium-range order of glass-forming liquids against their temperature-induced structural degradation, a glass transition temperature-scaled Arrhenius diagram (Angell plot [137, 138]) of the liquid viscosities has been established from which one defines the kinetic fragility (steepness index) *m* as [101]:

$$m = \frac{d \lg \eta}{d\,(T_g/T)}|_{(T=T_g)} \tag{5.2}$$

with the glass transition temperature T_g (T_g is defined as the isokom temperature $\eta(T_g)$ = 10^{12} Pa s; isokoms are temperatures of constant viscosity). The temperature-dependant viscosity can also be described by the MYEGA model [29, 30]:

$$\lg \eta = \lg \eta_\infty + \frac{B}{T} exp\left(\frac{C}{T}\right) \tag{5.3}$$

with the adjustable parameters η_∞ (= viscosity in the high temperature limit) and *B*, *C* (= constants that are related to the onset of rigidity in the liquid network) [30]. The MYEGA equation is used in the following analysis, as the accurateness of this model is superior in predicting low-temperature isokoms of glass-forming liquids using the same number of parameters as VFTH [30]. Thus, the combination of **Eqs. (5.2)** and **(5.3)** receives the kinetic fragility in the form [30]:

$$m = \frac{B}{T_g}\left(1 + \frac{C}{T_g}\right) exp\left(\frac{C}{T_g}\right) \tag{5.4}$$

Further, as a F–S crossover has been perceived upon supercooling of the here studied liquid alloys toward the glass transition [47, 48], an approach based on a single kinetic fragility of the liquid fails to describe the viscosity temperature dependence correctly. In order to capture the scaling of dynamics across both the fragile and strong regimes the generalized MYEGA expression has been introduced [49, 50]:

$$\lg \eta = \lg \eta_\infty + \frac{1}{T\left(W_{fragile} exp\left(-\frac{C_{fragile}}{T}\right) + W_{strong} exp\left(-\frac{C_{strong}}{T}\right)\right)} \tag{5.5}$$

with the adjustable parameters of the second term, $W_{fragile}$, W_{strong} (= normalized weighting factors) $C_{fragile}$, C_{strong} (= rigidity constants), which account for the fragile and strong liquid behaviour at high and low temperatures, respectively [49].

Alternatively, the change of the fictive temperature for cooling or heating with a

constant rate of change of temperature through the glass transition range can be accessed by calorimetric methods [17, 32, 139]. In correspondence to **Eq. (5.3)** one has [49]:

$$\lg q_{c,h} = \lg q_{c,h\infty} - \frac{B}{T_f} exp\left(\frac{C}{T_f}\right) \tag{5.6}$$

with $q_{c,h}$ the absolute value of the cooling rate q_c or heating rate q_h and T_f the fictive temperature. In particular, the constraint $|q_c|$ = $|q_h|$ of **Eq. (5.6)** is mandatory to retrieve viscosity at fictive temperatures free of artefacts stemming from the thermal history of the sample [74]. Further, as shown by Scherer [31] and Yue et al. [32], one can superimpose **Eqs. (5.3)** on **(5.6)** to determine a so-called parallel shift factor lg *K*. Thus, lg *K* allows to retrieve η without the need to conduct viscosity measurements. This is of crucial importance since the proneness to crystallise of the here studied metallic glasses prevent determination of liquid viscosity by rheological methods within a wide temperature range above T_g. The shift factor concept has been further developed to include three well-defined points (T_{onset}, T_{peak} and T_{end}) within the calorimetric glass transition region [5]. The corresponding shift factors lg K_{onset}, lg K_{peak} and lg K_{end} are related to the viscosity of the liquid at these temperatures by [5]:

$$\lg K_{onset}, \lg K_{peak}, \lg K_{end} = \lg \eta(T_{onset}, T_{peak}, T_{end}) + \lg q_{c,h} \tag{5.7}$$

It should be noted that T_{onset} is equal to the fictive temperature [17, 32, 63] determined by the enthalpy matching method [16, 64, 65]. lg K_{onset}, lg K_{peak} and lg K_{end} represent compositionally independent factors expressing the equivalency between structural relaxation and viscous flow, respectively calibrated to the average values of 11.2 ± 0.1, 9.8 ± 0.2 and 9.2 ± 0.2 [5]. **Fig. 5.1** shows the resulting superimposition for DGG I standard glass used for this prior calibration (DGG I = soda-lime-silica glass of the German Society of Glass Technology with viscosity data points certified by the National Metrology Institute of Germany (PTB) [43]). For this glass, viscosity is accessible over the entire range of temperatures (DGG I glass hardly crystallises), so that no gap between high and low viscosity data is present. Thus, fictive temperatures by DSC and FDSC can be related directly to viscosity even without the use of interpolating viscosity-temperature models.

5.3 Experimental

5.3.1 Bulk metallic glasses

Amorphous powders of two commercial bulk metallic glasses of nominal composition (at%) $Zr_{59.3}Cu_{28.8}Al_{10.4}Nb_{1.5}$ (AMZ4) and $Zr_{52.5}Cu_{17.9}Ni_{14.6}Al_{10}Ti_5$ (Vitreloy 105) were studied. The AMZ4 composition was developed based on the Vitreloy BMGs with the

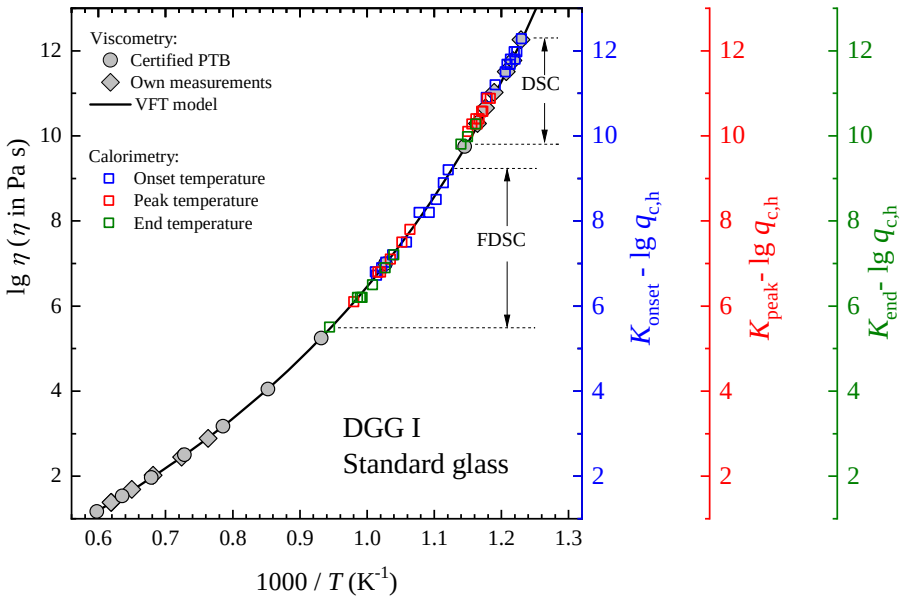

Figure 5.1: Superimposing viscosity and fictive temperature (T_{onset}, T_{peak} and T_{end}) of the glass transition range determined by DSC and FDSC for DGG I standard glass used for calibration. The figure is intended to verify that parallel shift factors can be used to determine viscosity down to $\sim 10^{5.5}$ Pa s from fictive temperatures using **Eq. (5.7)**. Viscosity data were collected from own measurements [89] and points certified by PTB for DGG I glass [43]. T_{onset}, T_{peak} and T_{end} by DSC were taken from Ref. [5], while T_{onset}, T_{peak} by FDSC were from Ref. [89]. T_{end} was retrieved from the FDSC measurements of this previous study. Superimposition was achieved using **Eq. (5.7)** with lg K values 11.2, 9.8 and 9.2 for onset, peak and end, respectively.

target to reduce alloying effort and cost while retaining a suitable glass forming ability [140]. Both glasses were produced by gas atomization as fully amorphous powders by Heraeus Amloy Technologies GmbH. The AMZ4 powder is characterised by a size distribution with D_{10} = 13 μm, D_{50} at 25 μm and D_{90} at 44 μm, which is similar to that of the Vitreloy 105 with a particle size distribution of D_{10} = 14 μm, D_{50} at 26 μm and D_{90} at 43 μm. Using ICP-OES (inductively coupled plasma optical emission spectrometry) according to DIN EN ISO 4491–4 the oxygen content for the AMZ4 powders used for this study was determined to be approximately 0.2 wt%, while the oxygen content of the Vit105 powder was determined to be about 0.06 wt%.

5.3.2 DSC and FDSC

A conventional differential scanning calorimeter (DSC 404 F3 Pegasus; Netzsch, Selb, Germany) was used to determine the characteristic temperatures of the glass transition range for relatively low cooling/heating rates. The temperature and sensitivity calibration of the instrument was performed prior to the glass experiments using melting temperatures and enthalpy of fusion of reference materials (pure metallic In, Sn, Bi, Zn,

Al, Ag and Au) up to 1337 K. The samples of Vitreloy 105 ($\approx$ 40 mg) were cooled to room temperature with rates of 5, 10, 20, 30 or 40 K min^{-1} from 713 K (to ensure "equilibration" in the supercooled liquid state) and then measured with a matching heating rate during the second upscan $|q_{c1}| = |q_{h2}|$. For 713 K, the stress relaxation time as approximated by the Maxwell relation is $\tau \approx 100$ ms (shear modulus G $\approx$ 30 GPa [141], $\eta = 10^{9.5}$ Pa s, see below) and, thus, at least 30 times shorter than the shortest time interval (2 × 1/40 K min^{-1} = 3000 ms K^{-1}) to reach and leave this temperature. Before this, a baseline correction was performed with two Al_2O_3 inlayed empty lidded Pt80Rh20 crucibles (height $\approx$ 2.6 mm, diameter $\approx$ 6.5 mm) under dry nitrogen (5.0) atmosphere (100 ml min^{-1}), using the above-described temperature program. This procedure could not be used for the AMZ4 metallic glass, due to its strong tendency to crystallise at these comparatively low cooling/heating rates.

A flash differential scanning calorimeter (FDSC 2+, Mettler Toledo, Greifensee, Switzerland) equipped with a UFH 1 chip sensor was used to get insights into the glass transition at higher cooling and heating rates up to 40,000 K s^{-1}. The sample support temperature of the device was set to cryogenic 178.15 K to receive the highest possible cooling rate over a broad temperature range. Pre-and post-measurement routines including temperature calibration (In) of each chip were performed as described in [89, 135]. A constant gas flow of 80 ml min^{-1} argon (5.0) was used as purge gas for all measurements and the measuring cell lid was mounted to guarantee a low oxygen atmosphere after purging for 60 min. For the measurements, a single grain of approximately 0.5 μg of bulk metallic glass was placed in the centre of the measurement area. For Vitreloy 105, the time-temperature protocol comprises a first heating to 1173 K and to 1273 K for AMZ4 (ca. 50 K above liquidus temperature) and a holding for 10 ms to melt possible frozen-in crystal nuclei. Then the sample was rapidly quenched at 40,000 K s^{-1} and subsequently heated at the same rate while taking the endotherm of the glass transition range. 7 cycles with $|q_c| = |q_h|$ were directly following with cooling/heating rates in decreasing order ($q_{c,h}$ = 35,000, 30,000, 25,000, 20,000, 15,000, 10,000, 7,500 K s^{-1}). Subsequently, the sample was quenched from liquid state with 30,000 K s^{-1} to room temperature and heated up with 5,000 K s^{-1} to at least 850 K for Vitreloy 105 (800 K for AMZ4) and held for 10 ms. At 850 K the approximated stress relaxation time for Vitreloy 105 is 0.005 ms (= $10^{5.2}$ Pa s/30 GPa), while $\tau \approx 0.021$ ms (= $10^{5.8}$ Pa s / 30 GPa) can be calculated for AMZ4. Thus, Maxwell stress relaxation time for both glasses was considerably shorter (2000 times shorter for Vitreloy 105 and 471 times shorter for AMZ4) than the dwell time, which ensured equilibrium viscosity of the liquid between the cycles. Then 8 cycles with $|q_c| = |q_h|$ were directly following with $q_{c,h}$ = 5,000, 2,500, 1,000, 500, 250, 100, 50, 5,000 K s^{-1}. The last cycle (5,000 K s^{-1}) was performed to check for these possible crystallisation artefacts caused by prior cycling at lower cooling/heating rates. Each experiment was repeated for one more time using a different sample and chip.

For FDSC experiments, the onset of the calorimetric glass transition (T_{onset}), the maximum of the endothermic event (T_{peak}) and the end value (T_{end}) were determined. **Fig. 5.2** shows exemplarily how the characteristic temperatures were extracted from the FDSC signal of the glass transition range for $q_{c,h}$ = 5,000, 1,000, 500 and 100 K s^{-1}.

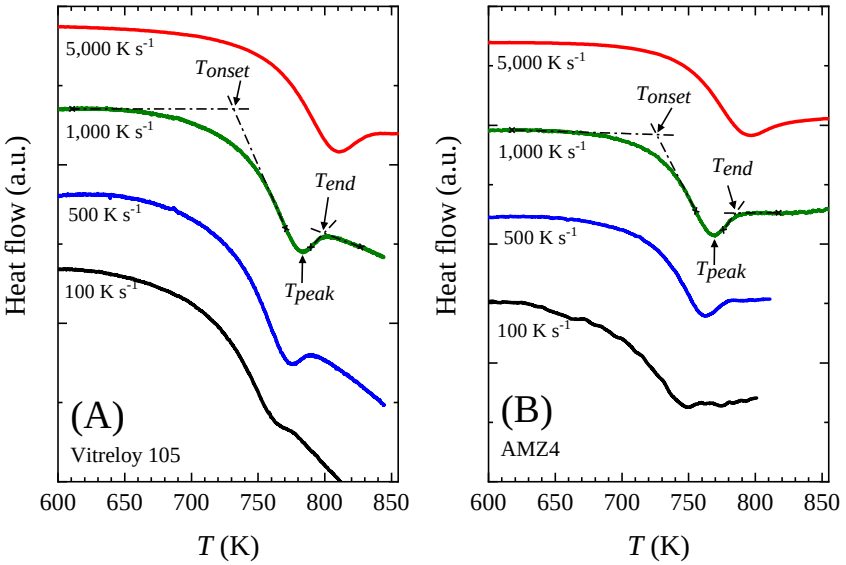

Figure 5.2: FDSC traces of the glass transition range of the analysed samples of Vitreloy 105 (A) and AMZ4 (B) as examples for $q_{c,h}$ = 5,000, 1,000, 500 and 100 K s^{-1}. T_{onset} corresponded to the intercept between the tangent to the glass signal before the glass transition region and the tangent to the signal inflection point during the glass transition, while T_{end} was constructed from the intercept between the tangent to the signal of the relaxed liquid after the glass transition region and the tangent to the second signal inflection point during the glass transition (tangents are marked by dashed lines). T_{peak} corresponded to the minimum of the signal during the glass transition. For clarity, a y -axis offset is used.

5.4 Results

5.4.1 DSC and FDSC

The values of T_{onset}, T_{peak} and T_{end} were obtained by conventional DSC and FDSC with $q_{c,h}$ ranging from 0.167 K s^{-1} (or 10 K min^{-1}) to 40,000 K s^{-1} (or 2,400,000 K min^{-1}). However, the relative strong tendency to crystallise of the AMZ4 liquid impedes glass formation for $q_{c,h}$ < 100 K s^{-1}, whereas a glass can be formed by quenching the Vitreloy 105 liquid with a cooling rate down to 0.176 K s^{-1}. Further, T_{end} was only evaluable for FDSC due to the onset of a crystallisation exotherm, when heated in the conventional DSC above the glass transition peak at rates up to 40 K min^{-1} (no constant signal level was assignable to the liquid). Furthermore, a strong thermal lagging [25] of the FDSC signals was evident, if samples of Vitreloy 105 were treated at high rates (7,500–40,000 K s^{-1}). Thus, T_{onset}, T_{peak} and T_{end} of these cooling rates

were discarded from further analysis. Despite these limitations, **Fig. 5.3** shows that T_{onset}, T_{peak} and T_{end} against the employed cooling/heating rate in logarithmic scale follow the trend predicted by **Eq. (5.6)**, i.e. an increase in the fictive temperatures for increasing the absolute heating/cooling rate $q_{c,h}$. Further, **Fig. 5.3** is clearly showing that the characteristic temperatures determined at low cooling rates by DSC and those at high cooling rates by FDSC matches the common trend. All measured and evaluated T_{onset}, T_{peak} and T_{end} data are listed in **Table 5.1**.

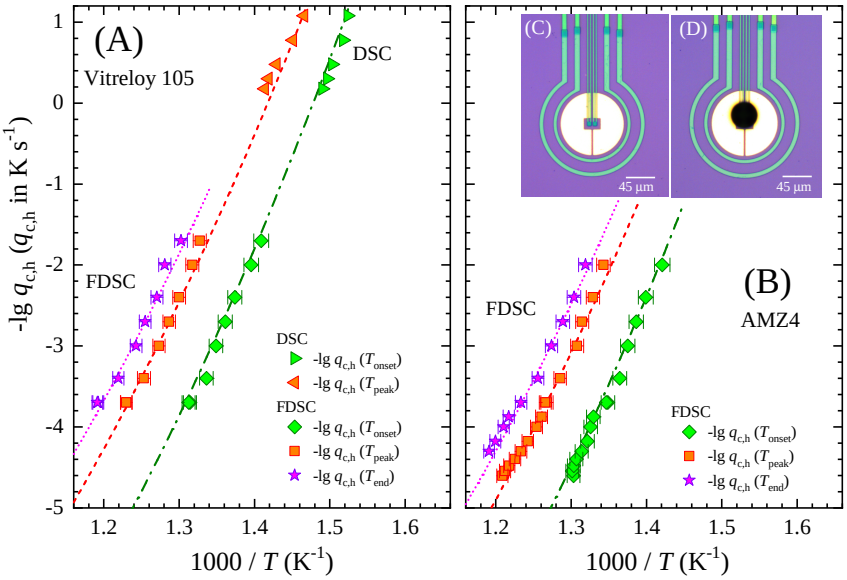

Figure 5.3: Arrhenian diagram of characteristic temperatures of the glass transition (T_{onset}, T_{peak} and T_{end}) for $|q_c| = |q_h|$. Vitreloy 105 (A) and AMZ4 (B) metallic glasses. UFH 1 sensor chip before loading (C) and loaded with AMZ4 glass droplet upon quenching at 30,000 K s^{-1} (D). Dashed and dashed-dotted lines are lg $\eta(T_{onset})$ - 11.2, lg $\eta(T_{peak})$ - 9.8 and lg $\eta(T_{end})$ - 9.2 for T_{onset}, T_{peak} and T_{end}, respectively. The lg $\eta(T)$ is from MYEGA-fit through calorimetric and viscosity data using lg η_∞, B, C parameter of the strong regime of **Table 5.2**.

5.4.2 Viscosity of Vitreloy 105 and AMZ4

By employing the shift factors lg K_{onset} = 11.2 ± 0.1, lg K_{peak} = 9.8 ± 0.2 and lg K_{end} = 9.2 ± 0.2 for the Vitreloy 105 and AMZ4 samples, it was possible to translate all calorimetric T_{onset}, T_{peak}, and K_{end} of **Table 5.1** into viscosity values according to **Eq. (5.7)**. **Fig. 5.4** reveals that this route led to a reliable agreement with measured viscosity and that for both compositions the strong character of the liquids is kept down to lg η = 4.9–5.5. Using the MYEGA viscosity model for the strong regime (**Eq. (5.3)**), lg $\eta(T)$ was best described with the parameters compiled in **Table 5.2**. As in previous research [47, 48, 136], the viscosity at infinite temperature η_∞ was set to 4 × 10^{-5} Pa s

Table 5.1: Characteristic glass transition temperatures T_{onset}, T_{peak} and T_{end} of Vitreloy 105 and AMZ4 metallic glasses as determined by conventional DSC and FDSC (mean value of two experiments and ordered by increasing $q_{c,h}$). These temperatures were determined with a maximum uncertainty of ± 1 K for conventional DSC and ± 5 K for FDSC.

		Vitreloy 105			AMZ4		
	$q_{c,h}$ (K s^{-1})	T_{onset} (K)	T_{peak} (K)	T_{end} (K)	T_{onset} (K)	T_{peak} (K)	T_{end} (K)
DSC	0.083	656.2	682.2				
	0.167	658.9	689.3				
	0.333	665.2	699.8				
	0.5	668.2	705.0				
	0.667	671.0	707.5				
FDSC	50	710	753	768			
	100	716	759	781	704	745	758
	250	728	769	787	715	752	767
	500	735	777	797	721	761	776
	1,000	741	785	805	727	765	785
	2,500	748	798	820	733	778	796
	5,000	761	813	839	741	789	811
	5,000	762	813	839	743	790	
	7,500				752	793	822
	10,000				754	797	826
	15,000				757	805	834
	20,000				761	811	840
	25,000				765	816	
	30,000				767	821	
	35,000				768	825	
	40,000				768	827	

(lg η_∞ = -4.4) and this value was kept constant when fitting **Eq. (5.3)** through the data.

5.5 Discussion

In general, narrowing down the temperature range of the F–S transition of Vitreloy 105 and AMZ4 liquids is impeded by their strong tendency to crystallise. Thus, viscometry and conventional calorimetric methods are limited to ranges above liquidus temperature and around glass transition (standard cooling) leaving a huge gap of ∼11 (Vitreloy 105) and ∼13 (AMZ4) orders of magnitude in viscosity between the liquid's fragile and strong regimes. **Fig. 5.5** shows that fast-scanning calorimetry was capable to provide improved access to the viscosity of Vitreloy 105 and AMZ4 liquids for temperatures down to $\sim 0.78 T_g/T$. Further, by employing the double exponential form of the MYEGA model (**Eq. (5.5)**) with a fragile term dominant at high temperatures and a strong term dominant at low temperatures, the overall viscous behaviour was entirely describable in quantitative

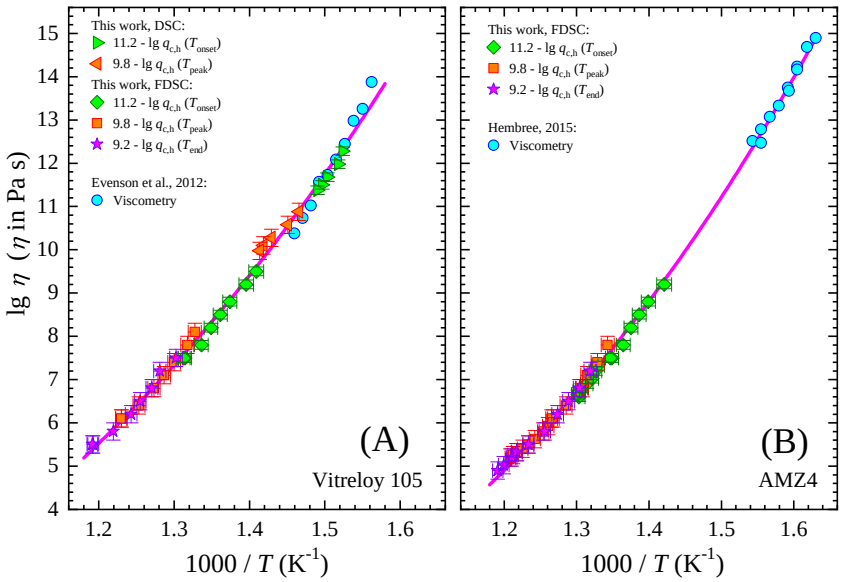

Figure 5.4: Measured viscosity together with DSC/FDSC-derived viscosity (**Eq. (5.7)**) using the shift factors lg K_{onset} = 11.2 ± 0.1, lg K_{peak} = 9.8 ± 0.2 and lg K_{end} = 9.2 ± 0.2 for Vitreloy 105 (A) and AMZ4 (B). Viscometry data: Vitreloy 105 from Evenson et al. [47], AMZ4 from Hembree [48]. Full magenta line is MYEGA-fit through all data. η_∞, B, C parameter as compiled for the strong regime in **Table 5.2**.

terms (**Table 5.2**). Particularly, inspection of **Fig. 5.5** let us believe that on the one hand the extent of the F-S transition as quantified by the transition factor f ($f = m_{fragile}/m_{strong}$) is larger for Vitreloy 105 (= 2.71) than for AMZ4 (= 1.75), while on the other hand the F–S crossover takes place with a maximum at around $0.69T_g/T$ (Vitreloy 105) and $0.66T_g/T$ (AMZ4) as pinpointed by the first derivative of the viscosity dependence with respect to T_g/T (**Fig. 5.6**). The latter temperature coordinate of the F–S transition is slightly higher than for Vitreloy 1, for which Way et al. [119] determined a crossover in the viscosity-temperature dependence depending on the heating/cooling path between 0.5 and $0.65T_g/T$. In other BMG systems [49], values between 0.7 and $0.8T_g/T$ were reported.

In general, there appears to be an inverse relation between the transition factor f and m_{strong} (**Fig. 5.7**). Although in the current study no direct correlation could be established between the F–S crossover temperature and the kinetic fragility m_{strong} of the strong regime (not shown), the data obtained in this study fit well into the general trend depicted in (**Fig. 5.7**). The Zr–based BMGs studied here and those of Hembree [48] precisely extend the apparent trend on the high-fragility boundary initially analysed by Zhang et al. [50].

The larger m_{strong} of an alloy, the more fragile is its low temperature phase, indicating that pronounced structural ordering is still present in the temperature regime in close vicinity to the glass transition, in line with the observation that these alloys are characterized by a larger heat capacity difference between the liquid and glassy or crystalline state around the glass transition [143]. On the other hand, a low m_{strong}

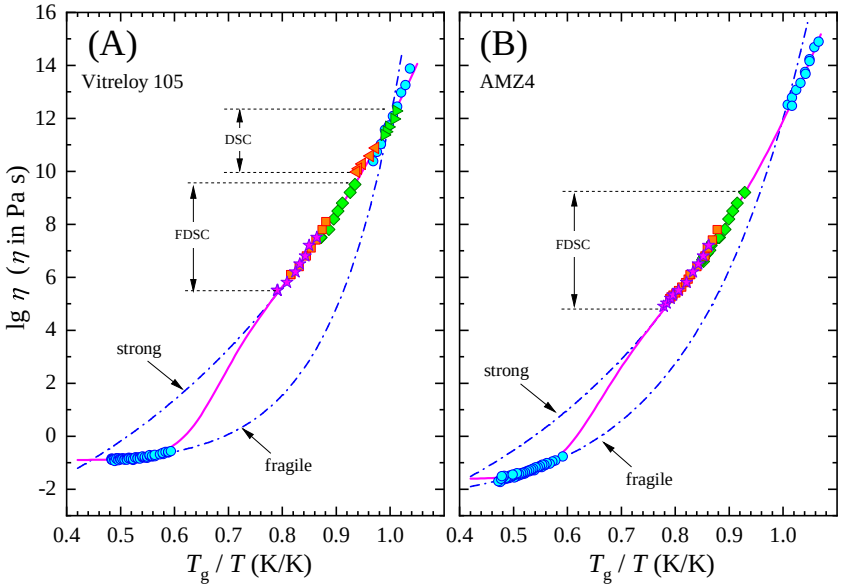

Figure 5.5: T_g/T-scaled representation of the temperature dependence of the viscosity (Angell-Plot) for Vitreloy 105 (A) and AMZ4 (B). Solid magenta line is best fit of **Eq. (5.5)** through all data. Blue dashed-dotted lines are best fits through the low-temperature data of the strong regime and through the high-temperature data of the fragile regime (**Eq. (5.3)**), respectively.

Table 5.2: Parameters of the temperature-dependant viscosity for Vitreloy 105 and AMZ4 liquids using the MYEGA model. Fit (**Eq. (5.3)**) of high-temperature viscosity data (Couette rheometer [142]) of the fragile regime only. Fit (**Eq. (5.3)**) of low-temperature viscosity data (calorimetry derived (this work) and beam bending viscometer [47, 48]) of the strong regime only. Fit (**Eq. (5.5)**) of all data (fragile and strong regimes). Specific parameters: glass transition temperature T_g and kinetic fragility m.

	Vitreloy 105			AMZ4		
Regimes	Fragile **Eq. (5.3)**	Strong **Eq. (5.3)**	Fragile-to-strong **Eq. (5.5)**	Fragile **Eq. (5.3)**	Strong **Eq. (5.3)**	Fragile-to-strong **Eq. (5.5)**
lg η_∞ (Pa s)	-1.08	-4.4[a]	-0.9	-2.5	-4.4[a]	-1.62
B (K)	8.75			182		
W (K^{-1})			23214			1965
C (K)	4578		18464	2586		16538
B (K)		2889			2381	
W (K^{-1})			0.00097			0.00094
C (K)		877	1400		984	1385
T_g[b] (K)	663.4[a]	663.4		653.7[a]	653.7	
m (**Eq. (5.4)**)	103.4	38.1		71.9	41.1	

Keys: [a]kept constant; [b]isokom temperature $\eta(T_g)$ = 10^{12} Pa s

indicates a stronger liquid behaviour in this temperature region, meaning that structural ordering has a less pronounced temperature dependence. The latter suggests that these alloys already have undergone pronounced structural ordering during cooling towards the glass transition in line with the observation of smaller heat capacity jumps around the glass transition. Accordingly, a lower m_{strong} value should generally correlate with a larger F–S transition factor and vice versa (**Fig. 5.7**).

As aforementioned, the nature of F–S transitions still has not been fully understood,

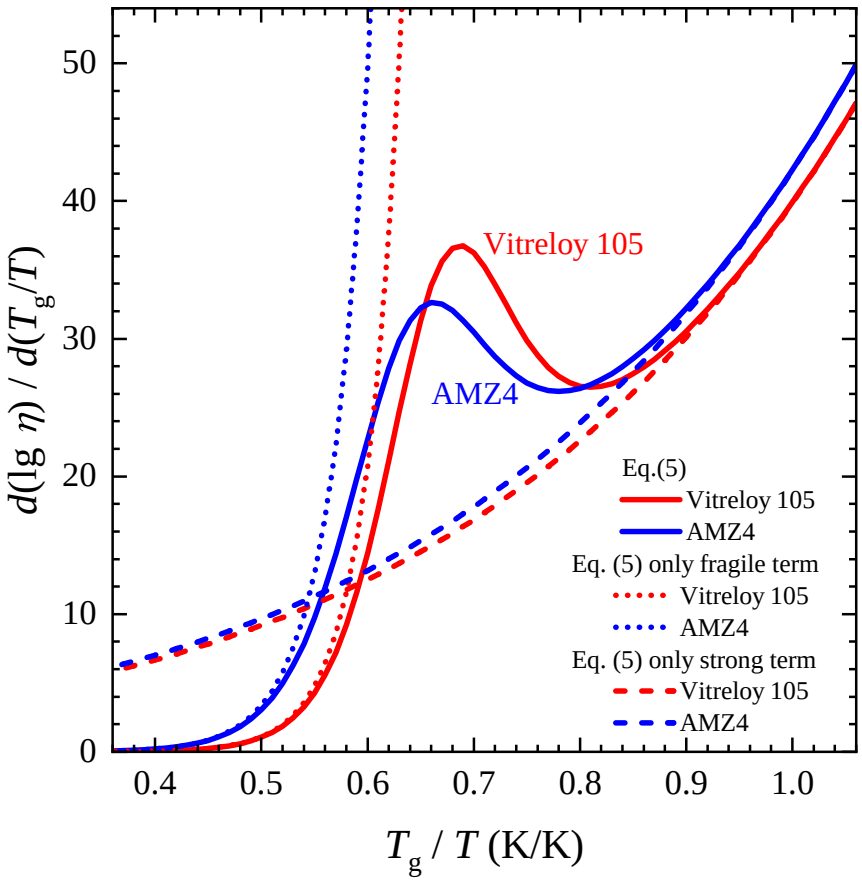

Figure 5.6: d(lg η)/d(T_g/T) as a function of the T_g-scaled temperature T for Vitreloy 105 and AMZ4 bulk metallic glass-forming liquids. The contributions of a fragile term dominant at high temperatures and a strong term dominant at low temperatures of **Eq. (5.5)** are marked by dotted and dashed lines, respectively.

but they have emerged as a common feature for metallic-glass forming liquids. The phenomenon has been linked to polyamorphism, which describes multiple distinct amorphous phases of the same composition with different properties. The distinctive characteristic between such two liquid or amorphous phases is thought to lie in the formation of locally favoured structures and not in their density [144]. This rationalises how metallic glasses, usually already exhibiting dense packing through short- and medium-range order in their liquid state [145], can undergo such transitions by chemical and topological ordering driven by the negative mixing enthalpies between their main constituents rather than by density. To establish a link between the observed viscosity behaviour and the thermodynamic and structural properties, metallic glasses provide an interesting case for study due to the experimentally accessible intermediate temperature ranges at which the transitions occur [48]. The present study has outlined a possibility to use fast-scanning calorimetry to bypass the remaining challenge of rapid crystallisation for the viscosity behaviour [146]. Linking the F–S transition to the destruction of ordering on the short- to medium range length-scales has been studied for Vitreloy 1 [121] and Vitreloy

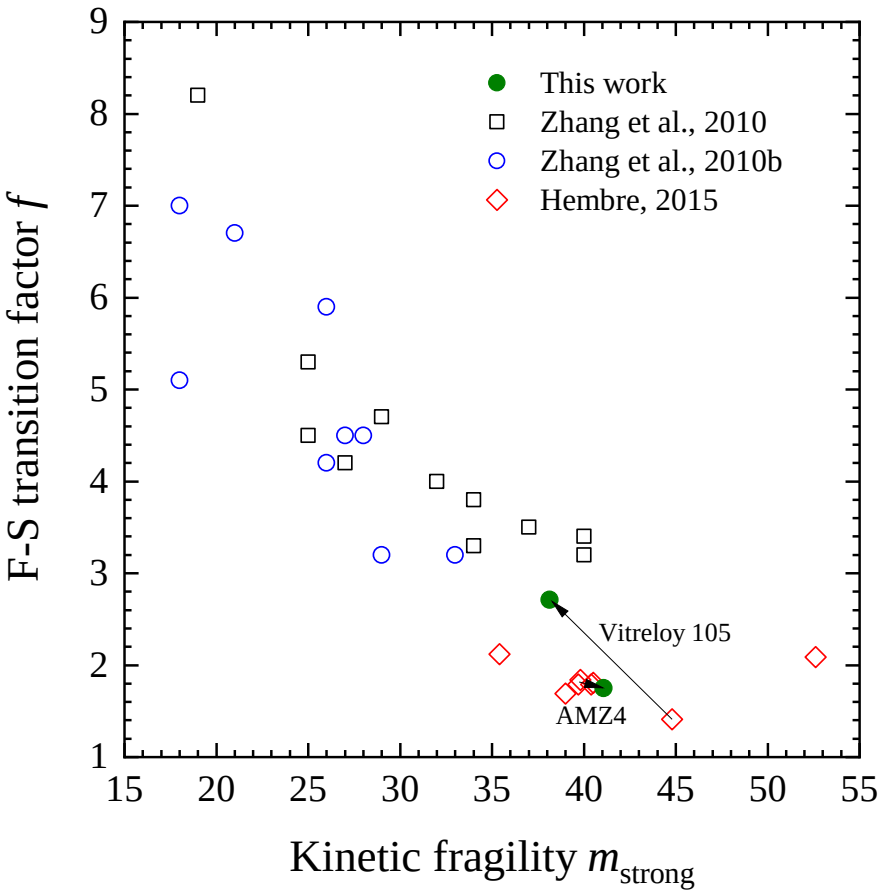

Figure 5.7: Dependence of the transition factor f on the kinetic fragility of the strong regime m_{strong} of bulk metallic glass-forming liquids. Note that arrows indicate the shift in Vitreloy 105 and AMZ4 data from previous research [48] to this study.

106a [125].

An empirical correlation between structural evolution and fragility has been explored for a wide range of metallic glass forming systems, including AMZ4 and Vitreloy 105, identifying structural changes in the first and in the 3rd to 4th coordination shell (around 1 nm) as the length-scale for the structural changes correlating with the low temperature fragility around the glass transition, i.e. the strong regime [147]. Making use of this empirical correlation, the structural changes associated with a liquid-liquid transition (LLT) in the deeply undercooled melt of the Vit106a bulk metallic forming alloy predict a two-order of magnitude change in the dynamics around $1.2T_g$, enabling to explain the course of viscosity data determined from conventional viscosity measurements [125]. However, the large inaccessible temperature related to conventional viscosity measurements makes it difficult to narrow down the position of the supposed underlying transformations. Using the methodology described above, the range of experimentally accessible viscosity data can be extended, enabling to narrow down the temperature regime of the dynamic crossover and furthermore might help to explore and identify further systems with LLTs or F-S transitions.

Finally, one has to note that the use of FDSC data in narrowing down the temperature regime of the dynamic crossover of bulk metallic glass-forming liquids necessitates composition independent (universal) shift factors for T_{onset}, T_{peak} and T_{end}. While the use of shift factors for the strong regime of Vitreloy 105 and AMZ4 is justified by the reference melt (DGG I) of close fragility (*m* DGG I = 37.8 [43]), a reference material for the fragile regime has not been presented in Section 5.2 (*m* fragile = 104 for Vitreloy 105 and *m* fragile = 71 for AMZ4). Since Chip- or Flash-DSC (FDSC) is a relatively novel technique to explore the glass transition at rates up to several thousand of Kelvin per second of small samples or thin films in the nano-gram range, this issue has been studied only for a few glass-forming liquids so far. Further, the proneness to crystallise of most fragile glass-forming liquids decreases the overlap of FDSC data points with viscosity measurements and makes the process more difficult in the search for a fragile reference material. Even though an increasing gap in the viscometric data was evident for a glass melt of diopside composition (*m* = 62.7) and a glass melt of a commercial fluorophosphate composition (*m* = 72.3), a prior study [89] showed that the use of the shift factors for fictive temperatures obtained from FDSC was successful in retrieving viscosity. However, fragile organic glass-forming liquids, such as polystyrene (PS) and polyethylene terephthalate (PET) could serve here as reference materials, as FDSC and dielectric spectroscopy data are available for broad temperature ranges. Dhotel et al. [148] performed a separate analysis of each data set and received comparable results for the fragility index *m* determined from FDSC/DSC measurements using cooling rates over 6 orders of magnitude (10^{-3} - 10^{3} K s^{-1}) and from broadband dielectric spectroscopy (136 vs. 126 for PS and 126 vs. 150 for PET). In the frequency domain of dielectric spectroscopy, the shift factor concept is known as the Frenkel-Kobeko-Reiner (FKR) constant $C = q_c/\omega$ (ω is the angular frequency of the glass (α) transition) [149, 150]. It is generally accepted to determine kinetic fragility from dielectric relaxation at $\omega(T_g)$ = 10^{-2} s [151] and, thus, one has lg K_{onset} = lg C + 10 for the limiting fictive temperature. Hence, it is remarkable that in the study of Dhotel et al. [148] the overlay of the broadband dielectric spectroscopy with DSC/FDSC data was achieved for lg C = 0.8 for PS and lg C = 1.5 for PET. Schawe [152] analysed cooling rates of PS samples from 0.003 to 4,000 K s^{-1}, which resulted in a FKR constant lg C = 1.5. In another study [153], lg C = 1.3 was obtained from the relation between freezing-in due to linear cooling and the dynamic glass transition temperature by temperature-modulated DSC of PS. For all PS studies, the same fully amorphous commercial polysterene (PS168N) from BASF was used.

These studies make us believe that FDSC/DSC enables to reproduce kinetic fragility correctly even for fragile liquids and at high cooling rates. However, they also emphasize that the fictive temperature has to be assessed from cooling rate over several lg units (the scaling is non-Arrhenius across the whole temperature range). In turn, the use of an Arrhenian approximation for the correlation -lg q_c versus $1/T_f$ leads to an increasing

deviation between calorimetric fragility and kinetic fragility as experienced for fragile organic [154] and inorganic [45] glass-forming liquids. Further, to determine the mean relaxation time for fragile liquids from the α-susceptibility peak of the dielectric [148] or mechanical loss [155], a broadband spectral analysis by temperature and frequency sweeps through the glass transition is required. If a large experimental bandwidth is incompatible with the material (crystallisation, demixing, etc.) one has to consider possible effects of the evolving heterogeneities on the frequency distribution of dielectric and mechanical loss spectra [155] or viscosity [2]. Further, the shift factor concept is based on the precondition that the cooling rate is sufficiently slow to ensure that in the time interval the mean temperature fluctuation δT of the fluctuating subsystems (cooperatively rearranging regions) can be measured [150]. If the cooling rate is too large, the time interval becomes too short to measure δT and the calorimetric experiment indicates a too high fictive temperature, which leads to an underestimation of kinetic fragility by FDSC. While the problem cannot be solved for fragile liquids within the framework of this study, the deviation from the VFTH or MYEGA dependence of -lg q_c on 1/T_f for cooling rates $\geq$ 5,000 K s^{-1} for the strong reference liquid (DGG I) [89] might be a hint for such a limitation by FDSC experiments.

5.6 Conclusions

Fast-scanning calorimetry has been successfully applied to retrieve the viscosity of supercooled liquids of Zr–based BMGs (Vitreloy 105 and AMZ4) for temperatures from standard glass transition down to $\sim$0.78T_g/T. This temperature range was largely inaccessible to viscosity determination in previous research, leaving a huge gap in viscosity of the supercooled liquids up to 13 orders of magnitude. By employing the calorimetry-derived viscosity together with data of previous rheology studies an available set of data could be established for supercooled Vitreloy 105 and AMZ4 liquids. The double exponential form of the MYEGA model with a fragile term dominant at high temperatures and a strong term dominant at low temperatures was found to describe the entire viscosity course well. This analysis revealed that both liquids are strong for lg $\eta \geq$ 4.9-5.5, the F–S crossover is centred on 0.69T_g/T (Vitreloy 105) and 0.66T_g/T (AMZ4), while the extent of the fragile-to-strong transition is larger for Vitreloy 105 than for AMZ4. Both values were found to agree well with the inverse relation established for BMG liquids between transition factor and kinetic fragility of the strong regime.

6 Discussion

This study comprises of three investigations (chapter 3-5) of different fragile glass systems to test the possibility to produce new viscosity data using the basic relation shown by Scherer and Yue et al. [31, 32] in combination with the high scanning rates of a FDSC.

In the first work (chapter 3), **Fig. 3.4** demonstrates the dependence of fictive temperature on the cooling rate for the three fragile melts Di, LS2 and N-PK52A over five orders of magnitude of $q_{c,h}$ received by combining three different DSC devices. Here, the melts showed an Arrehenian trend from $q_{c,h}$ = 0.08 K s^{-1} till $q_{c,h}$ = 5000 K s^{-1}. Furthermore, after exploring the relationship between calorimetry and viscometry for the standard soda-lime silicate glass DGG I (**Fig. 3.3**), the parallel shift factors lg K_{onset} = 11.19 $\pm$ 0.06 and lg K_{peak} = 9.68 $\pm$ 0.08 were applied to the calorimetric data of Di, LS2 and N-PK52A to obtain viscosity data (**Fig. 3.5**) by using **Eq. (3.1)**. A comparison of this resulting data with viscosimetric data (**Fig. 3.5**) showed a good agreement in the low-temperature (high viscosity) regime of micropenetration. Therefore, it can be concluded that the K_{onset} and K_{peak} obtained are independent of the chemical composition within the chemical interval investigated in this work. In addition, it can be seen that the FDSC-derived viscosity partially fills the $\eta(T)$ gap in which crystallisation occurs for most of the synthetic and natural systems with a low ability to form glass [12, 13, 71–74]. Afterwards, these findings were extended by a highly-constrained parameterisation of the viscosity obtained by the MYEGA equation (**Eq. 3.2**) [29, 30] using DSC-derived and measured viscosities. The derived fragility index *m* for LS2 is the lowest with 47.4 (*m* = 45.4 [76]), whereas the N-PK52A was found to have the highest fragility of 72.3. The Di exhibits a fragility index of 62.7 and agrees with data provided by the literature (*m* = 58.6 [75]). A comparison of the fragility indexes of LS2 and N-PK52A with those calculated by simply using measured viscosity revealed a $\sim$10% lower and higher value. Consequently, the additional use of FDSC-derived viscosities provides a better constraint to the estimation of the *m* parameter. Moreover, it can be concluded that the K_{onset} and K_{peak} provided in this work can be used for relatively strong glass former systems and more fragile systems such as LS2, Di and N-PK52A.

The subsequent work (chapter 4) demonstrated that the production of a pure TeO_2 glass is possible in a FDSC by applying fast quenching rates to a TeO_2 melt. The resulting glass 100Te (**Fig. 4.1**) was verified afterwards, together with two sodium tellurite glasses (86Te14Na and 80Te20Na) by Raman spectroscopy (**Fig. 4.2**) and showed a good matching with spectra from the literature [93, 97, 98]. Additional viscometric measurements by micropenetration of samples 80Te20Na and 86Te14Na (**Fig. 4.3**) revealed a good agreement with the literature available [99, 100]. Calorimetric measurements using $q_{c,h}$

from 0.02 K s^{-1} till $q_{c,h}$ = 30,000 K s^{-1} allowed identifying characteristic temperatures T_{onset} and T_{peak} over six orders of magnitude of $q_{c,h}$ (**Fig. 4.4A**). Furthermore, after exploring the relationship between calorimetry and viscometry for the samples 86Te14Na and 80Te20Na, the common best-fitting shift factor lg K_{onset} = 10.77 $\pm$ 0.06 was used to translate the calorimetric T_{onset} values of all three samples into viscosity according to **Eq. (4.2)**. Afterwards, a common lg K_{peak} = 9.73 $\pm$ 0.10 was obtained by adjusting the T_{peak} values to the T_{onset} trend. The entire viscosity data of all three samples is presented in **Fig. 4.4B** and shows the first viscosity data for pure TeO_2 in the range of $\eta(T)$ from $10^{5.7}$ to $10^{9.4}$ Pa s. It is necessary to stress that the lg K_{peak} used closely agreed with the shift factors previously computed for other melts [5, 89], while the lg K_{onset} obtained obviously differs from the average value of 11.2 $\pm$ 0.1 reported in the past. This could be related to the very high fragility of the melts, as previously suggested [102]. The resulting viscosity data of 100Te and 80Te20Na were added to high temperature data from rotating crucible viscometry generated by Tokunaga et al. [103] and were fitted by the MYEGA equation (**Eq. (4.2)**) [29, 30] to obtain a highly-constrained parameterisation of the viscosity (**Tab. 4.3**). This fit provided the first experimentally-determined viscosity curve for pure TeO_2, given that this component has a poor glass-forming ability and a strong tendency to crystallise. The fragility index *m* of 64(1) obtained represents the highest-known value for a single-component oxide glass, because all others (SiO_2, GeO_2, P_2O_5 and As_2O_3) showed strong Arrhenius behaviours and *m* values in the range from 17 to 20, with the exception of B_2O_3, which yields an intermediate value of *m* = $\sim$45. This should be associated with the very modest resistance against viscous flow offered by the structural units composing the TeO_2 liquid. In fact, new studies recommend a considerable short-range disorder surrounding the Tellurium atom, whose comparably weak interaction with oxygen (additionally, the presence of a lone electron pair) expresses the lack of a sharp cut-off between bonding and non-bonding partners, with a median coordination number near four [94, 95, 104–106]. A visualisation of the dependence of the viscosity to the reduced temperature T_g/T (Angell-plot) highlights the extraordinary role of the fragile TeO_2 melt among the single glass-forming oxides (**Fig. 4.6**). Furthermore, the MYEGA fit yielded a T_g of 559.5 $\pm$ 0.8 K, which is much lower in comparison to the scattered results reported by the literature [92, 93, 112–115]. This could be explained by the insufficient relaxation of the superquenched liquid and/or contamination of the sample (**Fig. 4.7**). In addition, the viscosity data obtained within this work for η = 10^{12} Pa s in the TeO_2–Na_2O system precisely match with those available in the literature [100]. In fact, studies in silicate and borate systems have repeatedly highlighted non-linear trends for T_g when the first mol% of modifier are added to the glass former end member [116–118].

In the final work (chapter 5), it was possible to create new viscosity data (**Fig. 5.4**) for Vitreloy 105 and AMZ4 melts in the temperature range from the glass transition down to $\sim 0.78 T_g/T$. This was achieved by applying scanning rates ranging from $\sim$0.083 K s^{-1}

(5 K min^{-1}) up to 40,000 K s^{-1} (2,400,000 K min^{-1}) to achieve the characteristic calorimetric temperatures T_{onset}, T_{peak} and T_{end} (**Fig. 5.2+5.3**) to the samples and using the parallel shift factors lg K_{onset} = 11.2 $\pm$ 0.1, lg K_{peak} = 9.8 $\pm$ 0.2 and lg K_{end} = 9.2 $\pm$ 0.2 [5] in combination with **Eq. (5.7)** [29, 30]. In addition, the whole viscous behaviour was described fully in quantitative terms (**Table 5.2**) by applying a double exponential form of the MYEGA model (**Eq. (5.5)**) with a strong term dominant at low temperatures and a fragile term dominant at high temperatures. A detailed inspection of the viscosity behaviour of both melts (**Fig. 5.5**) leads to the conclusion that the range of the F-S transition as quantified by the transition factor f ($f = m_{fragile}/m_{strong}$) is larger for Vitreloy 105 (= 2.71) than for AMZ4 (= 1.75), while the F–S crossover takes place with a maximum at around $0.69T_g/T$ (Vitreloy 105) and $0.66T_g/T$ (AMZ4), as localised by the first derivative of the viscosity behaviour with respect to T_g/T (**Fig. 5.6**). The position of the maximum of the F–S transition is slightly higher for AMZ4 than for Vitreloy 1, for which Way et al. [119] observed a crossover in the viscosity-temperature dependence depending on the heating/cooling path between 0.5 and $0.65T_g/T$. In the literature, values between 0.7 and $0.8T_g/T$ were reported for other BMG systems. Furthermore, when the transition factor f is plotted in dependence of the kinetic fragility m_{strong} (**Fig. 5.7**), there appears to be an inverse relation when adding the results from this work with data from the literature [48–50]. The apparent trend of the high-fragility side first described by Zhang et al. [50] was extended by the Zr–based BMGs studied by Hembree [48] and the ones from this work.

7 Conclusion

The observations found by measuring the different glass systems from chapters 3-5 with FDSC answered the main question set for this study. The updated version of the basic relation demonstrated by Scherer and Yue et al. [31, 32] was used to cover cooling and heating rates up to 40,000 K s^{-1} (2,400,000 K min^{-1}) and thereby obtain viscosities down to η = $10^{4.9}$ Pa s. These new viscosity data have been inaccessible so far due to crystallisation occurring in these glass systems during the measurements with comparatively slow running viscometric methods.

The first study (chapter 3) initially showed that a combination of fast scanning calorimetry with two conventional DSCs and viscometers results in reliable results over six orders magnitude of viscosity. It was demonstrated that the parallel shift factors K_{onset} and K_{peak} used to generate the viscosity data are independent of the chemical composition of silicate and fluorophosphate systems, which represent relatively strong and fragile glass systems. Additional constraints on the effect of sample mass on the thermal lag of the characteristic glass transition temperatures T_{onset} and T_{peak} were discussed.

For the second work (chapter 4), a combination of calorimetry and viscometry was used to calculate the full viscosity curve of pure TeO_2 with the help of two sodium tellurite glasses. Furthermore, the fragility index *m* and glass transition T_g were provided, discussed and compared with the existing literature. The received fragility index *m* of 64(1) represents the highest known value for a single-component oxide glass. Moreover, the T_g of 559.5 $\pm$ 0.8 K is much lower in comparison to the scattered results reported by the literature.

In the third work (chapter 5), FDSC measurements made it possible to access the viscosity of two Zr–based BMGs (Vitreloy 105 and AMZ4) for temperatures from standard glass transition down to $\sim 0.78 T_g/T$. Combining them with data from previous rheology studies resulted in a large dataset, which enabled for the use of a double exponential form of the MYEGA model with a strong term predominant at low temperatures and a fragile term predominant at high temperatures to describe the entire viscosity behaviour. The resulting viscosity fit narrowed down the appearance of a F-S transition to a temperature region with a centre at $0.69 T_g/T$ (Vitreloy 105) and $0.66 T_g/T$ (AMZ4), while the extent of the fragile-to-strong transition is larger for Vitreloy 105 than for AMZ4.

8 References

[1] M. L. Nascimento, L. A. Souza, E. B. Ferreira and E. D. Zanotto. 'Can glass stability parameters infer glass forming ability?' In: *Journal of Non-Crystalline Solids* 351 (2005), pp. 3296–3308. DOI: https://doi.org/10.1016/j.jnoncrysol.2005.08.013.

[2] J. Deubener. 'Viscosity of Glass-Forming Melts'. In: *Encyclopedia of Glass Science, Technology, History, and Culture*. John Wiley & Sons, Ltd, 2021. Chap. 4.1, pp. 431–451. ISBN: 9781118801017. DOI: https://doi.org/10.1002/9781118801017.ch4.1.

[3] S. Schuller, O. Pinet and B. Penelon. 'Liquid–Liquid Phase Separation Process in Borosilicate Liquids Enriched in Molybdenum and Phosphorus Oxides'. In: *Journal of the American Ceramic Society* 94 (2011), pp. 447–454. DOI: https://doi.org/10.1111/j.1551-2916.2010.04131.x.

[4] M. Tomozawa. 'Compositional Changes as Evidence for Spinodal Decomposition in Glass'. In: *Journal of the American Ceramic Society* 61 (1978), pp. 444–447. DOI: https://doi.org/10.1111/j.1151-2916.1978.tb09356.x.

[5] D. Di Genova, A. Zandona and J. Deubener. 'Unravelling the effect of nano-heterogeneity on the viscosity of silicate melts: Implications for glass manufacturing and volcanic eruptions'. In: *Journal of Non-Crystalline Solids* 545 (2020), p. 120248. DOI: https://doi.org/10.1016/j.jnoncrysol.2020.120248.

[6] D. Di Genova, R. A. Brooker, H. M. Mader, J. W. E. Drewitt, A. Longo, J. Deubener, D. R. Neuville, S. Fanara, O. Shebanova, S. Anzellini, F. Arzilli, E. C. Bamber, L. Hennet, G. La Spina and N. Miyajima. 'In situ observation of nanolite growth in volcanic melt: A driving force for explosive eruptions'. In: *Science Advances* 6 (2020). DOI: https://doi.org/10.1126/sciadv.abb0413. eprint: https://advances.sciencemag.org/content/6/39/eabb0413.full.pdf.

[7] Q. Fu, B. R. Wheaton, K. L. Geisinger, A. J. Credle and J. Wang. 'Crystallization, Microstructure, and Viscosity Evolutions in Lithium Aluminosilicate Glass-Ceramics'. In: *Frontiers in Materials* 3 (2016), p. 49. DOI: https://doi.org/10.3389/fmats.2016.00049.

[8] U. Fotheringham, R. Wurth and C. Rüssel. 'Thermal analyses to assess diffusion kinetics in the nano-sized interspaces between the growing crystals of a glass ceramics'. In: *Thermochimica Acta* 522 (2011), pp. 144–150. DOI: https://doi.org/10.1016/j.tca.2011.03.023.

[9] A. L. Greer. 'Metallic glasses…on the threshold'. In: *Materials Today* 12 (2009), pp. 14–22. DOI: https://doi.org/10.1016/S1369-7021(09)70037-9.

[10] E. D. Zanotto and J. C. Mauro. 'The glassy state of matter: Its definition and ultimate fate'. In: *Journal of Non-Crystalline Solids* 471 (2017), pp. 490–495. DOI: https://doi.org/10.1016/j.jnoncrysol.2017.05.019.

[11] S. Fanara and H. Behrens. 'Proton conduction in hydrous glasses of the join $CaAl_2Si_2O_8$–$CaMgSi_2O_6$: An impedance and infrared spectroscopic study'. In: *The Journal of Chemical Physics* 134 (2011), p. 194505. DOI: https://doi.org/10.1063/1.3589898.

[12] R. Al-Mukadam and J. Deubener. 'Effects of cooling rate and oxygen partial pressure on heterogeneous crystal nucleation of supercooled lithium disilicate melt in PtRh20 containers'. In: *Journal of Non-Crystalline Solids* 524 (2019), p. 119642. DOI: https://doi.org/10.1016/j.jnoncrysol.2019.119642.

[13] S. Krüger and J. Deubener. 'Heterogeneous surface nucleation of lithium disilicate glass: An isothermal DSC study'. In: *Journal of Non-Crystalline Solids* 417-418 (2015), pp. 45–51. DOI: https://doi.org/10.1016/j.jnoncrysol.2015.03.013.

[14] A. Q. Tool and C. G. Eicitlin. 'Variations caused in the heating curves of glass by heat treatment 1'. In: *Journal of the American Ceramic Society* 14 (1931), pp. 276–308. DOI: https://doi.org/10.1111/j.1151-2916.1931.tb16602.x.

[15] A. Q. Tool. 'Relation between inelastic deformability and thermal expansion of glass in its annealing range'. In: *Journal of the American Ceramic Society* 29 (1946), pp. 240–253. DOI: https://doi.org/10.1111/j.1151-2916.1946.tb11592.x.

[16] C. T. Moynihan, A. J. Easteal, M. A. De Bolt and J. Tucker. 'Dependence of the Fictive Temperature of Glass on Cooling Rate'. In: *Journal of the American Ceramic Society* 59 (1976), pp. 12–16. DOI: https://doi.org/10.1111/j.1151-2916.1976.tb09376.x.

[17] C. T. Moynihan. 'Structural relaxation and the glass transition'. In: *Reviews in Mineralogy and Geochemistry* 32 (1995), pp. 1–19. DOI: https://doi.org/10.1515/9781501509384-003.

[18] C. Moynihan, S.-K. Lee, M. Tatsumisago and T. Minami. 'Estimation of activation energies for structural relaxation and viscous flow from DTA and DSC experiments'. In: *Thermochimica Acta* 280-281 (1996). Vitrification, Transformation and Crytallization of Glasses, pp. 153–162. DOI: https://doi.org/10.1016/0040-6031(95)02781-5.

[19] D. J. Plazek and K. L. Ngai. 'The Glass Temperature'. In: *Physical Properties of Polymers Handbook, edited by JE Mark*. Springer, New York, NY, 2007, pp. 139–215. ISBN: 9780387312354. DOI: https://doi.org/10.1007/978-0-387-69002-5.

[20] J. C. Mauro, R. J. Loucks and P. K. Gupta. 'Fictive Temperature and the Glassy State'. In: *Journal of the American Ceramic Society* 92 (2009), pp. 75–86. DOI: https://doi.org/10.1111/j.1551-2916.2008.02851.x.

[21] Q. Zheng, Y. Zhang, M. Montazerian, O. Gulbiten, J. C. Mauro, E. D. Zanotto and Y. Yue. 'Understanding Glass through Differential Scanning Calorimetry'. In: *Chemical Reviews* 119 (2019), pp. 7848–7939. DOI: https://doi.org/10.1021/acs.chemrev.8b00510.

[22] W. A. Johnson and R. F. Mehl. 'Reaction kinetics in processes of nucleation and growth'. In: *Transactions of the American Institute of Mining, Metallurgical and Petroleum Engineers* 135 (1939), pp. 416–458.

[23] M. Avrami. 'Kinetics of Phase Change. I General Theory'. In: *The Journal of Chemical Physics* 7 (1939), pp. 1103–1112. DOI: https://10.1063/1.1750380.

[24] M. Avrami. 'Kinetics of Phase Change. II Transformation-Time Relations for Random Distribution of Nuclei'. In: *The Journal of Chemical Physics* 8 (1940), pp. 212–224. DOI: https://10.1063/1.1750631.

[25] M. Avrami. 'Granulation, Phase Change, and Microstructure Kinetics of Phase Change. III'. In: *The Journal of Chemical Physics* 9 (1941), pp. 177–184. DOI: https://10.1063/1.1750872.

[26] A. N. Kolmogorov. 'Zur Statistik der Kristallisationsvorgange in Metallen'. In: *Izvestiya Akademii Nauk SSSR. Seriya Matematicheskaya* 1 (1937), pp. 355–359.

[27] E. D. Zanotto. 'The applicability of the general theory of phase transformations to glass crystallization'. In: *Thermochimica Acta* 280-281 (1996). Vitrification, Transformation and Crytallization of Glasses, pp. 73–82. DOI: https://doi.org/10.1016/0040-6031(95)02636-3.

[28] S. Krüger and J. Deubener. 'The TTT Curves of the Heterogeneous and Homogeneous Crystallization of Lithium Disilicate – A Stochastic Approach to Crystal Nucleation'. In: *Frontiers in Materials* 3 (2016). DOI: https://10.3389/fmats.2016.00042.

[29] S. C. Waterton. 'The viscosity-temperature relationship and some inferences on the nature of molten and of plastic glass'. In: *Journal of the Society of Glass Technology* 16 (1932), pp. 244–247.

[30] J. C. Mauro, Y. Yue, A. J. Ellison, P. K. Gupta and D. C. Allan. 'Viscosity of glass-forming liquids'. In: *Proceedings of the National Academy of Sciences* 106 (2009), pp. 19780–19784. DOI: https://doi.org/10.1073/pnas.0911705106.

[31] G. W. Scherer. ‘Use of the Adam-Gibbs Equation in the Analysis of Structural Relaxation’. In: *Journal of the American Ceramic Society* 67 (1984), pp. 504–511. DOI: https://doi.org/10.1111/j.1151-2916.1984.tb19643.x.

[32] Y. Yue, R. von der Ohe and S. L. Jensen. ‘Fictive temperature, cooling rate, and viscosity of glasses’. In: *The Journal of Chemical Physics* 120 (2004), pp. 8053–8059. DOI: https://doi.org/10.1063/1.1689951.

[33] S. Vyazovkin. ‘Kissinger Method in Kinetics of Materials: Things to Beware and Be Aware of’. In: *Molecules* 25 (2020). DOI: https://10.3390/molecules25122813.

[34] M. Gao, C. Cao and J. H. Perepezko. ‘Analysis of Nucleation and Glass Formation by Chip Calorimetry’. In: *Applied Sciences* 11 (2021). DOI: https://10.3390/app11167652.

[35] H. E. Kissinger. ‘Reaction kinetics in differential thermal analysis’. In: *Analytical chemistry* 29 (1957), pp. 1702–1706. DOI: https://10.1021/ac60131a045.

[36] H. Vogel. ‘Das Temperaturabhängigkeitsgesetz der Viskosität von Flüssigkeiten’. In: *Phys. Z.* 22 (1921), pp. 645–646.

[37] G. S. Fulcher. ‘Analysis of recent measurements of the viscosity of glasses’. In: *Journal of the American Ceramic Society* 8 (1925), pp. 339–355. DOI: https://doi.org/10.1111/j.1151-2916.1925.tb16731.x.

[38] G. Tammann and W. Hesse. ‘Die Abhängigkeit der Viscosität von der Temperatur bie unterkühlten Flüssigkeiten’. In: *Zeitschrift für anorganische und allgemeine Chemie* 156 (1926), pp. 245–257. DOI: https://doi.org/10.1002/zaac.19261560121.

[39] O. S. Narayanaswamy. ‘A Model of Structural Relaxation in Glass’. In: *Journal of the American Ceramic Society* 54 (1971), pp. 491–498. DOI: https://doi.org/10.1111/j.1151-2916.1971.tb12186.x.

[40] C. T. Moynihan, P. B. Macedo, C. J. Montrose, C. J. Montrose, P. K. Gupta, M. A. DeBolt, J. F. Dill, B. E. Dom, P. W. Drake, A. J. Easteal, P. B. Elterman, R. P. Moeller, H. Sasabe and J. A. Wilder. ‘Structural relaxation in vitreous materials’. In: *Annals of the New York Academy of Sciences* 279 (1976), pp. 15–35. DOI: https://doi.org/10.1111/j.1749-6632.1976.tb39688.x.

[41] C. T. Moynihan, A. J. Easteal, J. Wilder and J. Tucker. ‘Dependence of the glass transition temperature on heating and cooling rate’. In: *The Journal of Physical Chemistry* 78 (1974), pp. 2673–2677. DOI: https://10.1021/j100619a008.

[42] A. Scarani, A. Vona, D. Di Genova, R. Al-Mukadam, C. Romano and J. Deubener. 'Determination of cooling rates of glasses over four orders of magnitude'. In: *Contributions to Mineralogy and Petrology* 177 (2022), pp. 1–17. DOI: https://doi.org/10.1007/s00410-022-01899-5.

[43] G. Meerlender. 'Viskositäts-Temperatur-Verhalten des Standardglases I der DGG'. In: *Glastechnische Berichte* 1 (1974), pp. 1–3.

[44] A. Masuhr, T. A. Waniuk, R. Busch and W. L. Johnson. 'Time Scales for Viscous Flow, Atomic Transport, and Crystallization in the Liquid and Supercooled Liquid States of $Zr_{41.2}Ti_{13.8}Cu_{12.5}Ni_{10.0}Be_{22.5}$'. In: *Physical Review Letters* 82 (1999), pp. 2290–2293. DOI: https://10.1103/physrevlett.82.2290.

[45] Q. Zheng, J. C. Mauro and Y. Yue. 'Reconciling calorimetric and kinetic fragilities of glass-forming liquids'. In: *Journal of Non-Crystalline Solids* 456 (2017), pp. 95–100. DOI: https://doi.org/10.1016/j.jnoncrysol.2016.11.014.

[46] SCHOTT AG. *N-PK52A - 497816.370*. 2021. URL: https://shop.schott.com/advanced_optics/Products/Optical-Glass/Optical-Glass/Phosphate-Crown/N-PK52A/c/optical-glass/glass-N-PK52A (visited on 15/01/2022).

[47] Z. Evenson, T. Schmitt, M. Nicola, I. Gallino and R. Busch. 'High temperature melt viscosity and fragile to strong transition in Zr–Cu–Ni–Al–Nb(Ti) and $Cu_{47}Ti_{34}Zr_{11}Ni_8$ bulk metallic glasses'. In: *Acta Materialia* 60 (2012), pp. 4712–4719. DOI: https://doi.org/10.1016/j.actamat.2012.05.019.

[48] W. Hembree. 'High temperature rheology of Zr-based bulk metallic glass forming liquids'. In: (2015). DOI: http://dx.doi.org/10.22028/D291-23174.

[49] C. Zhang, L. Hu, Y. Yue and J. C. Mauro. 'Fragile-to-strong transition in metallic glass-forming liquids'. In: *The Journal of Chemical Physics* 133 (2010), p. 014508. DOI: https://doi.org/10.1063/1.3457670.

[50] C.-Z. Zhang, L.-N. Hu, X.-F. Bian and Y.-Z. Yue. 'Fragile-to-Strong Transition in Al-Ni-M (M=La, Pr, Nd) Metallic Glasses'. In: 27 (2010), p. 116401. DOI: https://doi.org/10.1088/0256-307x/27/11/116401.

[51] V. Mathot, M. Pyda, T. Pijpers, G. Vanden Poel, E. van de Kerkhof, S. van Herwaarden, F. van Herwaarden and A. Leenaers. 'The Flash DSC 1, a power compensation twin-type, chip-based fast scanning calorimeter (FSC): First findings on polymers'. In: *Thermochimica Acta* 522 (2011), pp. 36–45. DOI: https://doi.org/10.1016/j.tca.2011.02.031.

[52] J. E. Schawe and K.-U. Hess. 'The kinetics of the glass transition of silicate glass measured by fast scanning calorimetry'. In: *Thermochimica Acta* 677 (2019), pp. 85–90. DOI: https://doi.org/10.1016/j.tca.2019.01.001.

[53] A. Sipp, Y. Bottinga and P. Richet. 'New high viscosity data for 3D network liquids and new correlations between old parameters'. In: *Journal of Non-Crystalline Solids* 288 (2001), pp. 166–174. DOI: https://doi.org/10.1016/S0022-3093(01)00527-0.

[54] D. Giordano, A. R. L. Nichols, M. Potuzak, D. Di Genova, C. Romano and J. K. Russell. 'Heat capacity of hydrous trachybasalt from Mt Etna: comparison with $CaAl_2Si_2O_8$ (An)–$CaMgSi_2O_6$ (Di) as basaltic proxy compositions'. In: *Contributions to Mineralogy and Petrology* 170 (2015), p. 48. DOI: https://doi.org/10.1007/s00410-015-1196-6.

[55] H. Taniguchi. 'Universal viscosity-equation for silicate melts over wide temperature and pressure ranges'. In: *Journal of Volcanology and Geothermal Research* 66 (1995), pp. 1–8. DOI: https://doi.org/10.1016/0377-0273(94)00053-J.

[56] S. Reinsch, M. L. F. Nascimento, R. Müller and E. D. Zanotto. 'Crystal growth kinetics in cordierite and diopside glasses in wide temperature ranges'. In: *Journal of Non-Crystalline Solids* 354 (2008), pp. 5386–5394. DOI: https://doi.org/10.1016/j.jnoncrysol.2008.09.007.

[57] J. Deubener, R. Brückner and M. Sternitzke. 'Induction time analysis of nucleation and crystal growth in di- and metasilicate glasses'. In: *Journal of Non-Crystalline Solids* 163 (1993), pp. 1–12. DOI: https://doi.org/10.1016/0022-3093(93)90638-E.

[58] J. Deubener and R. Brückner. 'Influence of nucleation and crystallisation on the rheological properties of lithium disilicate melt'. In: *Journal of Non-Crystalline Solids* 209 (1997), pp. 96–111. DOI: https://doi.org/10.1016/S0022-3093(96)00554-6.

[59] V. M. Fokin, E. D. Zanotto, N. S. Yuritsyn and J. W. Schmelzer. 'Homogeneous crystal nucleation in silicate glasses: A 40 years perspective'. In: *Journal of Non-Crystalline Solids* 352 (2006), pp. 2681–2714. DOI: https://doi.org/10.1016/j.jnoncrysol.2006.02.074.

[60] R. J. Kirkpatrick. 'Kinetics of crystal growth in the system $CaMgSi_2O_6$-$CaAl_2SiO_6$'. In: *American Journal of Science* 274 (1974), pp. 215–242. DOI: https://doi.org/10.2475/ajs.274.3.215.

[61] T. Licko and V. Danek. 'Viscosity and structure of melts in the system CaO-MgO-SiO_2'. In: *Physics and chemistry of glasses* 27 (1986), pp. 22–26.

[62] C. A. Angell. 'Entropy and fragility in supercooling liquids'. In: *Journal of Research of the National Institute of Standards and Technology* 102 (1997), p. 171. DOI: https://doi.org/10.6028/jres.102.013.

[63] C. T. Moynihan. ‘Correlation between the Width of the Glass Transition Region and the Temperature Dependence of the Viscosity of High-Tg Glasses’. In: *Journal of the American Ceramic Society* 76 (1993), pp. 1081–1087. DOI: https://doi.org/10.1111/j.1151-2916.1993.tb03724.x.

[64] X. Guo, M. Potuzak, J. C. Mauro, D. C. Allan, T. J. Kiczenski and Y. Yue. ‘Unified approach for determining the enthalpic fictive temperature of glasses with arbitrary thermal history’. In: *Journal of Non-Crystalline Solids* 357 (2011), pp. 3230–3236. DOI: https://doi.org/10.1016/j.jnoncrysol.2011.05.014.

[65] Y.-Z. Yue. ‘Characteristic temperatures of enthalpy relaxation in glass’. In: *Journal of Non-Crystalline Solids* 354 (2008), pp. 1112–1118. DOI: https://doi.org/10.1016/j.jnoncrysol.2006.11.027.

[66] J. E. K. Schawe and S. Pogatscher. ‘Material Characterization by Fast Scanning Calorimetry: Practice and Applications’. In: *Fast Scanning Calorimetry*. Ed. by C. Schick and V. Mathot. Cham: Springer International Publishing, 2016, pp. 3–80. DOI: https://doi.org/10.1007/978-3-319-31329-0_1.

[67] H. Behrens, U. Bauer, S. Reinsch, P. Kiefer, R. Müller and J. Deubener. ‘Structural relaxation mechanisms in hydrous sodium borosilicate glasses’. In: *Journal of Non-Crystalline Solids* 497 (2018), pp. 30–39. DOI: https://doi.org/10.1016/j.jnoncrysol.2018.05.025.

[68] D. Di Genova, C. Romano, M. Alletti, V. Misiti and P. Scarlato. ‘The effect of CO_2 and H_2O on Etna and Fondo Riccio (Phlegrean Fields) liquid viscosity, glass transition temperature and heat capacity’. In: *Chemical Geology* 377 (2014), pp. 72–86. DOI: https://doi.org/10.1016/j.chemgeo.2014.04.001.

[69] R. Douglas, W. Armstrong, J. Edward and D. Hall. ‘A penetration viscometer’. In: *Glass Technology* 6 (1965), pp. 52–55.

[70] J. Deubener, H. Bornhöft, S. Reinsch, R. Müller, J. Lumeau, L. Glebova and L. Glebov. ‘Viscosity, relaxation and elastic properties of photo-thermo-refractive glass’. In: *Journal of Non-Crystalline Solids* 355 (2009), pp. 126–131. DOI: https://doi.org/10.1016/j.jnoncrysol.2008.10.002.

[71] S. Kolzenburg, D. Di Genova, D. Giordano, K. Hess and D. Dingwell. ‘The effect of oxygen fugacity on the rheological evolution of crystallizing basaltic melts’. In: *Earth and Planetary Science Letters* 487 (2018), pp. 21–32. DOI: https://doi.org/10.1016/j.epsl.2018.01.023.

[72] S. Campagnola, A. Vona, C. Romano and G. Giordano. ‘Crystallization kinetics and rheology of leucite-bearing tephriphonolite magmas from the Colli Albani volcano (Italy)’. In: *Chemical Geology* 424 (2016), pp. 12–29. DOI: https://doi.org/10.1016/j.chemgeo.2016.01.012.

[73] D. D. Genova, C. Cimarelli, K.-U. Hess and D. B. Dingwell. 'An advanced rotational rheometer system for extremely fluid liquids up to 1273 K and applications to alkali carbonate melts'. In: *American Mineralogist* 101 (2016), pp. 953–959. DOI: doi:10.2138/am-2016-5537CCBYNCND.

[74] N. Pronina, S. Krüger, H. Bornhöft, J. Deubener and A. Ehrenberg. 'Cooling history of a wet-granulated blast furnace slag (GBS)'. In: *Journal of Non-Crystalline Solids* 499 (2018), pp. 344–349. DOI: https://doi.org/10.1016/j.jnoncrysol.2018.07.054.

[75] O. N. Senkov and D. B. Miracle. 'Description of the fragile behavior of glass-forming liquids with the use of experimentally accessible parameters'. In: *Journal of Non-Crystalline Solids* 355 (2009), pp. 2596–2603. DOI: https://doi.org/10.1016/j.jnoncrysol.2009.09.020.

[76] M. L. F. Nascimento, V. M. Fokin, E. D. Zanotto and A. S. Abyzov. 'Dynamic processes in a silicate liquid from above melting to below the glass transition'. In: *The Journal of Chemical Physics* 135 (2011), p. 194703. DOI: https://doi.org/10.1063/1.3656696.

[77] D. Di Genova, C. Romano, D. Giordano and M. Alletti. 'Heat capacity, configurational heat capacity and fragility of hydrous magmas'. In: *Geochimica et Cosmochimica Acta* 142 (2014), pp. 314–333. DOI: https://doi.org/10.1016/j.gca.2014.07.012.

[78] Y. Yue. 'The iso-structural viscosity, configurational entropy and fragility of oxide liquids'. In: *Journal of Non-Crystalline Solids* 355 (2009), pp. 737–744. DOI: https://doi.org/10.1016/j.jnoncrysol.2009.01.032.

[79] E. Rössler, K.-U. Hess and V. Novikov. 'Universal representation of viscosity in glass forming liquids'. In: *Journal of Non-Crystalline Solids* 223 (1998), pp. 207–222. DOI: https://doi.org/10.1016/S0022-3093(97)00365-7.

[80] W. Holand and G. H. Beall. *Glass-ceramic technology*. John Wiley & Sons, 2019. ISBN: 9781119423690.

[81] R. N. Singh. 'Sealing Technology for Solid Oxide Fuel Cells (SOFC)'. In: *International Journal of Applied Ceramic Technology* 4 (2007), pp. 134–144. DOI: https://doi.org/10.1111/j.1744-7402.2007.02128.x.

[82] M. Eberstein, S. Reinsch, R. Müller, J. Deubener and W. A. Schiller. 'Sintering of glass matrix composites with small rigid inclusions'. In: *Journal of the European Ceramic Society* 29 (2009), pp. 2469–2479. DOI: https://doi.org/10.1016/j.jeurceramsoc.2009.02.007.

[83] R. Müller, R. Meszaros, B. Peplinski, S. Reinsch, M. Eberstein, W. A. Schiller and J. Deubener. 'Dissolution of Alumina, Sintering, and Crystallization in Glass Ceramic Composites for LTCC'. In: *Journal of the American Ceramic Society* 92 (2009), pp. 1703–1708. DOI: https://doi.org/10.1111/j.1551-2916.2009.03089.x.

[84] D. Di Genova, S. Kolzenburg, S. Wiesmaier, E. Dallanave, D. Neuville, K. Hess and D. Dingwell. 'A compositional tipping point governing the mobilization and eruption style of rhyolitic magma'. In: *Nature* 552 (2017), pp. 235–238. DOI: https://doi.org/10.1038/nature24488.

[85] D. Di Genova, A. Caracciolo and S. Kolzenburg. 'Measuring the degree of "nanotilization" of volcanic glasses: Understanding syn-eruptive processes recorded in melt inclusions'. In: *Lithos* 318-319 (2018), pp. 209–218. DOI: https://doi.org/10.1016/j.lithos.2018.08.011.

[86] C. Liebske, H. Behrens, F. Holtz and R. A. Lange. 'The influence of pressure and composition on the viscosity of andesitic melts'. In: *Geochimica et Cosmochimica Acta* 67 (2003), pp. 473–485. DOI: https://doi.org/10.1016/S0016-7037(02)01139-0.

[87] M. Mujin, M. Nakamura and A. Miyake. 'Eruption style and crystal size distributions: Crystallization of groundmass nanolites in the 2011 Shinmoedake eruption'. In: *American Mineralogist* 102 (2017), pp. 2367–2380. DOI: https://doi.org/10.2138/am-2017-6052CCBYNCND.

[88] 'Crystallisation in basaltic magmas revealed via in situ 4D synchrotron X-ray microtomography'. In: *Scientific Reports* 8 (2018), p. 8377. DOI: https://doi.org/10.1038/s41598-018-26644-6.

[89] R. Al-Mukadam, D. Di Genova, H. Bornhöft and J. Deubener. 'High rate calorimetry derived viscosity of oxide melts prone to crystallization'. In: *Journal of Non-Crystalline Solids* 536 (2020), p. 119992. DOI: https://doi.org/10.1016/j.jnoncrysol.2020.119992.

[90] T. Y. M. Imaoka. 'Studies of the Glass-formation Range of Tellurite Systems'. In: *Journal of the Ceramic Association, Japan* 76 (1968), pp. 160–172. DOI: https://doi.org/10.2109/jcersj1950.76.873_160.

[91] E. R. Barney, A. C. Hannon, D. Holland, N. Umesaki, M. Tatsumisago, R. G. Orman and S. Feller. 'Terminal Oxygens in Amorphous TeO_2'. In: *The Journal of Physical Chemistry Letters* 4 (2013), pp. 2312–2316. DOI: https://doi.org/10.1021/jz4010637.

[92] A. G. Kalampounias, G. Tsilomelekis and S. Boghosian. 'Glass-forming ability of TeO_2 and temperature induced changes on the structure of the glassy, supercooled, and molten states'. In: *The Journal of Chemical Physics* 142 (2015), p. 154503. DOI: https://doi.org/10.1063/1.4917536.

[93] N. Tagiara, D. Palles, E. Simandiras, V. Psycharis, A. Kyritsis and E. Kamitsos. 'Synthesis, thermal and structural properties of pure TeO_2 glass and zinc-tellurite glasses'. In: *Journal of Non-Crystalline Solids* 457 (2017), pp. 116–125. DOI: htt ps://doi.org/10.1016/j.jnoncrysol.2016.11.033.

[94] M. N. Garaga, U. Werner-Zwanziger, J. W. Zwanziger, A. DeCeanne, B. Hauke, K. Bozer and S. Feller. 'Short-Range Structure of TeO_2 Glass'. In: *The Journal of Physical Chemistry C* 121 (2017), pp. 28117–28124. DOI: https://doi.org/10.102 1/acs.jpcc.7b08978.

[95] M. A. Marple, M. Jesuit, I. Hung, Z. Gan, S. Feller and S. Sen. 'Structure of TeO_2 glass: Results from 2D ^{125}Te NMR spectroscopy'. In: *Journal of Non-Crystalline Solids* 513 (2019), pp. 183–190. DOI: https://doi.org/10.1016/j.jnoncrysol.2019 .03.019.

[96] J. Jiusti, E. D. Zanotto, S. A. Feller, H. J. Austin, H. M. Detar, I. Bishop, D. Manzani, Y. Nakatsuka, Y. Watanabe and H. Inoue. 'Effect of network formers and modifiers on the crystallization resistance of oxide glasses'. In: *Journal of Non-Crystalline Solids* 550 (2020), p. 120359. DOI: https://doi.org/10.1016/j.jno ncrysol.2020.120359.

[97] T. Sekiya, N. Mochida, A. Ohtsuka and M. Tonokawa. 'Raman spectra of $MO_{1/2}TeO_2$ (M = Li, Na, K, Rb, Cs and Tl) glasses'. In: *Journal of Non-Crystalline Solids* 144 (1992), pp. 128–144. DOI: https://doi.org/10.1016 /S0022-3093(05)80393-X.

[98] A. Šantić, A. Moguš-Milanković, K. Furić, M. Rajić-Linarić, C. S. Ray and D. E. Day. 'Structural properties and crystallization of sodium tellurite glasses'. In: *Croatica Chemica Acta* 81 (2008), pp. 559–567.

[99] B. Tincher, J. Massera, L. Petit and K. Richardson. 'Viscosity properties of tellurite-based glasses'. In: *Materials Research Bulletin* 45 (2010), pp. 1861–1865. DOI: https://doi.org/10.1016/j.materresbull.2010.09.008.

[100] S. V. Nemilov, A. K. Yakhkind and L. S. Davydenko. 'A Study on the Viscosity of TeO_2-Na_2O Glasses'. In: *Izvestiya Akademii Nauk SSSR, Neorganicheskie Materialy* 2(4) (1966), pp. 702–706.

[101] C. A. Angell. 'Formation of Glasses from Liquids and Biopolymers'. In: *Science* 267 (1995), pp. 1924–1935. DOI: https://doi.org/10.1126/science.267.5206.1924.

[102] T. Komatsu, K. Aida, T. Honma, Y. Benino and R. Sato. 'Decoupling between Enthalpy Relaxation and Viscous Flow and Its Structural Origin in Fragile Oxide Glass-Forming Liquids'. In: *Journal of the American Ceramic Society* 85 (2002), pp. 193–199. DOI: https://doi.org/10.1111/j.1151-2916.2002.tb00065.x.

[103] H. Tokunaga, S. Haruki, S. Sukenaga, N. Saito and K. Nakashima. 'Viscosity and refractive index of M_2O-TeO_2 (M= Li, Na and K) melts'. In: *Nippon Kinzoku Gakkaishi/Journal of the Japan Institute of Metals* 74 (2010), pp. 331–336. DOI: https://doi.org/10.2320/jinstmet.74.331.

[104] M. Smirnov, A. Mirgorodsky, O. Masson and P. Thomas. 'Quantum Mechanical Study of Pre-Dissociation Enhancement of Linear and Nonlinear Polarizabilities of (TeO_2)n Oligomers as a Key to Understanding the Remarkable Dielectric Properties of TeO2 Glasses'. In: *The Journal of Physical Chemistry A* 116 (2012), pp. 9361–9369. DOI: https://doi.org/10.1021/jp303014k.

[105] O. L. G. Alderman, C. J. Benmore, S. Feller, E. I. Kamitsos, E. D. Simandiras, D. G. Liakos, M. Jesuit, M. Boyd, M. Packard and R. Weber. 'Short-Range Disorder in TeO_2 Melt and Glass'. In: *The Journal of Physical Chemistry Letters* 11 (2020), pp. 427–431. DOI: https://doi.org/10.1021/acs.jpclett.9b03231.

[106] A. G. Papadopoulos, N. S. Tagiara, E. D. Simandiras and E. I. Kamitsos. 'On the Absence of Doubly Bonded Te=O Groups in TeO_2 Glass'. In: *The Journal of Physical Chemistry B* 124 (2020), pp. 5746–5753. DOI: https://doi.org/10.1021/acs.jpcb.0c02499.

[107] S. W. Martin and C. A. Angell. 'On the glass transition and viscosity of phosphorus pentoxide'. In: *The Journal of Physical Chemistry* 90 (1986), pp. 6736–6740. DOI: https://doi.org/10.1021/j100283a030.

[108] G. Urbain, Y. Bottinga and P. Richet. 'Viscosity of liquid silica, silicates and alumino-silicates'. In: *Geochimica et Cosmochimica Acta* 46 (1982), pp. 1061–1072. DOI: https://doi.org/10.1016/0016-7037(82)90059-X.

[109] E. H. Fontana and W. A. Plummer. 'A study of viscosity-temperature relationships in GeO_2 and SiO_2 systems'. In: *Physics and Chemistry of Glasses* 7 (1966), p. 139.

[110] A. Napolitano, P. B. Macedo and E. G. Hawkins. 'Viscosity and Density of Boron Trioxide'. In: *Journal of the American Ceramic Society* 48 (1965), pp. 613–616. DOI: https://doi.org/10.1111/j.1151-2916.1965.tb14690.x.

[111] P. B. Macedo and A. Napolitano. 'Inadequacies of Viscosity Theories for B_2O_3'. In: *The Journal of Chemical Physics* 49 (1968), pp. 1887–1895. DOI: https://doi.org/10.1063/1.1670321.

[112] N. Mochida, K. Takahashi, K. Nakata and S. Shibusawa. 'Properties and structure of the binary tellurite glasses containing mono-and di-valent cations'. In: *Journal of the Ceramic Association, Japan* 86 (1978), pp. 316–326. DOI: https://doi.org/10.2109/jcersj1950.86.995_316.

[113] E. Lambson, G. Saunders, B. Bridge and R. El-Mallawany. 'The elastic behaviour of TeO_2 glass under uniaxial and hydrostatic pressure'. In: *Journal of Non-Crystalline Solids* 69 (1984), pp. 117–133. DOI: https://doi.org/10.1016/0022-3093(84)90128-5.

[114] R. El-Mallawany. 'Thermal properties and crosslinking of binary TeO_2–Nb_2O_5 and TeO_2–WO_3 glasses'. In: *Journal of Non-Crystalline Solids* 379 (2013), pp. 177–179. DOI: https://doi.org/10.1016/j.jnoncrysol.2013.07.037.

[115] H. A. A. Sidek, S. Rosmawati, B. Z. Azmi and A. H. Shaari. 'Effect of ZnO on the thermal properties of tellurite glass'. In: *Advances in Condensed Matter Physics* 2013 (2013). DOI: https://doi.org/10.1155/2013/783207.

[116] S.-K. Lee, M. Tatsumisago and T. Minami. 'Transformation-Range Viscosity and Thermal Property of Sodium Silicate Glasses'. In: *Journal of the Ceramic Society of Japan* 101 (1993), pp. 1018–1020. DOI: https://doi.org/10.2109/jcersj.101.1018.

[117] M. Kodama and S. Kojima. 'Anharmonicity and fragility in lithium borate glasses'. In: *Journal of thermal analysis and calorimetry* 69 (2002), pp. 961–970. DOI: https://doi.org/10.1023/A:1020684712439.

[118] J. Deubener, R. Müller, H. Behrens and G. Heide. 'Water and the glass transition temperature of silicate melts'. In: *Journal of Non-Crystalline Solids* 330 (2003), pp. 268–273. DOI: https://doi.org/10.1016/S0022-3093(03)00472-1.

[119] C. Way, P. Wadhwa and R. Busch. 'The influence of shear rate and temperature on the viscosity and fragility of the $Zr_{41.2}Ti_{13.8}Cu_{12.5}Ni_{10.0}Be_{22.5}$ metallic-glass-forming liquid'. In: *Acta Materialia* 55 (2007), pp. 2977–2983. DOI: https://doi.org/10.1016/j.actamat.2006.12.032.

[120] R. Busch and I. Gallino. 'Kinetics, thermodynamics, and structure of bulk metallic glass forming liquids'. In: *Jom* 69 (2017), pp. 2178–2186. DOI: https://doi.org/10.1007/s11837-017-2574-5.

[121] S. Wei, F. Yang, J. Bednarcik, I. Kaban, O. Shuleshova, A. Meyer and R. Busch. 'Liquid–liquid transition in a strong bulk metallic glass-forming liquid'. In: *Nature communications* 4 (2013), pp. 1–9. DOI: https://doi.org/10.1038/ncomms3083.

[122] F. Spaepen and D. Turnbull. 'Kinetics of motion of crystal-melt interfaces'. In: *AIP Conference Proceedings* 50 (1979), pp. 73–83. DOI: https://doi.org/10.1063/1.31738.

[123] B. G. Bagley and H. S. Chen. 'A calculation of the thermodynamic first order amorphous semiconductor to metallic liquid transition temperature'. In: *AIP Conference Proceedings* 50 (1979), pp. 97–101. DOI: https://doi.org/10.1063/1.31740.

[124] C. A. Angell. 'Glass formation and glass transition in supercooled liquids, with insights from study of related phenomena in crystals'. In: *Journal of Non-Crystalline Solids* 354 (2008), pp. 4703–4712. DOI: https://doi.org/10.1016/j.jnoncrysol.2008.05.054.

[125] M. Stolpe, I. Jonas, S. Wei, Z. Evenson, W. Hembree, F. Yang, A. Meyer and R. Busch. 'Structural changes during a liquid-liquid transition in the deeply undercooled $Zr_{58.5}Cu_{15.6}Ni_{12.8}Al_{10.3}Nb_{2.8}$ bulk metallic glass forming melt'. In: *Phys. Rev. B* 93 (2016), p. 014201. DOI: https://doi.org/10.1103/PhysRevB.93.014201.

[126] H. Sheng, H. Liu, Y. Cheng, J. Wen, P. Lee, W. Luo, S. Shastri and E. Ma. 'Polyamorphism in a metallic glass'. In: *Nature materials* 6 (2007), pp. 192–197. DOI: https://doi.org/10.1038/nmat1839.

[127] W. Xu, M. T. Sandor, Y. Yu, H.-B. Ke, H.-P. Zhang, M.-Z. Li, W.-H. Wang, L. Liu and Y. Wu. 'Evidence of liquid–liquid transition in glass-forming $La_{50}Al_{35}Ni_{15}$ melt above liquidus temperature'. In: *Nature communications* 6 (2015), pp. 1–9. DOI: https://doi.org/10.1038/ncomms8696.

[128] X. Zhao, C. Wang, H. Zheng, Z. Tian and L. Hu. 'The role of liquid–liquid transition in glass formation of CuZr alloys'. In: *Phys. Chem. Chem. Phys.* 19 (2017), pp. 15962–15972. DOI: https://doi.org/10.1039/C7CP02111A.

[129] B. Bochtler, O. Gross and R. Busch. 'Indications for a fragile-to-strong transition in the high- and low-temperature viscosity of the Fe43Cr16Mo16C15B10 bulk metallic glass-forming alloy'. In: *Applied Physics Letters* 111 (2017), p. 261902. DOI: https://doi.org/10.1063/1.5013108.

[130] S. Hechler, B. Ruta, M. Stolpe, E. Pineda, Z. Evenson, O. Gross, A. Bernasconi, R. Busch and I. Gallino. 'Microscopic evidence of the connection between liquid-liquid transition and dynamical crossover in an ultraviscous metallic glass former'. In: *Phys. Rev. Materials* 2 (2018), p. 085603. DOI: https://doi.org/10.1103/PhysRevMaterials.2.085603.

[131] J. Shen, Z. Lu, J. Q. Wang, S. Lan, F. Zhang, A. Hirata, M. W. Chen, X. L. Wang, P. Wen, Y. H. Sun, H. Y. Bai and W. H. Wang. 'Metallic Glacial Glass Formation by a First-Order Liquid–Liquid Transition'. In: *The Journal of Physical Chemistry Letters* 11 (2020), pp. 6718–6723. DOI: https://doi.org/10.1021/acs.jpclett.0c01789.

[132] H. Tanaka. ‘General view of a liquid-liquid phase transition’. In: *Phys. Rev. E* 62 (2000), pp. 6968–6976. DOI: https://doi.org/10.1103/PhysRevE.62.6968.

[133] H. Tanaka. ‘Relationship among glass-forming ability, fragility, and short-range bond ordering of liquids’. In: *Journal of Non-Crystalline Solids* 351 (2005), pp. 678–690. DOI: https://doi.org/10.1016/j.jnoncrysol.2005.01.070.

[134] C. Angell. ‘Glass-formers and viscous liquid slowdown since David Turnbull: Enduring puzzles and new twists’. In: *MRS bulletin* 33 (2008), pp. 544–555. DOI: https://doi.org/10.1557/mrs2008.108.

[135] R. Al-Mukadam, A. Zandona and J. Deubener. ‘Kinetic fragility of pure TeO_2 glass’. In: *Journal of Non-Crystalline Solids* 554 (2021), p. 120595. DOI: https://doi.org/10.1016/j.jnoncrysol.2020.120595.

[136] Z. Evenson, I. Gallino and R. Busch. ‘The effect of cooling rates on the apparent fragility of Zr-based bulk metallic glasses’. In: *Journal of Applied Physics* 107 (2010), p. 123529. DOI: https://doi.org/10.1063/1.3452381.

[137] C. Angell. ‘Spectroscopy simulation and scattering, and the medium range order problem in glass’. In: *Journal of Non-Crystalline Solids* 73 (1985), pp. 1–17. DOI: https://doi.org/10.1016/0022-3093(85)90334-5.

[138] C. Angell. ‘Strong and fragile liquids’. In: *Relaxations in complex systems*. Springer-Verlag New York, 1985, pp. 3–11.

[139] Z. P. Lu, Y. Li and C. T. Liu. ‘Glass-forming tendency of bulk La–Al–Ni–Cu–(Co) metallic glass-forming liquids’. In: *Journal of Applied Physics* 93 (2003), pp. 286–290. DOI: https://doi.org/10.1063/1.1528297.

[140] J. Heinrich, R. Busch and B. Nonnenmacher. ‘Processing of a bulk metallic glass forming alloy based on industrial grade Zr’. In: *Intermetallics* 25 (2012), pp. 1–4. DOI: https://doi.org/10.1016/j.intermet.2012.02.011.

[141] J. Schneibel, J. Horton and P. Munroe. ‘Fracture toughness, fracture morphology, and crack-tip plastic zone of a Zr-based bulk amorphous alloy’. In: *Metallurgical and Materials Transactions A* 32 (2001), pp. 2819–2825. DOI: https://doi.org/10.1007/s11661-001-1032-7.

[142] W. Hembree, B. Bochtler and R. Busch. ‘High-temperature rotating cylinder rheometer for studying metallic glass forming liquids’. In: *Review of Scientific Instruments* 89 (2018), p. 113904. DOI: https://doi.org/10.1063/1.5039318.

[143] I. Gallino. ‘On the Fragility of Bulk Metallic Glass Forming Liquids’. In: *Entropy* 19 (2017). DOI: https://doi.org/10.3390/e19090483.

[144] H. Tanaka. 'Liquid–liquid transition and polyamorphism'. In: *The Journal of Chemical Physics* 153 (2020), p. 130901. DOI: https://doi.org/10.1063/5.0021045.

[145] E. Ma. 'Tuning order in disorder'. In: *Nature materials* 14 (2015), pp. 547–552. DOI: https://doi.org/10.1038/nmat4300.

[146] Z. Yang, R. Al-Mukadam, M. Stolpe, M. Markl, J. Deubener and C. Körner. 'Isothermal crystallization kinetics of an industrial-grade Zr-based bulk metallic glass'. In: *Journal of Non-Crystalline Solids* 573 (2021), p. 121145. DOI: https://doi.org/10.1016/j.jnoncrysol.2021.121145.

[147] S. Wei, M. Stolpe, O. Gross, Z. Evenson, I. Gallino, W. Hembree, J. Bednarcik, J. J. Kruzic and R. Busch. 'Linking structure to fragility in bulk metallic glass-forming liquids'. In: *Applied Physics Letters* 106 (2015), p. 181901. DOI: https://doi.org/10.1063/1.4919590.

[148] A. Dhotel, B. Rijal, L. Delbreilh, E. Dargent and A. Saiter. 'Combining Flash DSC, DSC and broadband dielectric spectroscopy to determine fragility'. In: *Journal of Thermal Analysis and Calorimetry* 121 (2015), pp. 453–461. DOI: https://doi.org/10.1007/s10973-015-4650-9.

[149] I. Gutzow and J. Schmelzer. *The vitreous state*. Springer, 1995, p. 84. ISBN: 9783642346323.

[150] E.-J. Donth. 'Slowing Down Mechanisms'. In: *The Glass Transition: Relaxation Dynamics in Liquids and Disordered Materials*. Berlin, Heidelberg: Springer Berlin Heidelberg, 2001, p. 352. ISBN: 9783662043653. DOI: https://doi.org/10.1007/978-3-662-04365-3_4.

[151] C. Angell. 'Relaxation in liquids, polymers and plastic crystals — strong/fragile patterns and problems'. In: *Journal of Non-Crystalline Solids* 131-133 (1991), pp. 13–31. DOI: https://doi.org/10.1016/0022-3093(91)90266-9.

[152] J. E. Schawe. 'Measurement of the thermal glass transition of polystyrene in a cooling rate range of more than six decades'. In: *Thermochimica Acta* 603 (2015), pp. 128–134. DOI: https://doi.org/10.1016/j.tca.2014.05.025.

[153] A. Hensel and C. Schick. 'Relation between freezing-in due to linear cooling and the dynamic glass transition temperature by temperature-modulated DSC'. In: *Journal of Non-Crystalline Solids* 235-237 (1998), pp. 510–516. DOI: https://doi.org/10.1016/S0022-3093(98)00607-3.

[154] Z. Chen, Z. Li, Y. Zhang, R. Liu, Y. Tian and L.-M. Wang. 'Calorimetric determination of fragility in glass forming liquids: T_f vs. $T_{g-onset}$ methods'. In: *The European Physical Journal E* 37 (2014), pp. 1–7. DOI: https://doi.org/10.1140/epje/i2014-14052-y.

[155] K. Müller, N. Bagdassarov, M. James, H. Schmeling and J. Deubener. ‘Internal friction spectroscopy in Li_2O–$2SiO_2$ partially crystallised glasses’. In: *Journal of Non-Crystalline Solids* 319 (2003), pp. 44–56. DOI: https://doi.org/10.1016/S0022-3093(02)01966-X.